A Final Report

Grant No. NSG-1652-2

TERRESTRIAL GROWTH OF LEAD-TIN-TELLURIDE BY TECHNIQUES RELATED TO LOW G GROWTH

Submitted to:

National Aeronautics and Space Administration
Langley Research Center
Hampton, VA 23665

Attention: Archibald L. Fripp, Jr.
FED

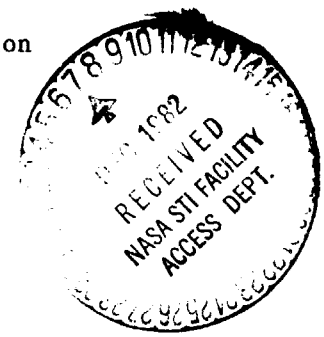

Submitted by:

W. A. Jesser
Professor

Department of Materials Science
RESEARCH LABORATORIES FOR THE ENGINEERING SCIENCES
SCHOOL OF ENGINEERING AND APPLIED SCIENCE
UNIVERSITY OF VIRGINIA
CHARLOTTESVILLE, VIRGINIA

Report No. UVA/528185/MS82/101

Copy No. 5*

October 1982

1. Report No.	2. Government Accession No.	3. Recipient's Catalog No.

4. Title and Subtitle	5. Report Date
TERRESTRIAL GROWTH OF LEAD-TIN-TELLURIDE BY TECHNIQUES RELATED TO LOW G GROWTH	November 1982
	6. Performing Organization Code: 5-28185
7. Author(s): W. A. Jesser, Professor; T. I. Ejim, Graduate Research Assistant	8. Performing Organization Report No.: UVA/528185/MS82/101
	10. Work Unit No.
9. Performing Organization Name and Address: Department of Materials Science, University of Virginia, Thornton Hall, Charlottesville, VA 22901	11. Contract or Grant No.: NSG-1652-2
	13. Type of Report and Period Covered: Final Report
12. Sponsoring Agency Name and Address: NASA Langley Research Center, Hampton, VA 23665, Attn: Archibald L. Fripp, Jr., FED	14. Sponsoring Agency Code

15. Supplementary Notes

16. Abstract

A modified Bridgman-Stockbarger furnace was constructed for a study of the solidification of silver, germanium and lead-tin-telluride. The melt-solid interface position with respect to the furnace and its temperature profile was determined by measuring the discontinuity in the slope of temperature as a function of position in the melt and in the solid. The results show that the interface position of the semiconductors germanium and lead-tin-telluride was essentially constant with respect to the furnace. and hence the growth rate was constant and equal to the sample translation rate of 0.046 cm/min and 0.178 cm/min in each case. The metal, silver, on the other hand showed a continuous interface migration toward the hot zone of the furnace and always exhibited a growth rate which was higher than the ampoule translation rate.

The K_L/K_S ratio of lead-tin-telluride was determined to be 2.33 ± 0.06 where $K_{L,S}$ denotes the thermal conductivity of the liquid, solid respectively. The value of K_L was calculated to be about 0.054 Watt $cm^{-1}K^{-1}$.

The diffusion boundary layer thickness was calculated for lead-tin-telluride to be about 0.05 cm using a liquid diffusivity of 7×10^{-5} cm^2/sec.

17. Key Words (Suggested by Author(s))	18. Distribution Statement
Bridgman-Stockbarger furnace, lead-tin-telluride, germanium, single crystal growth, directional solidification	Unclassified-Unlimited

19. Security Classif. (of this report)	20. Security Classif. (of this page)	21. No. of Pages	22. Price
Unclassified	Unclassified	154	

ACKNOWLEDGEMENTS

This final report is the Ph.D. dissertation of Dr. Theo Ejim who completed his Ph.D. work at the University of Virginia in September 1982 after spending two years of effort in the NASA Langley Research Center in Hampton, Virginia. Extensive and generous use was made of NASA equipment which is not available at the University. The guidance and advice of NASA staff in the use of equipment and during the pursuit of the goals of this research is gratefully acknowledged.

TABLE OF CONTENTS

LIST OF FIGURES

LIST OF TABLES

LIST OF SYMBOLS

A	Cross sectional area
C_A	Concentration of element "A" in the sample
C_L	Solute concentration in the melt
C_P	Heat capacity of constant pressure
C_S	Solute concentration in the solid
D_L	Solute diffusion coefficient in the melt
D_S	Solute diffusion coefficient in the solid
f	Position of thermocouple junction with respect to the bottom of the ampoule
F	Volume fraction
G_{CS}	Concentration gradient in the solid
G_L	Temperature gradient in the melt
G_S	Temperature gradient in the solid
g_s	fraction solidified
H	Latent heat of fusion
h_L	Heat transfer coefficient in the melt
h_S	Heat transfer coefficient in the solid
i	Interface position with respect to FRP
i_N	Normalized interface position, $(Z - i)/L_T$
I_A	X-ray intensity due to pure element "A"
I_A^S	X-ray intensity due to element "A" in the sample
K_L	Thermal conductivity in the melt
K_S	Thermal conductivity in the solid
k	Solute segretation coefficient, C_S/C_L
L	Length solidified at a given instance, Z - i

L_T	Total length of grown rod (boule)
m_L	Slope of the liquidus curve versus composition
m_S	Slope of the solidus curve versus composition
Pe	Peclet number
q	Heat flow rate
R	Growth rate
S	Radius of the sample cross section
t	Time
T_L	Equilibrium liquidus temperature
TC	Thermocouple
TH	Tickler heater
T_C	Cold zone temperature
T_H	Hot zone temperature
V	Translation rate
X'	Distance from the interface into the melt
Z	Translated length measured from the FRP
Z_a	Bottom of ampoule with respect to FRP
α	Length of tickler heater
β	Biot number
ρ	Density
δ	Width of diffusion boundary layer

CHAPTER I

INTRODUCTION

Directional Solidification (DS) and normal freezing carried out in a controlled environment are particularly important in the field of single crystal growth and, therefore, to the electronics industry. The Bridgman-Stockbarger[1] technique is one of the common methods of growing bulk single crystals. This technique draws heavily from DS studies. The one common aim of crystal growers is to produce a homogeneous single crystal of controlled composition free of line, point and volume defects, which are detrimental to device applications of the crystals. Some important controllable factors which determine the extent to which the grower's aim is met include the rate of growth and the temperature gradients in the phases. These factors influence the heat flow pattern in a given material.[2]

In the Bridgman technique used in the present work, much like DS experiments, heat is introduced into the material from a heater, through an adiabatic zone and out of the cooler in a vertical mode. The cooling device in a typical system can be coolant such as water or liquid metal for direct immersion, or in the present case it can be a heater block with a lower temperature setting than the hot zone. The choice of the cooling method may depend on the knowledge of the temperature gradient necessary for the avoidance of constitutional supercooling, the magnitude of the thermal gradient and cooling rates that will not introduce defects

in the grown crystal by the subsequent thermal strain and point defect aggregation.

The macroscopic melt-solid interface shape may greatly influence the generation and propagation of defects during directional solidification. It is generally accepted that a convex shape (looking from the melt side) favors grain selection.[3] The well known constitutional supercooling concept[4] indicates that slow rates of growth and a high temperature gradient in the liquid phase are necessary conditions for homogeneous growth of alloy materials. These concerns are particularly important in the field of semiconductor device applications. Developments in this field call for very high quality single crystals in order to achieve uniform electrical response within the crystal. This means, among other things, the homogeneous distribution of dopants and solutes and a very low dislocation density. In an alloy semiconductor like $Pb_{1-x}Sn_xTe$, homogeneity means the absence of convection in the melt and the avoidance of constitutional supercooling with its resultant dendritic growth. The absence of convection can only be achieved in a system that exhibits both thermal and solutal stability in the melt at all times during the growth. If for any configuration, the lighter material (lighter either by differences in temperature or solute concentration) is at the bottom of the system then the density gradient can couple with gravity to start convection in the melt. Looking at the phase diagram of a binary alloy system and

employing the lever rule, it is easily seen that the composition of the first-to-freeze solid may be higher or lower than the bulk melt composition depending on the appropriate segregation coefficient. The segregation coefficient, here, means the ratio of the solute concentration in the solid phase and the solute concentration in the melt from which the solid froze. This rejection or depletion of solute creates a diffusion boundary layer in the melt immediately ahead of the interface. Within this layer mass transfer should be by concentration gradient-driven diffusion alone resulting in homogeneous steady-state growth. However, this is not always true and much of the quality of the grown crystal depends on the behavior of this layer. If any region of this layer sees a temperature that is lower than the freezing point, that region will break down leading to dendritic or cellular growth. Also strong gravity-driven convection can sweep away this boundary layer into the bulk melt leading to nonsteady state and nonhomogeneous growth.

The microgravity environment of space is being proposed as an environment in which the problem associated with gravity-driven convection can be lessened if not entirely eliminated. The present research is part of a general effort to develop experiments for materials processing in space aboard the space shuttle. It is, therefore, a part of an intensive attempt to understand all factors that can influence crystal quality. Until recently the ampoule translation rate during

directional solidification had been regarded as the crystal growth rate. The two rates are now known to be able to differ by as much as 100%.[5] Experimental furnace characterization has been minimal. While there has been much theoretical work in this area, the mathematical difficulties involved have led to the introduction of assumptions that may not fit experimental conditions. Much experimentation is still needed in order to understand the thermal environmental changes that take place in a Bridgman-Stockbarger system during crystal growth.

Three different materials were used in this investigation. These include two semiconductors, germanium and $Pb_{1-x}Sn_xTe$ and one metal, silver. The alloy semiconductor $Pb_{1-x}Sn_xTe$ is a technologically very important material being proposed as one of the materials to be processed in the space laboratory experiments. It has an energy gap that is dependent on the composition and can be as low as zero.[6],[7] With the low energy gap and the advantage that its energy gap can be controlled by varying composition, the semiconductor may be used in photovoltaic detectors and laser over a range of wavelengths.

It has been mentioned earlier in this chapter that the shape of the melt-solid interface influences grain selection.[3] Theoretical work[2],[3] also indicates that the position of the melt-solid interface with respect to the furnace determines the shape of the interface. The present work concentrates on understanding how the melt-solid

interface position changes in relation to a furnace reference point and with respect to a number of furnace parameters and ampoule translation rates. With the knowledge of the interface movements the actual growth rate of the material will be determined as opposed to the translation rate. A careful characterization of the empty furnace will be carried out in order to understand possible shifts in temperature profile on loading. Finally, the concentration profile of a grown alloy will be correlated with the freezing temperature determined at selected points along the crystal.

CHAPTER II

BACKGROUND AND PREVIOUS WORK

A. INTERFACE BREAKDOWN

1. Constitutional Supercooling Criterion

One of the many published works dealing with the problems of solidification is the classic paper by Rutter and Chalmers[4] in which they treated the problem of constitutional supercooling (CS) during the directional solidification of single crystals of tin doped with lead. For a given set of growth conditions like dopant concentration and temperature gradient in the melt, a critical growth rate was reached at which interface breakdown occurred leading to a hexagonal array of protrusions. They explained this "cellular" structure with the theory of constitutional supercooling. This supercooling ahead of the interface is a result of either solute buildup or depletion in the melt immediately ahead of the liquid-solid interface. Factors that affected the interface breakdown included the rate of translation of the ampoule or withdrawal of the furnace, the amount of impurity and the temperature gradient in the melt. To develop quantitatively the C.S. criterion, the heat and mass flow are considered only at the liquid-solid interface. The gradient of the solute in the liquid at the interface for a steady-state condition is given as

$$\left(\frac{dC_L}{dX'}\right)_{x'=0} = -\frac{R}{D_L} C^*_L(1-k) \qquad (1)$$

where C^*_L = solute concentration in the melt at the interface

R = growth rate

D_L = solute diffusion coefficient in the melt

k = solute segregation coefficient, C_S/C^*_L

C_S = solute concentration in the solid

X' = distance from the interface into the melt

Assuming equilibrium at a flat interface the derivative of the equilibrium liquidus temperature T_L with respect to distance from the interface into the melt is given as

$$\left(\frac{dT_L}{dx'}\right)_{x'=0} = m_L\left(\frac{dC_L}{dx'}\right)_{x'=0} \qquad (2)$$

where m_L = the slope of the liquidus curve versus composition. Constitutional supercooling is absent when the actual temperature gradient in the melt is equal to or greater than the gradient of the liquidus temperature curve.

Assuming that k is independent of composition and substituting Eq. (1) into Eq. (2) gives the C.S. criterion[8] for interface breakdown.

$$\frac{G_L}{R} \leq \frac{|m_L| C^*_S (1-k)}{D_L k} \qquad (3)$$

where G_L = actual temperature gradient in the melt

C^*_S = solute concentration in the solid at the interface

Hurle[9] has treated the case where the melt is stirred. The temperature gradient in the melt at the interface is given as

$$\left(\frac{dT}{dx}\right)_{x'=0} = \frac{|m_L| R}{D_L} (C_S - C^*_L) \ \ldots \qquad (4a)$$

where C^*_L = the steady-state melt concentration at the interface

C_S = solute concentration in the solid

He obtained the C.S. criterion for interface breakdown with a stirred melt as

$$\frac{G_L}{R} \leq \frac{|m_L| C_o (1-k)}{D_L \, k + (1-k) \exp(-R\delta/D_L)} \ \ldots \qquad (4b)$$

where C_o = average composition of the bulk melt

δ = width of a diffusion layer

In deriving Eq. (4b) he used the effective distribution coefficient proposed by Burton et al.[10] for a system with some diffusion layer of width δ, within which mass transport is by diffusion only. This will be discussed later in this chapter.

2. Stability Criterion

The C.S. criterion of Eq. (3) is based on static thermodynamic considerations. A supercooled region is one where the solid phase of the material is thermodynamically more stable than the melt and therefore crystals at the interface with the right orientation will rapidly grow out to this region, leading to an interface breakdown.

A more fundamental theory that describes interface breakdown was developed by Mullins and Sekerka.[11] The interface stability theory differs from the C.S. principles in two main respects. The theory is based upon the dynamics of the whole system rather than upon the thermodynamics of the melt ahead of the interface. Such things as heat flow in the solid and latent heat of fusion are not accounted for in the C.S. principle. The C.S. principle deals with the question of which state, liquid or solid is thermodynamically favorable in the region of melt ahead of the interface, but the real question is what state is dynamically achievable. Second, the stability theory of Mullins and Sekerka[11] describes the time evolution of a perturbed interface and the resulting concentration and temperature fields. With the assumption that the bulk of the phase was isotropic and that a local equilibrium existed at the interface, they solved the Laplace equations of both the thermal and mass fields taking into account the solid-liquid interfacial energy, latent heat of fusion and the thermal

conductivities of both the liquid and solid phases. They conclude that high surface tension and a high temperature gradient favor interface stability whereas the solute buildup or depletion, depending on the value of the segregation coefficient, is destabilizing.

Ignoring the "capillary" term (surface tension) which is always stabilizing, the interface stability criterion can be simplified to the form below.

$$-G_L + m_1 G_{CL} + \left(\frac{K_S - K_L}{K_S + K_L}\right) G_L - \left(\frac{H}{K_S + K_L}\right) R \leq 0 \qquad (5)$$

where $K_{S,L}$ = thermal conductivity in solid, liquid

H = latent heat of fusion

G_{T_L} = temperature gradient in the liquid

G_{CL} = solute concentration gradient in the liquid

The latent heat term makes the interface more stable than would be predicted by the C.S. criterion. Again, if $K_L >> K_S$ the conductivity term makes the interface more stable than predicted by the C.S. criterion. It is therefore possible to have constitutional supercooling without an instability and instability without constitutional supercooling.

B. MASS REDISTRIBUTION

1. Liquid Diffusion Controlled

A quantitative treatment of the solute redistribution and the C.S. criterion was developed by Tiller et al.[3] and Smith et al.[12]

The segregation of impurities in a dilute binary alloy system is described by the segregation coefficient. This is the ratio of the solute concentration in the solid to the concentration in the melt from which the solid forms. They assumed a system with a segregation coefficient of less than unity and negligible convective mixing in the liquid. With the above assumptions, they solved the following diffusion equation

$$D_L \frac{\partial^2 C_L}{\partial x'^2} + R \frac{\partial C_L}{\partial x'} = \frac{\partial C_L}{\partial t} \qquad (6)$$

where t = time.

Solving the time independent form of the equation gives the solute concentration of the frozen portion and the liquid ahead of the interface respectively as

$$C_S = C_O \{(1-k) \left[1-\exp(-k \frac{RX}{D_L})\right] + k\} \qquad (7a)$$

$$C_L = C_O \{1+(\frac{1-k}{k}) \exp(- \frac{RX'}{D})\} \qquad (7b)$$

where C_O is the starting bulk melt concentration.

2. Partial and Complete Mixing in the Melt

In most cases of crystal growth from the melt, convection is present and solute redistribution in these cases has been treated by Burton et al.[10] and by Wagner.[13] In a solidification process from the melt of an alloy, there is always a solute buildup or depletion in the melt immediately ahead of the solid-liquid interface. In their treatment, it is assumed that there is a diffusion layer of width δ, which is independent of the convection in the bulk melt. Outside this layer, the melt composition is maintained uniform by convection and inside it, mass transport is by diffusion only. Again the same time independent diffusion equation is solved but with modified boundary conditions:

$$C_L = C_L^* \quad (x'=0) \text{ at the interface} \tag{8a}$$

$$C_L = C_0 \quad (x' \geq \delta) \text{ in the bulk melt} \tag{8b}$$

The solution to the diffusion equation is

$$\frac{C_L^* - C_S^*}{C_o - C_S^*} = e^{R\delta/D_L} \tag{9}$$

where C_L^*, C_S^* are liquid and solid solute concentrations at the interface

δ = width of the diffusion boundary layer

C_o = average concentration in the bulk melt

In the same work, they proposed the value of an effective segregation coefficient, k_{eff}, as

$$k_{eff} = \frac{k}{k + (1-k)\, e^{-R\delta/D_L}} \tag{10}$$

where k = equilibrium segregation coefficient, C_S/C_L^*

$k_{eff} = C_S^*/C_o$

As indicated by Flemings,[14] besides the treatments of mass redistribution by Tiller et al.[8] and by Burton et al.[10] discussed above, there is the earlier treatment by a number of investigators[15],[16],[17] in which complete mixing in the liquid is assumed. Consider a column of melt of an alloy material being lowered into the cold zone of a furnace in a normal freezing process. The first to freeze is kC_o. As cooling and solidification progresses, there is a solute buildup in the melt near the interface. At temperature T^* (temperature at the interface), a solid of composition C_S^* freezes out of a liquid of composition C_L^*. Equating the solute rejected when a small amount of solid forms with the resulting solute increase in the melt will give

$$(C_L - C_S^*)\, dg_s = (1-g_s)\, dC_L \tag{11}$$

Substituting the equilibrium segregation coefficient and integrating from $C_S^* = kC_o$ at $g_s = 0$ yields the composition of the solid at

the liquid-solid interface as

$$C_S^* = kC_o\,(1-g_s)^{k-1} \tag{12}$$

where C_o = average composition in the melt.

C. HEAT ANALYSIS

1. Effect of Ampoule Motion and Insulation Thickness

A theoretical heat analysis work by Chang et al.[3] has considered the effects of ampoule movement (Peclet number) on the shape and position of the isotherms, in a Bridgman-type furnace. The work assumes an infinitely long ampoule, isotropic properties (the section of the boule in the hot zone and the section in the cold zone have the same physical constants), negligible latent heat of fusion and a step function in the temperature profile of the furnace. Using these assumptions, they solved a two-dimensional steady-state differential equation for the temperature field as given by

$$\frac{K}{\rho C_P}\left[\frac{\partial^2 T}{\partial r^2} + \frac{1}{r}\frac{\partial T}{\partial r} + \frac{\partial^2 T}{\partial z^2}\right] - V\frac{\partial T}{\partial z} = 0 \tag{13}$$

where K = thermal conductivity of the boule

ρ = density of the boule

C_P = heat capacity of the boule

V = boule translation rate

r = radial position

z = axial position

The boundary conditions were as follows:

$$\text{at } z \to \infty,\ T \to T_c \text{ (cold end temperature)} \tag{14a}$$

$$\text{at } z \to -\infty,\ T \to T_h \text{ (hot end temperature)} \tag{14b}$$

$$\text{at } r = 0 \text{ (centerline, } \partial T/\partial r = 0 \text{ (symmetry)} \tag{14c}$$

$$\text{at } r = S \text{ (surface of sample) for } z > 0,\ -K\ \partial T/\partial r = h(T-T_c) \tag{14d}$$

$$\text{at } r = S \text{ for } z < 0,\ -K\ \partial T/\partial r = h(T-T_h) \tag{14e}$$

$$\text{at } z = 0,\ T_+ = T_- \text{ and } (\partial T/\partial z)_+ = (\partial T/\partial z)_- \tag{14f}$$

where h is the heat transfer coefficient at the sample surface.

The solution to these equations was obtained by Chang[18] as

$$\phi = \frac{T-T_c}{T_h-T_c} = \sum_{n=1}^{\infty} C_m J_o \left(\frac{a_n r}{S}\right) \exp\left\{\tfrac{1}{2}\left[Pe-(Pe^2 + 4\ a_n^2)^{\frac{1}{2}}\right]\frac{Z}{S}\right\} \tag{15a}$$

for $z > 0$ (cold zone)

and

$$\phi = 1 + \sum_{n=1}^{\infty} C_n J_o \left(\frac{a_n r}{S}\right) \exp\left\{\tfrac{1}{2}\left[Pe + (Pe^2 + 4\ a_n^2)^{\frac{1}{2}}\right]\frac{Z}{S}\right\} \tag{15b}$$

for $z < 0$ (hot zone)

where $J_o\ (a_n r/S)$ is the Bessel function of the first kind of order zero of the argument $a_n r/S$.

$$Pe = V\ C_p S/K \tag{16}$$

is the Peclet number (ratio of heat carried by motion of sample to the heat by conduction), a_n are the eigenvalues determined by $a_n J_1(a_n) - \beta j_o(a_n) = 0$ where J_1 is the Bessel function of the first kind of first order.

$$\beta = \frac{hS}{K} \tag{17}$$

is the Biot number (ratio of heat loss from the sample surface to the heat conduction).

$$C_m = \frac{\beta\left[Pe+(Pe^2 + 4\ a_n^2)^{\frac{1}{2}}\right]}{(\beta^2+a_n^2)\ J_o(a_n)\ (Pe^2 + 4\ a_n^2)^{\frac{1}{2}}}$$

$$C_n = \frac{\beta\left[Pe-(Pe^2 + 4\ a_n^2)^{\frac{1}{2}}\right]}{(\beta^2+a_n^2)\ J_o(a_n)\ (Pe^2 + 4\ a_n^2)^{\frac{1}{2}}}$$

The work showed that the sensitivity of the interface position (a chosen isotherm) to relative heater and cooler temperatures is greater for small Biot numbers; that means small ampoule diameters, ineffective heat transfer from the ampoule surface and high thermal conductivity. They showed that the interface becomes increasingly concave (looking

from the melt) as the ampoule translation rate increases for constant thermal conditions. Of course this statement assumes that the interface does not break down due to the increased growth rate. Three factors combine to cause this increasing concavity of the interface. These are the decrease in the interface temperature due to segregation (alloy system), the sensible heat carried by the ampoule, and the latent heat liberation at the interface during freezing. They also pointed out that stirring of the melt has roughly the same influence on the interface position and shape as does a greater thermal conductivity in the melt than in the solid. Both move the interface toward the cooler and make the interface less convex.

Fu and Wilcox[2] have theoretically investigated the influence of insulation on the stability of the interface shape and position. They used a finite difference technique to solve the steady-state two dimensional differential equation for heat conduction in a cylindrical rod moving with a known axial velocity. Inserting a layer of insulation between the heater and cooler strongly decreased the curvature of the isotherms in this region. Thus the axial temperature gradient at the planar interface is expected to be uniform over a larger region with increasing thickness of the insulation zone. They showed that for a stationary ampoule, the planar isotherm lies in the lower part of the insulation region when the Biot number (hS/K) in the hot zone is larger than that in the cold zone. For equal thermal conductivity in both the

hot and cold zones, this result means that the rate of heat transfer from the furnace wall to the surface of the sample in the hot zone is higher than the rate of heat loss. Finally the work showed a shift in isotherms toward the cold zone with increasing Peclet number (increasing ampoule velocity). This simply means that more heat is being pushed down toward the cold zone.

2. Tickler Heater Analysis

A one-dimensional analysis of a booster heater, otherwise known as a "tickler" heater, inserted in the adiabatic zone, has been performed by Naumann.[24] He assumed that for a poor conductor, characterized by high Biot number, the tickler heater would probably introduce a high radial gradient which would distort the isotherms near the solid-liquid interface; and no appreciable increase in axial gradient without overheating the material near the sample surface. So the analysis was for good conductors with a Biot number of about 10^{-2} in which the radial gradients may be neglected. With the further assumption of steady state, the problem reduces to the classical one dimensional steady-state heat flow in a rod. In dimensionless form it is as follows

$$\frac{\partial^2 T}{\partial Z'^2} - 2\beta\,(T-T_i) = Pe\,\frac{\partial T}{\partial Z'} \qquad (18)$$

where $Z' = Z/a$

β = Biot number

Pe = Peclet number

a = radius of the cylindrical rod

Z = axial position

The analytical solution to the equation may be described as follows:

$$T_Z = \begin{cases} T_H - De^{W(Z+Z_3)} & , -\infty < Z < -Z_3 \\ T_t + Ae^{W(Z+Z_2)} + Be^{-W(Z+Z_2)} & , -Z_3 < Z < -Z_1 \\ T_o + G_m Z & , -Z_1 < Z < 0 \\ T_o + G_s Z & , 0 < Z < Z_1 \\ T_c + Ce^{-(Z-Z_1)} & , Z_1 < X < \infty \end{cases} \qquad (19)$$

where A, B, C, D are fourier coefficients

$W = \sqrt{2\beta_H}, = \sqrt{2\beta_C}$

$\beta_{H,C}$ = Biot number in hot, cold zones and the furnace is described as a hot zone, T_H from $-\infty < Z < -Z_3$

tickler heater, T_t from $-Z_3 < Z < -Z_1$

adiabatic zone, $\beta = 0$ from $-Z_1 < Z < Z_1$

cold zone, T_c from $Z_1 < Z < \infty$

The function of the tickler heater is to compensate for the roll off in sample temperature due to the conduction of heat thereby increasing the temperature gradient in the melt. However it is necessary to

restrict the temperature of the tickler heater region such that the maximum temperature attainable in any part of the furnace is T_H. This is required in order to avoid a "hump" in the temperature profile since such a condition may enhance convection in the melt which in turn introduces inhomogeneity into the crystal. Naumann[24] calculated that the maximum tickler heater temperature for his furnace configuration which is given as follows:

$$(T_t - T_{H_{max}}) = \frac{2(T_H - T_o)}{(1+\beta Z_1)\, e^{2\beta L} + (1-\beta Z_1)\, e^{-2\beta L} - 2} \qquad (20)$$

where L = half the length of the tickler heater.

D. CONVECTION IN THE MELT

Kim et al.[19] have investigated the effects of destabilizing vertical thermal gradients on crystal growth and segregation in an inverted (cold zone on top) Bridgman configuration using a Ga-doped germanium. It was found that as solidification progressed the melt exhibited successively turbulent convection, oscillatory thermal instabilities and finally thermal stability. Growth under turbulent convection was shown to be characterized by pronounced and rapid fluctuations of growth rate.

The results indicated that the convective melt flow behavior depends strongly on the melt height (aspect ratio) and is in principle analogous to the result obtained with an InSb system of similar configuration.[20]

In these works, turbulent convection was indicated between the aspect ratio of 2.4 and 1.8 in the germanium system and between 3 and 2 in the InSb system. As the melt height decreased, the turbulent convection gave way to oscillatory thermal instability and at an aspect ratio of about 0.9, thermal stability was indicated by the results of the germanium system.

Recent work by A. I. Witt et al.[21] has treated segregation in a Bridgman-type furnace configuration for crystals grown in the low gravity of space. It was established that the segregation behavior is diffusion controlled without interference from residual gravity, and surface tension gradients. This experiment was conducted during the Apollo-Soyuz mission as a part of NASA's program to determine the potential of zero-gravity conditions for basic research and materials processing applications. Ga-doped germanium crystals grown on Earth were partially remelted and regrown in space while current pulses were applied to achieve interfacial demarcation. A number of ground-based control experiments were carried out in an identical furnace to permit comparison of growth and segregation behavior in space and on Earth. It was shown that crystals from the ground-based experiments exhibited complete loss of single crystallinity after a growth length of about 2 cm. In contrast, single crystallinity was preserved in the space-grown crystal up to the last stages of growth in spite of internal matrix breakdown due to constitutional supercooling effects which were expected

under the prevailing growth conditions. The microscopic growth rate on Earth was found to be, within the experimental error, the same as that observed in space. Thus, while unavoidable convection in the melt on Earth interfers with the segregation process, it had no significant effect on the microscopic crystal growth rate of a doped element.

Given the remelting process needed in an experiment like the one mentioned above, and some first-to-freeze problems, there is an increased effort in the investigation of the melt-back process. Yue and Clark[22] in their work with a magnesium alloy of copper reported a disproportionately high solute (copper) concentration in the first-to-freeze portion of the rod. This is probably due to the nucleation problems that arise because of the undercooling required to overcome the nucleation energy barrier. It is hoped that with the introduction of a solid-liquid interface this initial transient may be avoided. It is of interest therefore to study the meltback process. Of prime importance is the stability of the phase boundary during melt-back. The condition of the interface may influence the crystal structure on regrowth. Woodruff[23] has treated the melting process of an alloy following the same method used by Mullins and Sekerka,[11] but with the additional consideration of solute diffusion in the growing phase. It is shown as in figure 1 that a region of constitutional superheating will occur ahead of the melting interface if

CONSTITUTIONAL SUPERHEATING

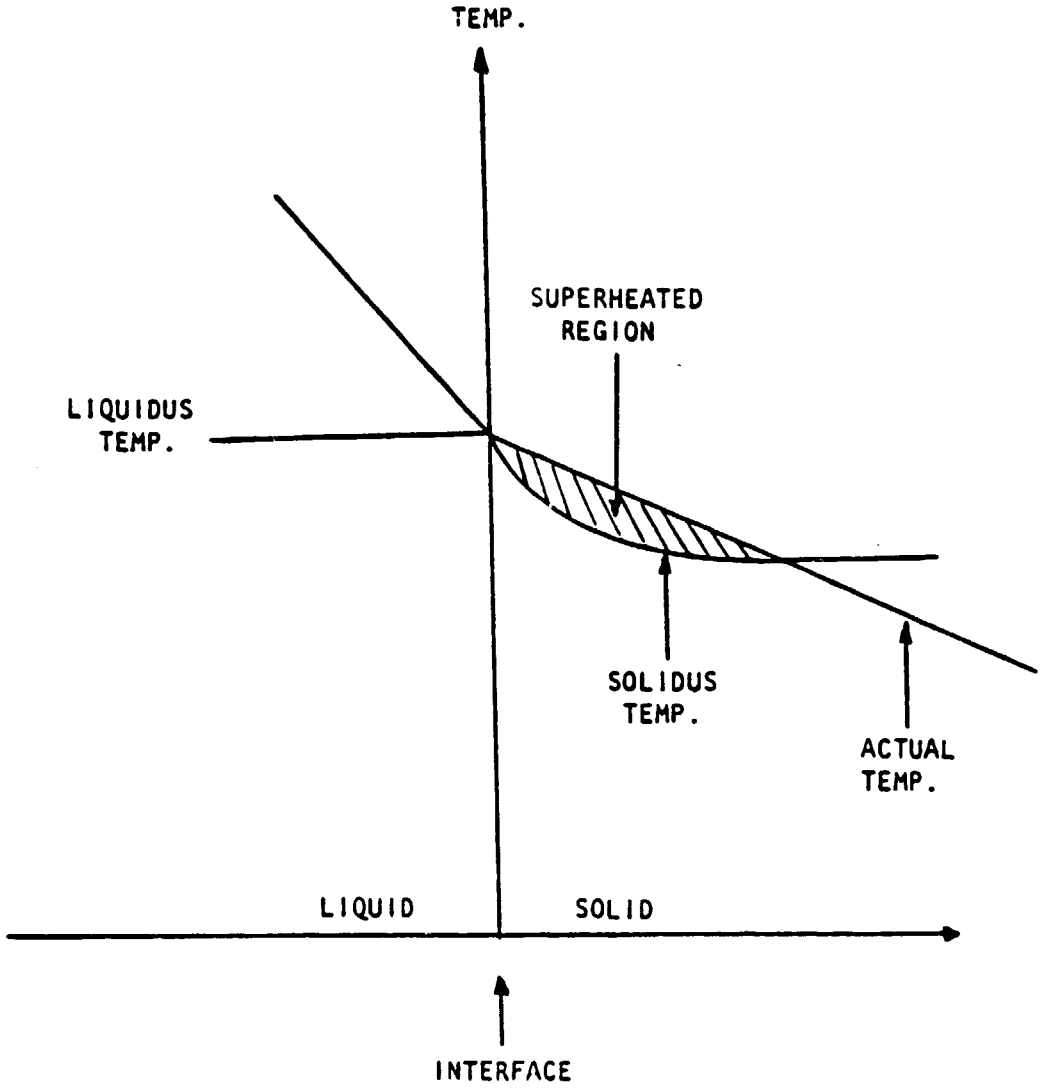

Figure 1: The condition under which a region of a given material may superheat during melting.

$$G_s \leq m_s G_{CS}/K \qquad (21)$$

where K = solute segregation coefficient

G_{CS} = conc. gradient in the solid

G_s = temperature gradient in the solid

M_s = slope of solidius curve versus composition

CHAPTER III

APPARATUS AND EXPERIMENTAL DETAILS

A. APPARATUS

1. Heater Blocks

The furnace that was constructed and characterized in this investigation has a Bridgman-type configuration consisting of a hot zone, an insulation (adiabatic) zone, and a cold zone. The furnace was required to withstand temperatures up to 1100° C and exhibit a temperature gradient of at least 100° C/cm or more at mperatures of not less than 900° C. The heater blocks were obtained commercially and according to manufacturer's specifications, they could withstand temperatures up to 1400° C. The heater blocks consist of spirally-wound Kanthal resistance wires embedded in ceramic cement. These come in halves, two of which will match to form a 4- to 12-inch heater with a cylindrical opening between them. The first furnace that was constructed and used for some of this investigation is shown in figure 2. It consists of the three different regions mentioned above. The adiabatic or insulation zone is a region between the hot and cold zones within which there are no heater wires and therefore no heat generation. This region is well insulated with fiberfax material (alumina fibers in a binder), to avoid heat loss. Both the hot and cold zones are lined with quartz tubes. This is intended to protect the heater coils and the isothermal liners from contamination in case of ampoule breakage during an experiment.

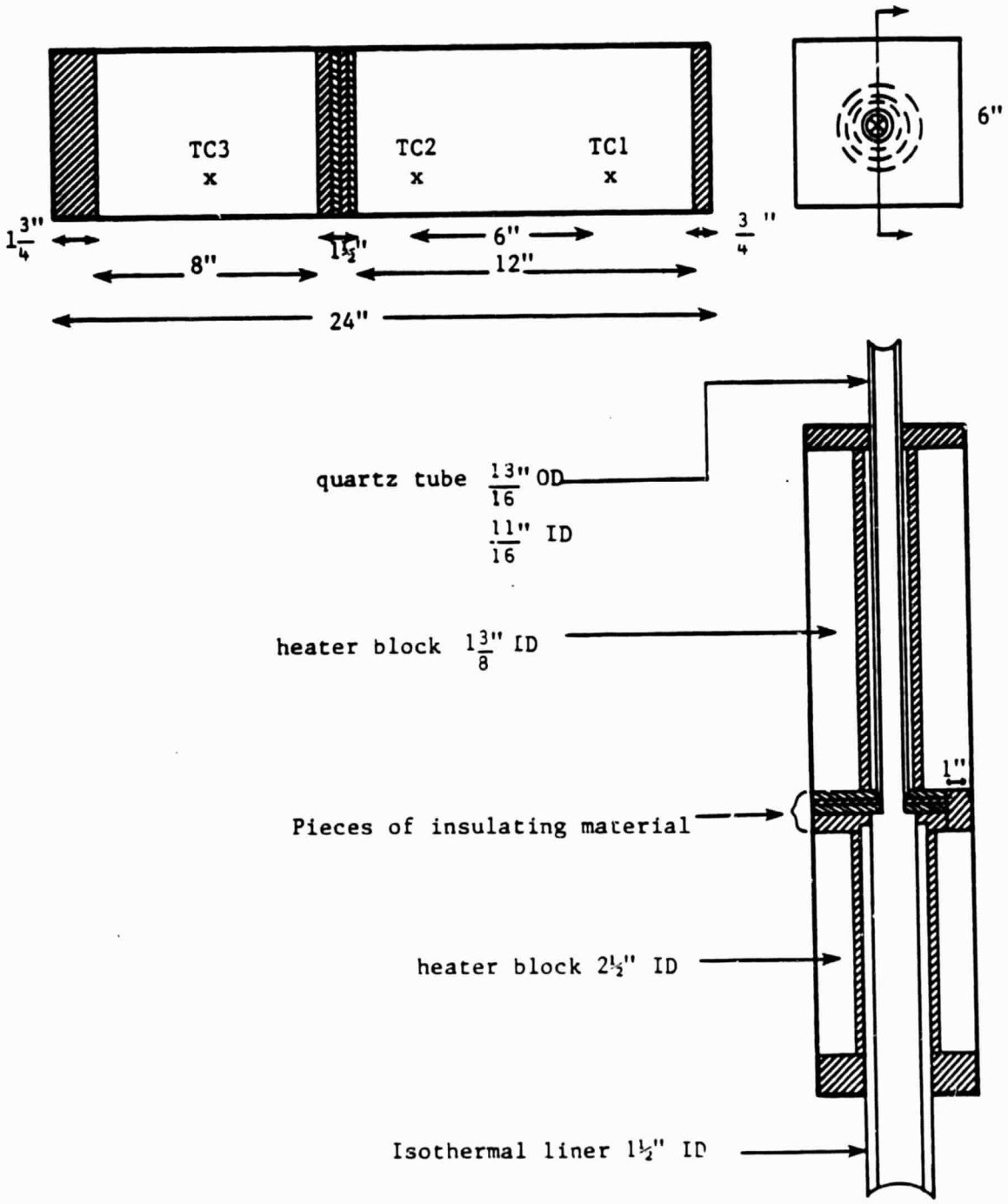

Figure 2: Two zone Bridgman Furnace

2. Controllers and Isothermal Liners

Temperature stability is very important in any crystal growth system. It is particularly important in solidification from the melt of alloys since temperature fluctuations can introduce compositional variations and may lead to cellular growth. The three furnace thermocouples shown in figure 2 are connected to a Eurotherm proportional plus integral (reset) temperature controllers. The controller eliminates "droop" by moving the proportional band up or down the temperature scale until the point at which control actually occurs coincides with the set point. "Droop" here means the difference between the set point and the actual point of control. A proportional band is a region around the set point within which power cycles on and off automatically without a temperature change. With the Eurotherm controllers, temperature oscill.. ..a can be eliminated using the appropriate rate and integral control settings. All the control thermocouples used in this work were platinum/rhodium-platinum (r-type).

A number of modifications were done on the furnace to get the final form used for most of the experiments. This final form is shown in figure 3. The furnace has an isothermal linear in both the hot and cold zones. It also contains a booster heater which will be referred to as a tickler heater from here on.

The isothermal liners are basically cylindrical heat pipes. The inner surfaces of a heat pipe are lined up with a porous capillary wick.[21]

This wick is saturated with the liquid phase of a "working" fluid and the remaining volume of the tube contains the vapor phase. Heat applied at the evaporator (liquid phase region) by an external source is absorbed through the vaporization of the working fluid resulting to a pressure differential along the heat pipe column. This pressure differential drives vapor from the evaporator (heated region) to the condenser (colder region) where it condenses thereby releasing the latent heat of vaporization. Through this process, heat is transferred from the evaporator region to the condenser region. The main function of the isothermal liner is to distribute heat more uniformily all through a given region by the wicking action. Another function of the isothermal liner is to add temperature stability to the furnace through its thermal mass.

3. Tickler Heater

The final form of the furnace constructed and used in this investigation is shown in the photograph of figure 3a. A schematic of this furnace showing all its important features is figure 3b. One of the important features of this furnace is the presence of a tickler heater which as a unit is shown in figure 4. A Kenthal A-1 wire which is 0.081 cm in diameter is wound on a quartz tube of 1.7 cm ID and 2.1 cm OD. The wire is wound around the quartz tube in such a way that the possible magnetic field created by current in one set of coils is cancelled by an opposite field created by current in another set of coils.

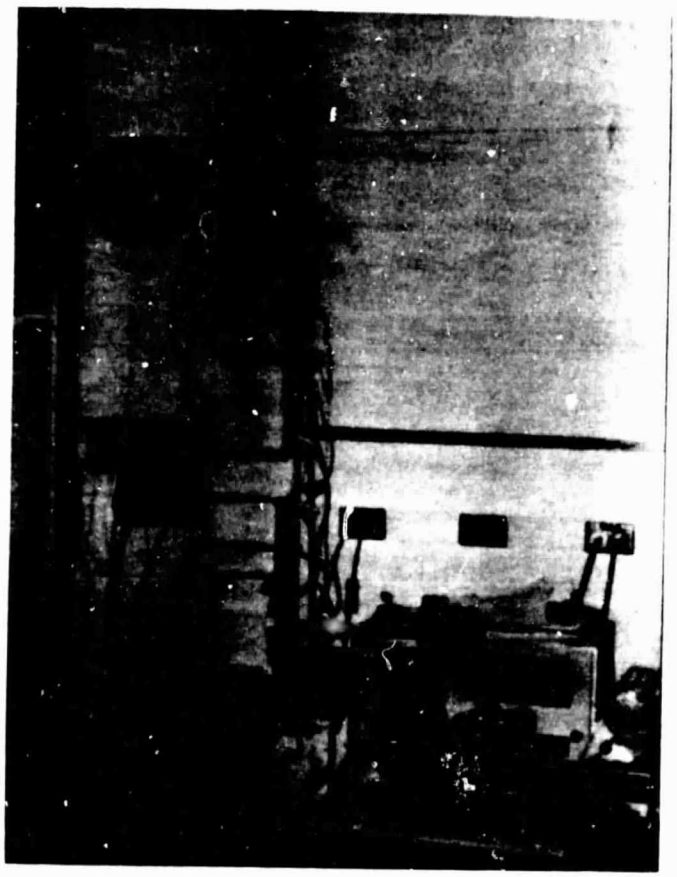

Figure 3a: The Bridgman-Stockbarger furnace constructed and used in this investigation.

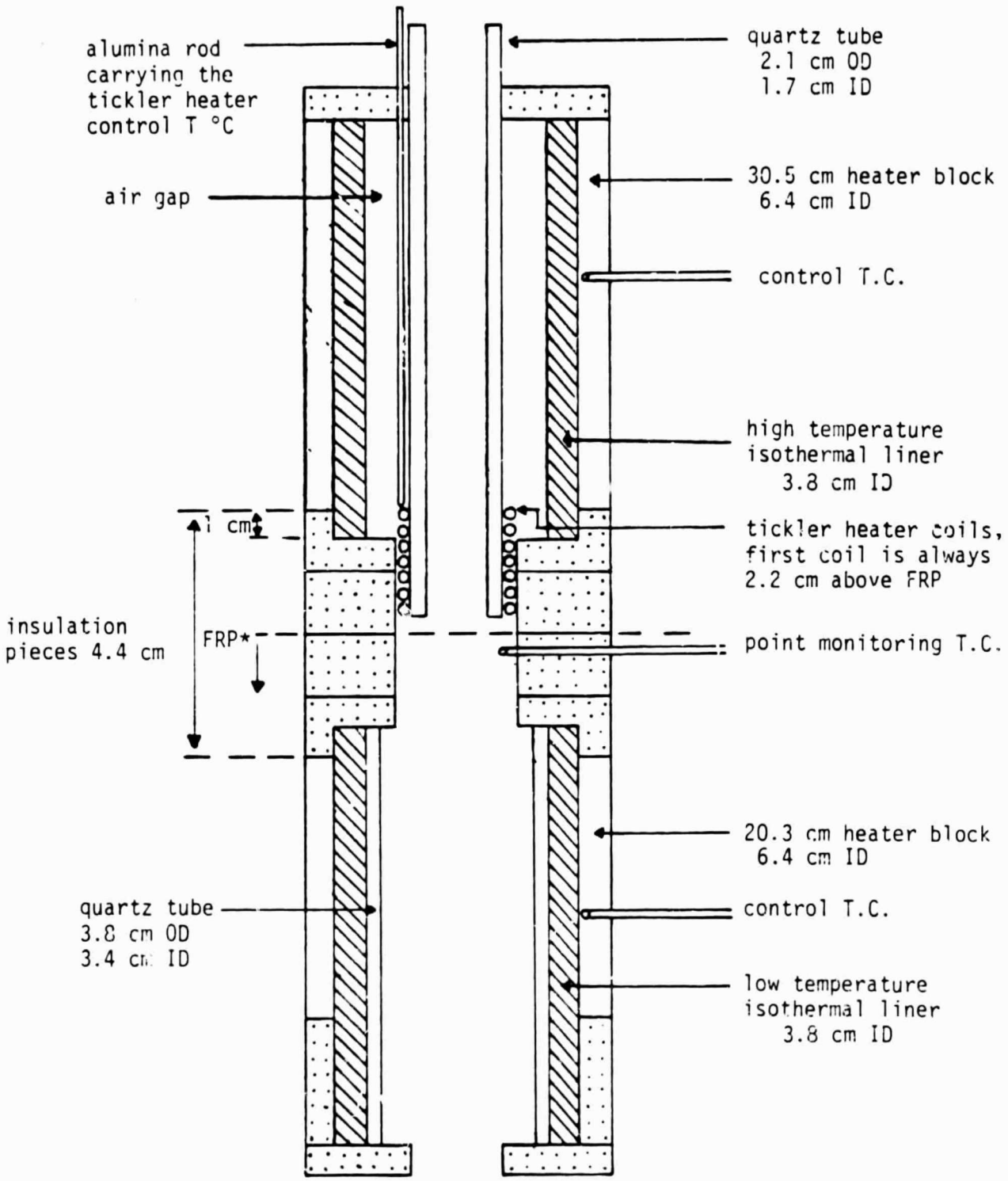

Figure 3b: Three Zone Bridgman-Stockbarger Furnace
(not to scale)
*Furnace reference point

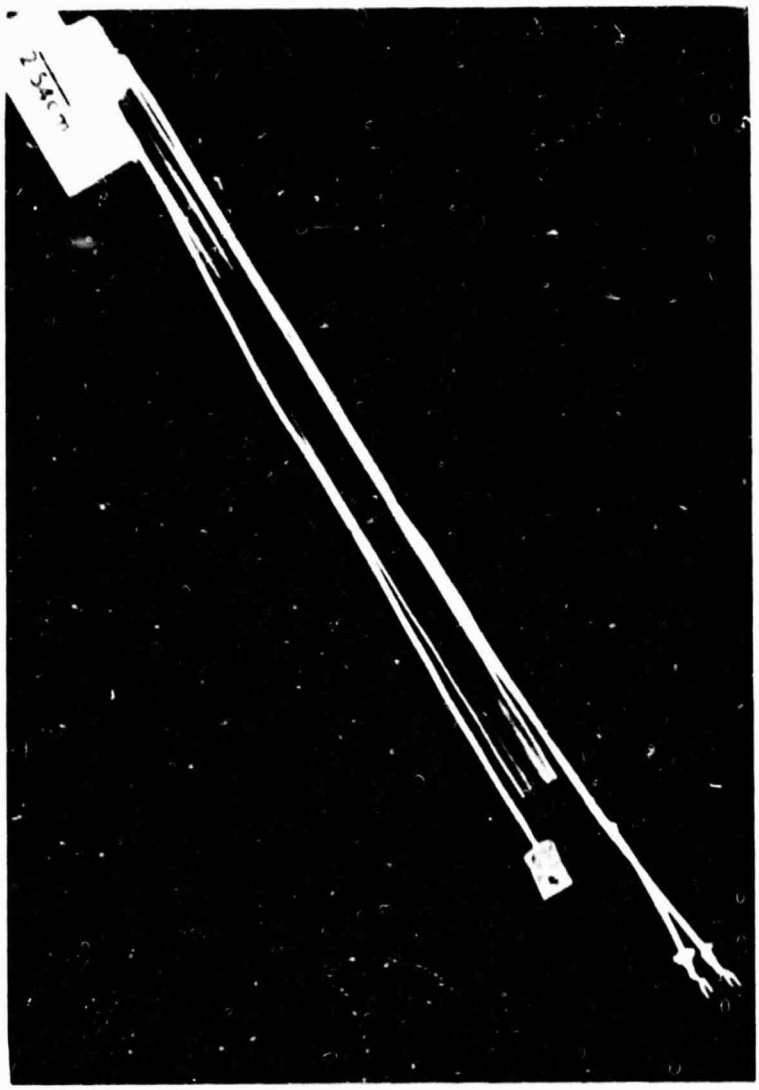

Figure 4: Tickler Heater with a 2.54 cm long heater winding (6 turns/cm).

In effect a non-inductive coil is created by this type of winding. Three tickler heaters were made with 16, 14, and 10 turns of wires, respectively. These gave heater coil lengths of 2.54 cm, 2.3 cm, and 1.43 cm, respectively. These units are then introduced into the adiabatic zone as the need arose. The introduction of a tickler heater in each case reduced the adiabatic zone length (insulation thickness) from 4.45 cm without a tickler heater to (4.45 - α) cm were α is any of the tickler heater lengths given above. Each turn of the resistance wires is insulated from the others to prevent short circuits. This is accomplished by covering them with a ceramic material.

4. Ampoule Design and Vacuum System

Using the furnace described above, initial attempts were made to measure the temperature profile in the melt of $Pb_{1-x}Sn_xTe$ during normal freezing, by dipping a thermocouple junction directly into the melt. Several coatings were used to try to protect the thermocouple junction from being attacked by the melt. However both bare and coated thermocouple junctions dissolved in the melt during the experiment. This problem coupled with the need to measure the temperature profile both in the growing solid phase and the melt called for a special ampoule design. An ampoule was designed with a 1-mm walled capillary tube attached to protect the thermocouples. This is shown in figure 5.

In order to grow materials, it was necessary to clean both the ampoule and the charge material and finally to pump on the loaded ampoule

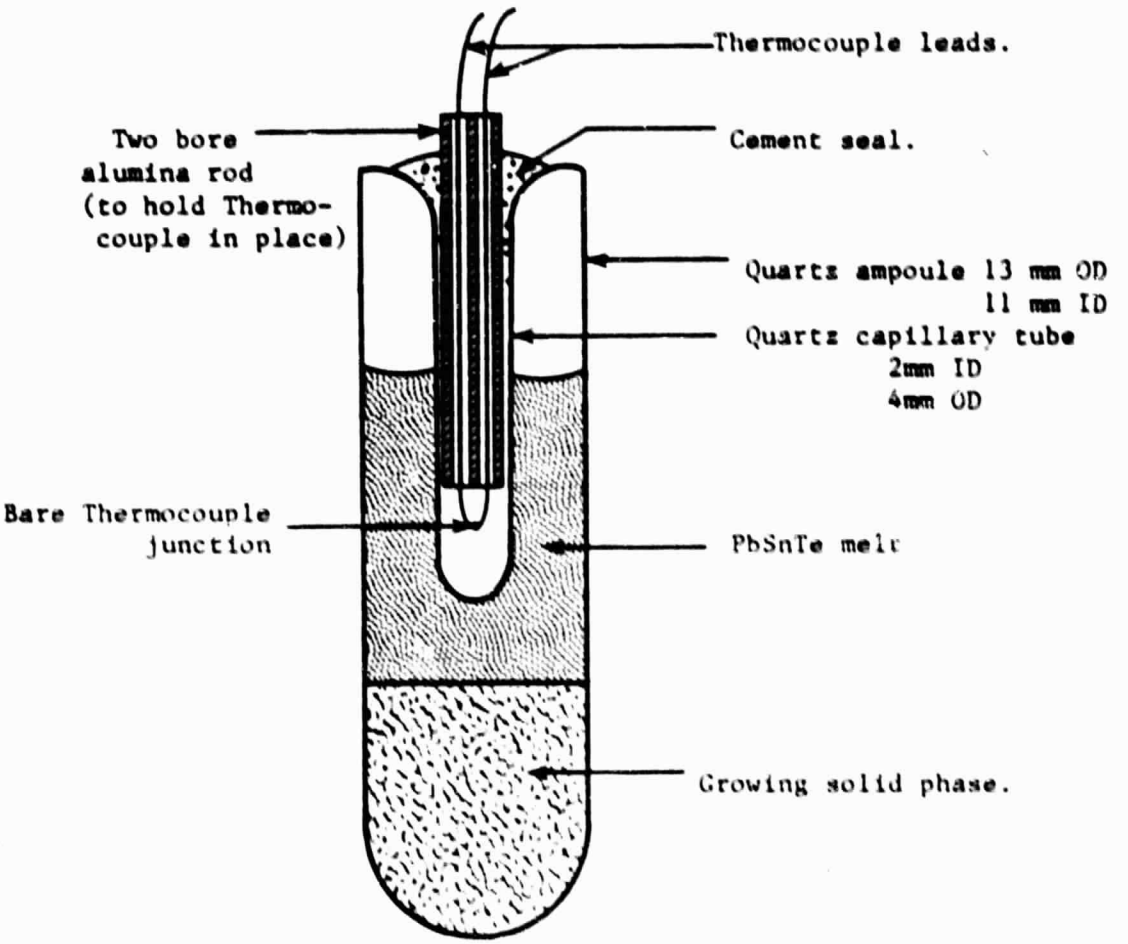

Figure 5: The capillary design for Temperature Measurement from the melt into the growing solid phase (not to scale).

under a high vacuum. This of course will help evaporate some contaminants that might be in the system. The vacuum unit used in this investigation has a cryogenic pump which acts as the roughing pump and an ion pump which has the ultimate low pressure capability of 10^{-11} torr. Attached to the vacuum system is a mass spectrometer unit for the analysis of the gases in the system as the loaded ampoule out gases. Given the high purity requirements in the single crystal growth of electronic materials, this vacuum system has an obvious advantage over a mechanical oil sealed pump which might introduce oil droplets or vapor into the sample.

B. EXPERIMENTAL TECHNIQUE

1. Bridgman Technique

Generally crystal growth methods can be divided into three categories, namely solid-solid, liquid-solid, and vapor-solid transformations. In this investigation the method employed is the liquid-solid transformation. A basic consideration in crystal growth by this method is the containment of the molten phase. The technique with which containment is achieved can have an appreciable effect on the growth conditions and the structural and chemical properties of the resulting crystal. Specifically, such things as strain, contamination, spurious nucleation and chemical reaction may be a direct result of method of containment. The melt-solid transformation as a method of crystal growth can be divided into three techniques with reference to the type

of containment. These are: (a) the melt and solid phases are in contact with a container, (b) only the melt is in contact with a container, and (c) no phase is in a container. These techniques are known as Bridgman-Stockbarger, Czochralski, and floating-zone melting, respectively.

The Bridgman-Stockbarger technique was used in this investigation. A completely molten phase of the sample and the container (ampoule) are pulled from the hot zone of a two zone furnace towards the cold zone until all the melt column solidifies. There are a number of factors worth mentioning here, that pertain to the growth of crystals by this technique. An attempt is made to achieve a planar melt-solid interface in order to reduce dislocation density.[22], [23] An attempt is also made to eliminate or minimize nonuniform segregation of impurities. These factors require that the furnace exhibit no radial temperature gradients and also that the G/R ratio be high. Finally, in the vertical Bridgman-Stockbarger technique the exact shape of the bottom of the ampoule is important for the selection of a single seed from the many that may nucleate spontaneously.

2. X-Ray Analysis

Another important experimental technique employed in this investigation, has to do with the quantitative x-ray analysis of the $Pb_{1-x}Sn_xTe$ rod grown by the Bridgman technique. Even before 1920, it was well known that each chemical element emitted characteristic x-ray wavelengths when

excited by electrons or primary x-rays of sufficient energy.[24] It was also observed that the intensity of the characteristic lines of an element depended on the amount of the element present in the specimen. So quantitative analysis by electron probe requires the measurement of wavelength and intensity of characteristic x-rays generated in the specimen. There are two systems used to separate the characteristic wavelengths for measurement. These are the wavelength dispersive spectrometer (WDS) and the energy dispersive spectrometer (EDS). Most of the analysis in this work was done with the energy dispersive spectrometer using a solid-state detector. The x-ray signal from the sample passes through a beryllium window and hits a Si(Li) detector generating electron-hole pairs. These are converted to voltage pulses and a multichannel analyzer sorts the pulses by voltages in proportion to their incident energies. In the wavelength dispersive spectrometer, an analyzing crystal is used to diffract x-rays from the sample in accordance with the Bragg's law. So at any given angle an x-ray of a particular wavelength is diffracted by the crystal and detected by a proportional counter. The x-ray quantum causes a number of ionizations in the detector which in turn creates a single output pulse whose amplitude is proportional to the number of ionizations. The total number of x-ray quanta is a measure of the relative number of atoms of the element giving off the particular characteristic x-ray quantum. It was Castaing[25] who first stated that the ratio of the characteristic

x-rays generated from element A in a specimen to that from pure A was equivalent to the concentration of element A in the specimen. That is

$$I_A/I_A^S = C_A$$

where I_A = the intensity of pure A x-rays

I_A^S = intensity of x-rays from element A in the sample for analysis

C_A = the concentration of A in the sample.

However, this C_A value commonly referred to as K value is adjusted for several effects. These include (1) the differences in electron scattering and retardation in the specimen and the standard; (2) the absorption of x-rays within the specimen, and (3) the x-ray fluorescence due to the different elements. This gives the following

$$C_A = \frac{I_A}{I_A^S} K_Z K_A K_F \qquad (22)$$

where K_Z, K_A, K_F represent the correction factors for the above mentioned effects respectively.

C. EXPERIMENTAL PROCEDURE

1. Furnace Characterization

The furnace constructed for this investigation was characterized experimentally before it was used for the solidification experiments. In

order to determine both the axial and radial temperature profiles of the furnace, the temperature profiles in the center of the furnace, the wall of the furnace quartz lining, and the wall of the isothermal liner were measured. This was done using three thermocouple junctions lined up with a light microscope so that in a vertical position the junctions maintain equal furnace axial position but different radial position according to the furnace positions mentioned above. These thermocouples are run down the furnace starting from a recorded position with respect to the furnace reference point (FRP) using a motor and gear system. As the thermocouples are run through the furnace, a programmable Fluke thermometer records the temperature at set time intervals. This empty furnace characterization is done first with both top and bottom ends of the vertical furnace kept open. It is then repeated with both ends plugged up with glass wool and some fiberfax. Both the unplugged and plugged modes of the above experiment are done first without a tickler heater and then with each of the three tickler heaters described in the last section. A tickler heater was physically in the furnace at all times. So an experiment without a tickler heater simply means that the tickler heater power supply is cut off. It needs to be pointed out that the furnace design did not allow a complete temperature profile to be obtained between the isothermal liner and the quartz liner (see Fig. 3). All three thermocouples for empty furnace temperature measurement are run through the hot zone. The thermocouple between the isothermal liner

and the quartz tube (liner) is removed before the other two are continued into the cold zone. The hot and cold zones heater controllers are set at 11.32 millivolts and 3.13 millivolts, respectively. This gives a temperature of 1100° C and 350° C respectively. These settings remain unchanged for all the experiments done with the furnace of figure 3.

2. Melt-Solid Temperature Measurement

The furnace was used to grow rods of $Pb_{1-x}Sn_xTe$, Ge and Ag. The silver that was used in this investigation was 99.99 pure but the other two materials were 99.9999 pure. These were obtained commercially. A carefully weighed out portion of any of the three materials mentioned above is loaded into an ampoule cleaned as described above and then attached to one of the vacuum pots. This loaded ampoule is pumped on as shown in figure 6, for about 12 hours. The weighing of the charges is especially important in the case of the alloy semiconductor, $Pb_{1-x}Sn_xTe$. The reason for this will be discussed in the next section of this chapter. However in all three materials, enough charges are weighed out to give about 18 cm of melt column in the 11 millimeter (ID) ampoule. After the loaded ampoule has been vacuum pumped for about 12 hours, it is then sealed under the vacuum. The vacuum gauge would typically read about 10^{-8} torr before sealing and about 10^{-6} torr just before the completion of sealing. A platinum-platinum/rhodium thermocouple threaded through a two bore alumina rod is slid down the ampoule capillary tube which has a 2-mm ID. This is shown in figure 5. The loaded ampoule, with the TC

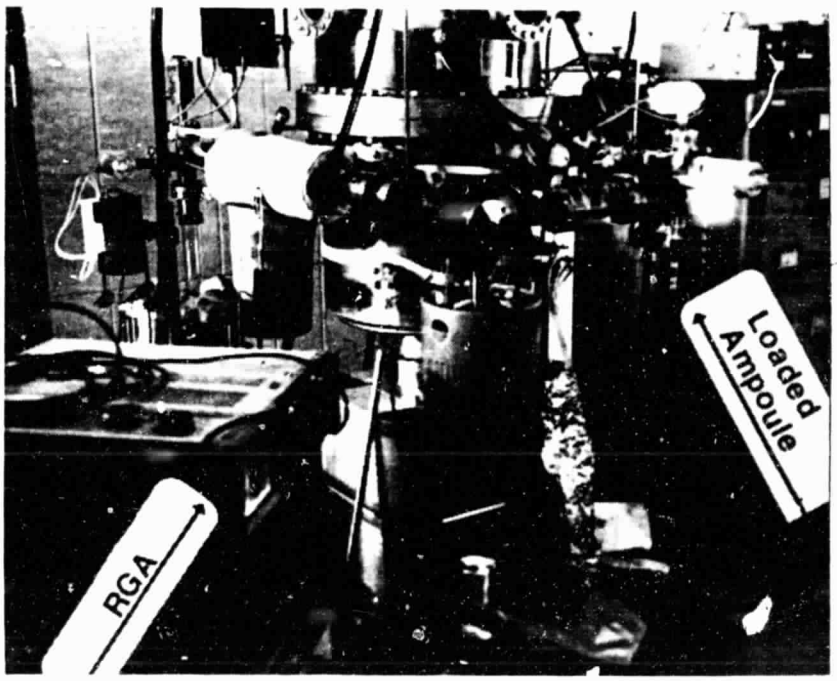

Figure 6: The vacuum system showing a loaded ampoule being pumped down, and a mass spectrometer (RGA).

in the capillary, is lowered into the nearly isothermal region of the hot zone of the furnace as determined by the empty furnace characterization. This region is between 1100° C to 1050° C. With a scale mounted on the furnace supporting beam, the position of the bottom of the ampoule and the capillary TC junction are recorded with respect to the FRP. The whole system is then allowed to sit for at least 12 hours to allow for melting, complete mixing in case of the $Pb_{1-x}Sn_xTe$ and thermal equilibration. The TC in the ampoule capillary tube (henceforth referred to as capillary TC) is connected to a programmable thermometer by Fluke. This Fluke unit is then programmed to take temperature readings at some time interval--usually ranging from 30 seconds to 30 minutes. The ampoule and the capillary TC are lowered towards the cold zone by a drive motor with a predetermined velocity. The capillary TC measures the temperature in the melt at the set time intervals as the system is lowered. Eventually, a solid phase forms and the advancing solid-melt interface in due time reaches the capillary TC junction. As the ampoule is lowered further, the capillary TC starts to measure the temperature in the solid phase at the same set time intervals. The temperature measurement usually continues for about 1 centimeter into the solid phase as determined by the distance scale on the furnace. Then the capillary TC junction is pulled up manually back into the melt as determined by the temperature reading. This is done while the ampoule is still being lowered. So at no time is the ampoule movement stopped. On completion of the

capillary TC pull-up the thermocouple is clamped down and allowed to be lowered again together with the ampoule. This makes it possible to obtain another set of temperature measurements. Each time this experiment is repeated, the thermocouple reads the temperature profile from the melt phase through the melt-solid interface into the solid phase. Typically this process is repeated at least five times for any run. The experiments described above in which the ampoule is in continuous motion are referred to as dynamic runs.

On completion of the above described dynamic runs, the drive motor is turned off. The system is allowed to equilibrate for at least 4 hours. This allows for the dissipation of heat generated due to the latent heat of fusion and/or heat carried due to ampoule movement (Peclet effect). A constant temperature reading over a period of about 30 minutes was taken as indication of complete thermal equilibration. With the ampoule held stationary, the temperature measurement experiment is repeated by running the capillary TC down the capillary tube. The tickler heater setting is lowered and the system is again left to equilibrate before another temperature measurement. All the temperature measurement experiments done with the ampoule at one position are referred to as stationary runs. The important variable in the stationary runs is the tickler heater millivolt power supply setting. A example of $Pb_{1-x}Sn_xTe$ and Ag directionally solidified as described above is shown in figure 7.

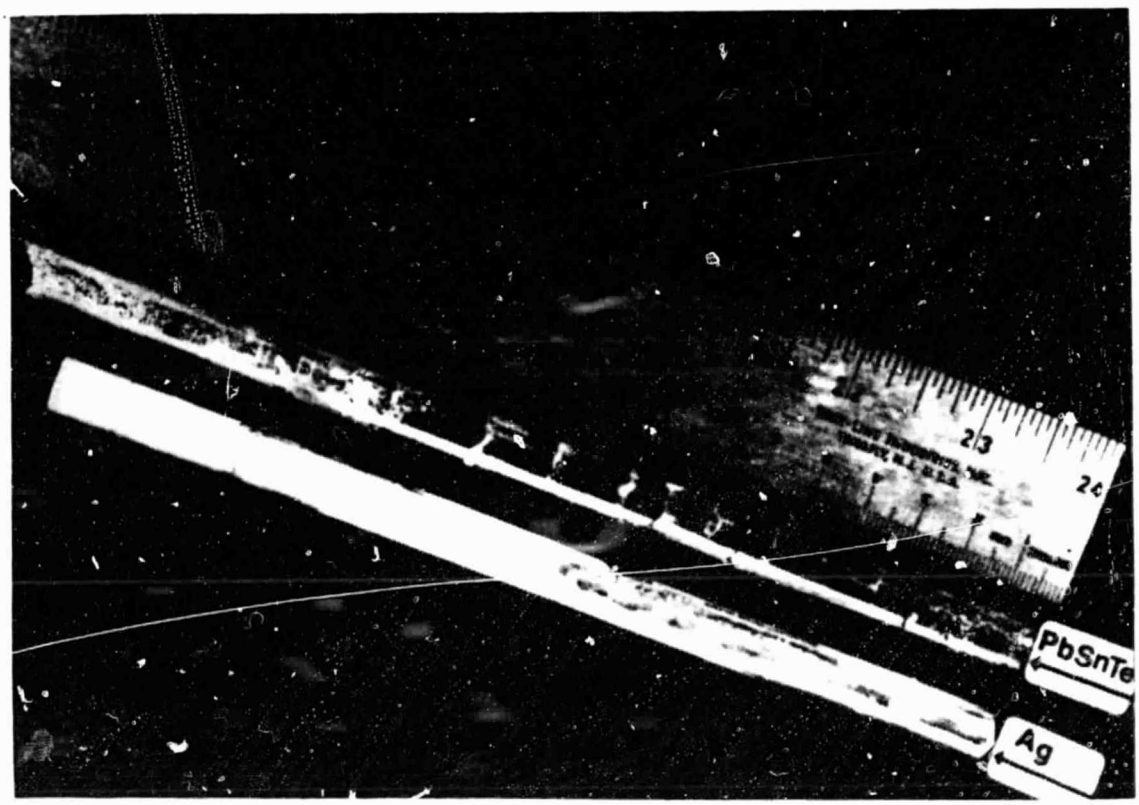

Figure 7: Directionally Solidified Rods of $Pb_{1-x}Sn_xTe$ and Ag.

3. Quantitative X-Ray Analysis

The alloy semiconductor, $Pb_{1-x}Sn_xTe$, grown by the above procedure, was analyzed for compositional variations along the grown crystal rod. This was done using quantitative energy dispersive x-ray analysis. The energy dispersive analysis was done using a JOEL scanning electron microscope (SEM) in conjunction with a TRACOR TN 2000. Binary alloy standards PbTe and SnTe were used to collect reference spectra at recorded beam current, count rate and total count time. The electron beam current used in all the analysis is set using a Faraday cup for beam collection and an ammeter for signal readout. The x-ray spectra from the samples taken from the grown rod of $Pb_{1-x}Sn_xTe$ are collected under the same conditions mentioned above. Other conditions that remained the same in all the analysis are the take-off angle and detector to sample distance. These x-ray spectra are then analyzed for compositions using the "super ML" program of the TRACOR unit. The unit also has a "ZAF" program for the corrections for atomic absorption or enhancement, matrix and fluorescence effects.

D. SAMPLE PREPARATION

1. Compounding $Pb_{1-x}Sn_xTe$

Lead and tin combine with tellerium to form binary compounds PbTe and SnTe. These possess the cubic B1 (rocksalt) crystal structures.[26] The composition range within which PbTe and SnTe and exist, as shown in figure 8a, is so narrow that they can be represented as compounds with a

single line at 50 atomic percent.[30] Also shown in figure 8a is the fact that there is some range to the composition within which the compound can exist. In this investigation the ternary systems $Pb_{1-x}Sn_xTe$ is treated as a pseudobinary system as shown in figure 8b. This is simply the shaded isopleth of figure 8c and is based on the assumption of a 50 atomic precent pure compound PbTe and SnTe. It was therefore very important to weigh out the elements carefully enough to have a one to one ratio between the metals (Pb,Sn) and nonmetal (Te) in order to maintain stoichiometry. Once stoichiometric proportions are maintained it becomes a good approximation to treat the system as an isomorphous pseudobinary. The appropriate stoichiometric weights of the elements are loaded in a quartz ampoule, melted in a vertical furnace and left to react for about 12 hours before the solidification experiment. Sometimes the charge is melted in a rocking-furnace which may enhance proper mixing and reaction.

2. Cleaning and Etching of Samples

Both the germanium and the silver charges used in this work were cleaned by a chemical etc. The cleaning solution for the germanium was as follows:

3:5:3 by volume of HF: HNO_3: Acetic acid plus a drop of Bromine.

The germanium charge was left in this solution for 2 minutes and then rinsed copiously with deionized water. The silver charge was cleaned in a solution of ammonium hydroxide (NH_4OH) and hydrogen peroxide (H_2O_2) in a 1:1 ratio by volume, using the standard laboratory

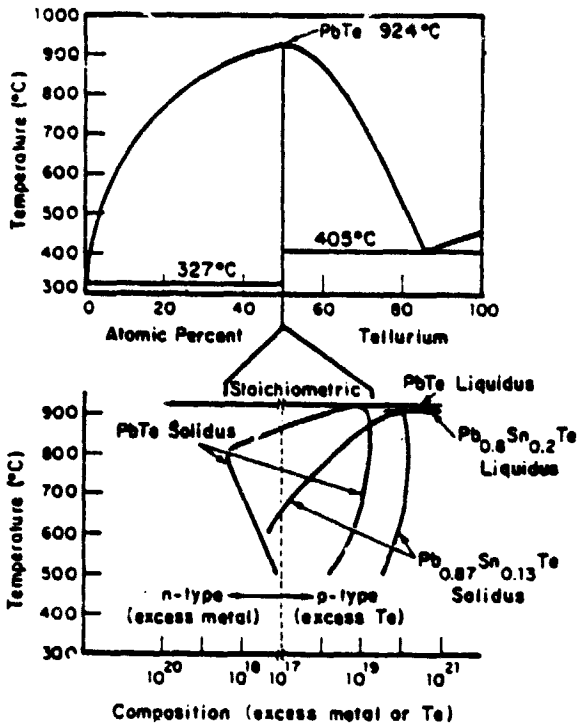

FIGURE 8a The upper part is the temperature-composition binary phase diagram of Pb and Te. The lower part is a greatly expanded portion of the Pb–Te phase diagram in the vicinity of the stoichiometric composition.

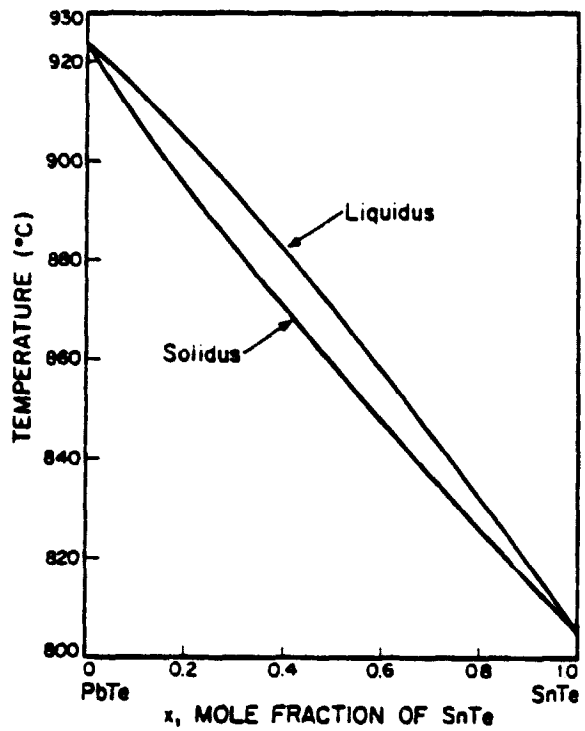

FIGURE 8b The pseudobinary temperature-composition phase diagram for $Pb_{1-x}Sn_xTe$.

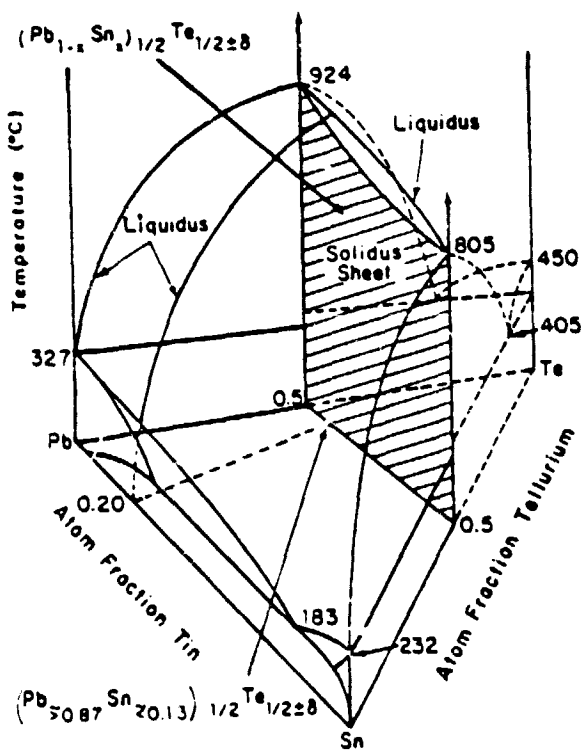

FIGURE 8c Temperature-composition phase diagram for the Pb-Sn-Te ternary system.

Note: These figures are taken from Ref. 30.

stocks. The cleaning takes about 1 minute after which the silver is rinsed in water and then in acetone. Typically, the quartz ampoules in which these materials are grown, are cleaned as follows:

a) Clean with trichloroethlene

b) Rinse with methanol

c) Rinse with deionized water copiously

d) Etch for 10 minutes in a mixture of 60% deionized water, 35% nitric acid and 5% hydrofluoric acid all by volume

e) Rinse with methanol copiously

f) Torch-dry with oxy-acetylene flame

g) 1000° C bake-out under a vacuum system

A grain boundary etch was done on the grown $Pb_{1-x}Sn_xTe$ crystal using the Norr solution.[27] The composition of the etchant is 20 gm of KOH in 45 ml of H_2O; 35 ml of $C_3H_8O_3$; and 20 ml of C_2H_5OH. This electrolytic etch is done with 1 volt potential for 15 secs and then rinsed 3 to 4 times in ethanol.

3. Samples for X-Ray Analysis

In the preparation of samples for the quantitative x-ray analysis, both mechanical and chemical polishing was used. The $Pb_{1-x}Sn_xTe$ rod is carefully sectioned into samples for analysis using a diamond wheel cutter. These samples are polished mechanically starting with a dry 400 grid emery paper and then taken progressively through the finer papers. The final mechanical polish is done on clothe mounted on steel wheels using a

1 micron alumina abrasive first and then a 0.05 micron alumina abrasive. It is possible to get smearing of the material on the polished surface. To eliminate this possible smearing problem, the mechanically polished samples are given a 1 to 2 minute chemical polish. The chemical polish is 95% HBr and 5% Br by volume.[27]

CHAPTER IV

EXPERIMENTAL DATA AND RESULTS

A. Introduction of System Geometry

In order to follow the data and results to be presented in this chapter, it is important to introduce the system geometry and definition of coordinates adopted in this investigation. The system geometry and coordinates are shown in figure 9. A line half way along the insulation zone is taken as the furnace reference point (FRP), from which all furnace axial positions are measured. The symbol Z represents any position along the furnace axis. The symbol i denotes the position of the melt-solid interface with respect to the furnace reference point. Both Z and i have a zero value at the FRP, are positive toward the cold zone and negative toward the hot zone. If the bottom of the ampoule is located at a particular value of Z, say Za, then the length, L, of solidified material is given by

$$L = Za - i \tag{23}$$

and the fraction of the melt column solidified at any given instant, g_s, is to first order $(Za - i)/L_T$ where L_T is the total length of the boule when it is completely liquid.

B. Furnace Characterization

The empty furnace characterization was accomplished by pulling a set of thermocouple junctions through the furnace of a known pull rate

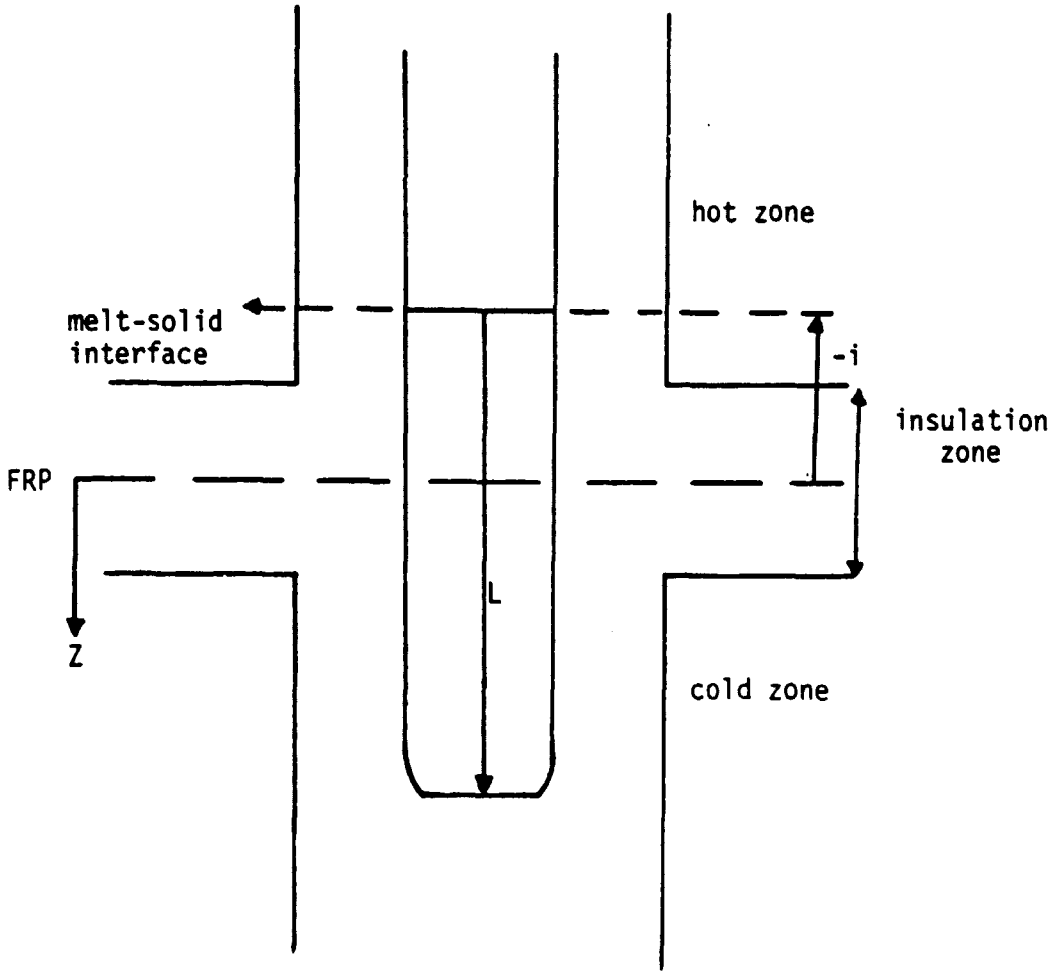

Figure 9: System geometry and definition of coordinates.

while a digital thermometer prints the temperature of the thermocouples at a preprogrammed time interval. The raw data obtained from the digital thermometer is in the form of temperature versus time. These data are fed into a computer which converts time to distance, z, and then generates temperature and/or temperature gradient versus distance plots by use of the programs shown in Appendix I.

The empty furnace temperature profiles are shown in figures 10 and 11 for the case of the tickler heater's power supply cutoff. That means that the tickler heater was in position in the furnace but was not generating any heat. The difference between figures 10 and 11 is that for figure 10, both the hot and cold zone ends were open to air flow, whereas both ends were plugged with quartz wool in the case of figure 11. Notice in figure 10 the large difference between the near-wall and the center-line temperatures, up to 300° C. Figure 11 shows that plugging the furnace ends results in a remarkable reduction in the temperature differences between the near-wall and the center line, less than 100° C. Notice also that the maximum differences in near-wall and center-line temperature occurs at the boundary of the hot zone and the insulation zone. The above mentioned figures also show that the center-line temperature gradient increased from 22° C/cm at 800° C to 75° C/cm at 800° C in the plugged furnace. The furnace design did not permit the temperature measurement near the wall of the isothermal liner to continue through to the cold zone. So only the hot zone profiles are shown in the figures

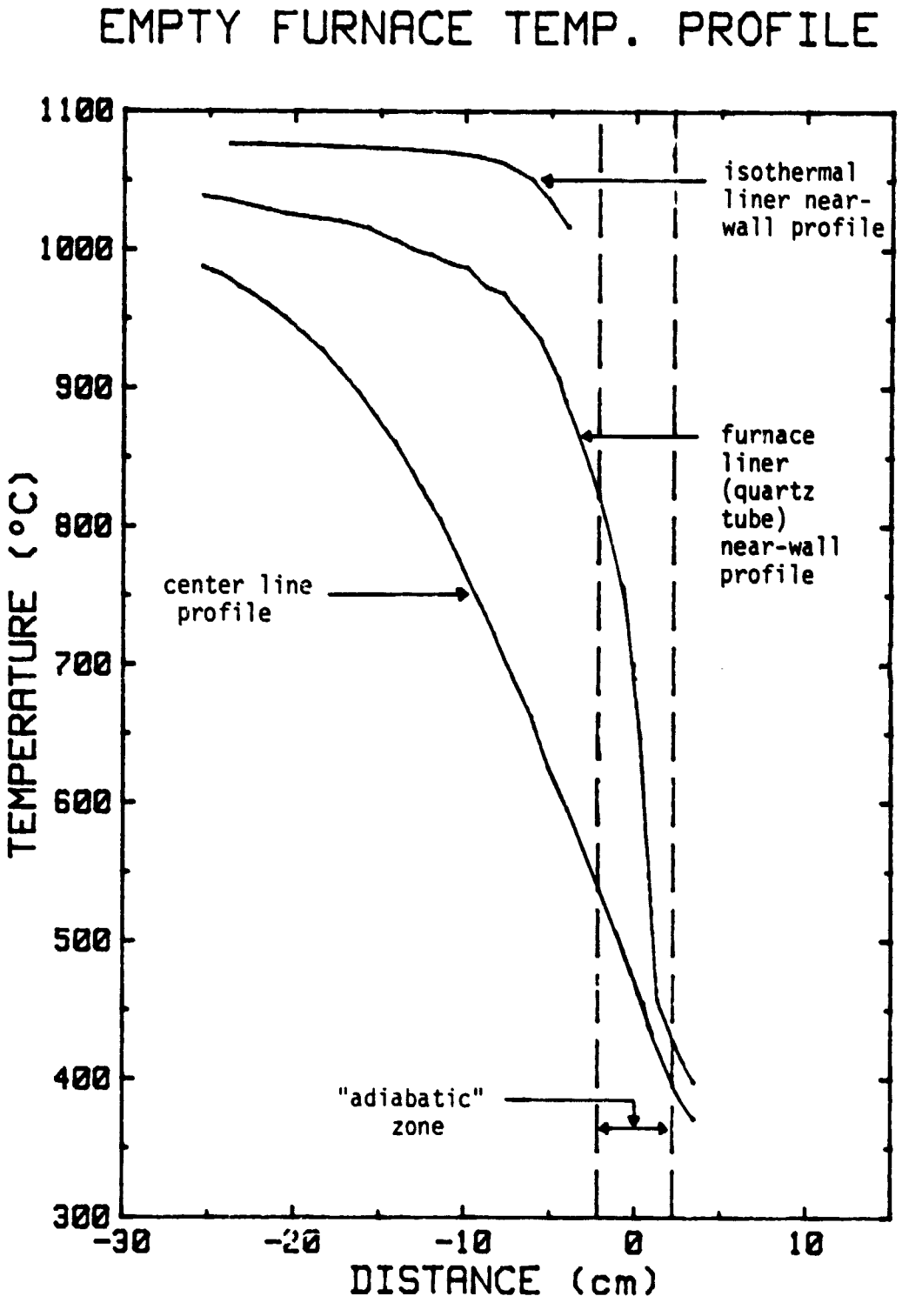

Figure 10: Unplugged temperature profile with a 2.3 cm tickler heater off. A few minutes after plugging the curve changed to that in Fig. 11.

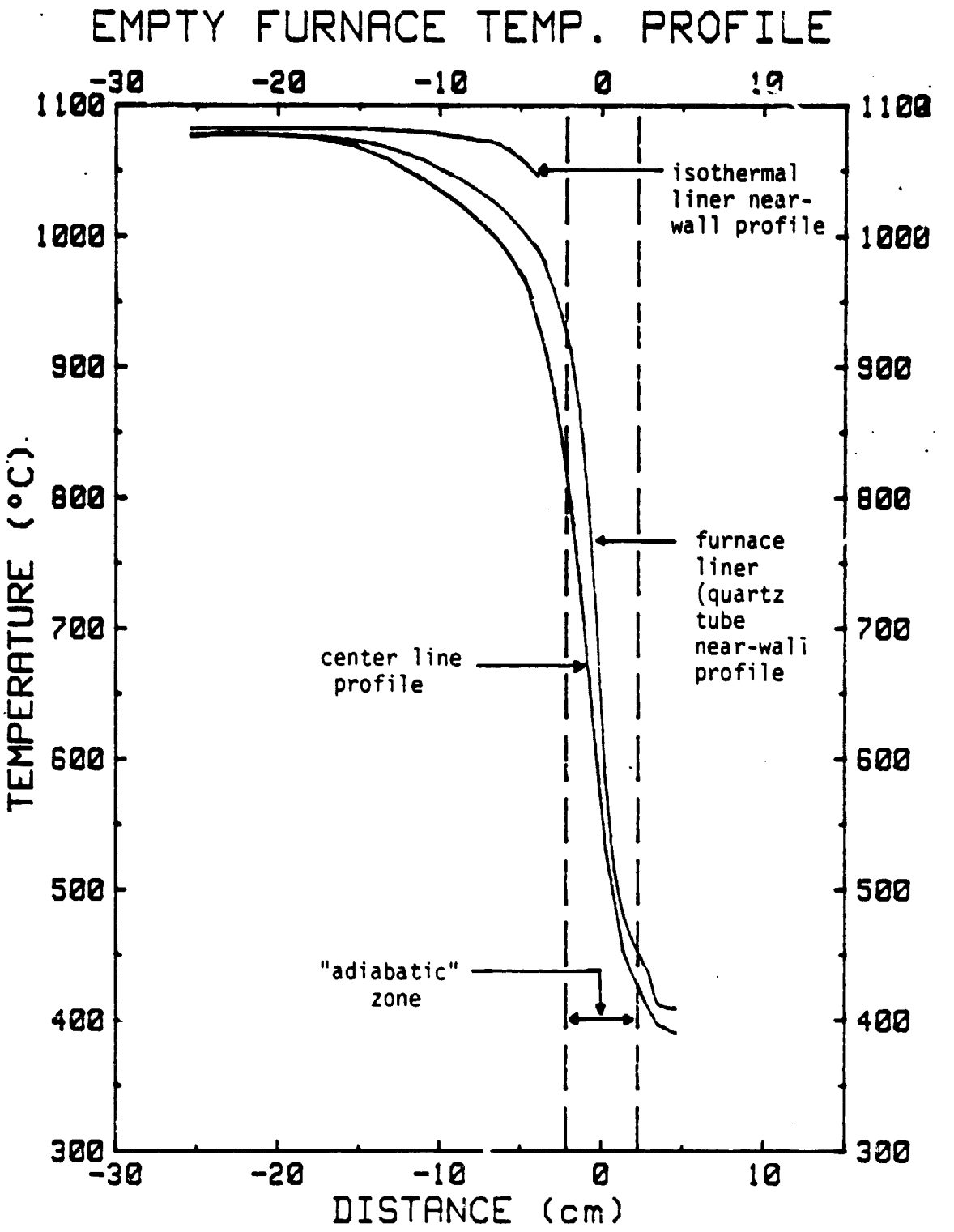

Figure 11: Plugged empty furnace temperature profile with a 2.3 cm tickler heater off plugged with quartz wool.

mentioned above. If a possible furnace misalignment is neglected and a perfectly symmetric furnace geometry is assumed, figure 11 can be used for the construction of isotherms along the furnace as is shown in figure 12. This figure is typical of most of the empty furnace temperature profiles in the sense that the isotherms remained convex (looking from the hot zone) all through the furnace but with a decrease in convexity as it approaches the cold zone. As will be noted later this is not the case for a loaded furnace.

Measurements of the plugged-furnace temperature profile was repeated but this time with a 1.43-cm long tickler heater activated to hold a reference thermocouple at about 1045° C. The resulting temperature profile is shown in figure 13. This figure shows a center-line temperature gradient of 87° C/cm at 800° C which means an increase in temperature gradient over that of figure 11. Figure 14 is a plot of the temperature gradient exhibited by the quartz liner's near-wall profile shown in figure 13. It shows a near-wall temperature gradient of 120° C/cm at 800° C as opposed to the 87° C/cm mentioned above for the center-line.

A much better plugging of the furnace ends was later achieved by using quartz wool first and then covering it with fiberfax (alumina) specially grooved to fit the furnace ends better. This relatively better plugging resulted in the temperature profile of figure 15 which

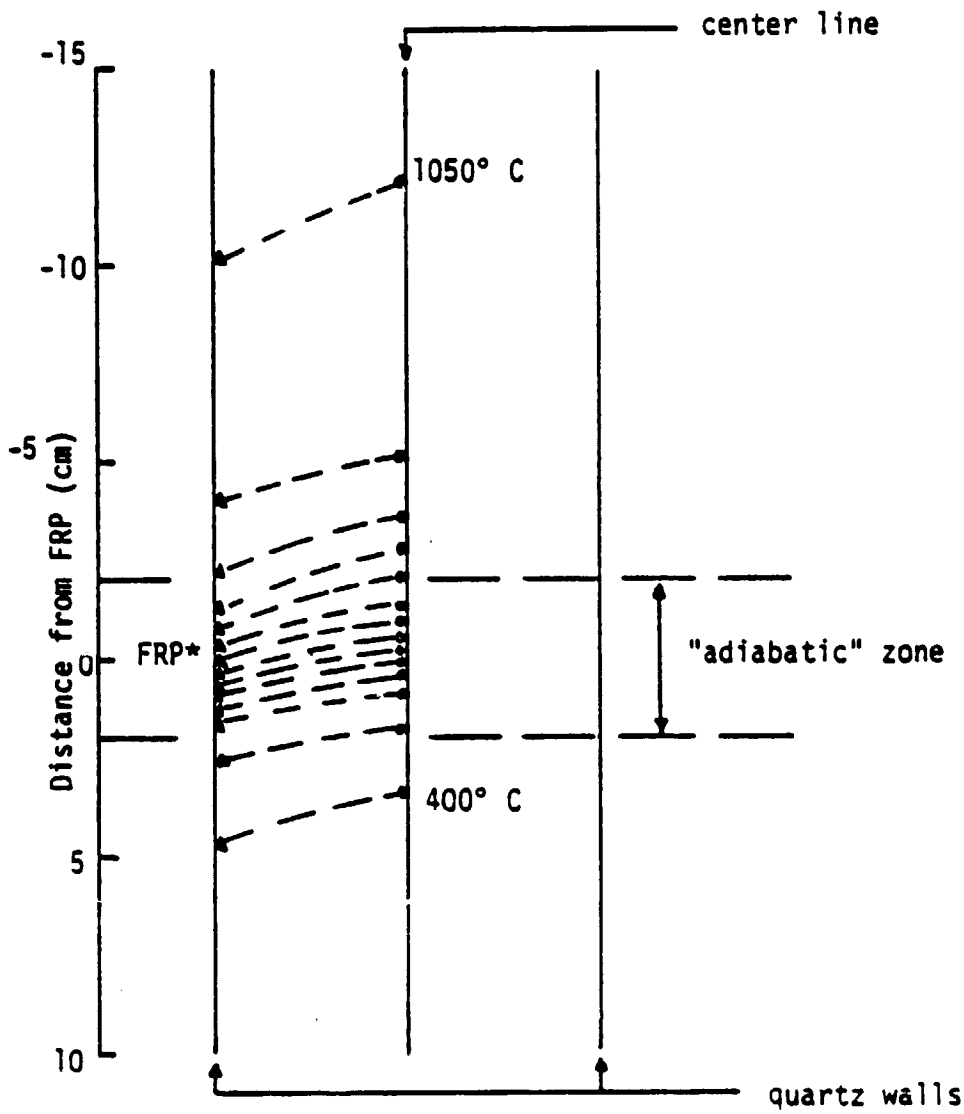

Figure 12: Isotherms of plugged empty furnace with 2.3 cm tickler heater off. See Figure 11.

*Furnace reference point.

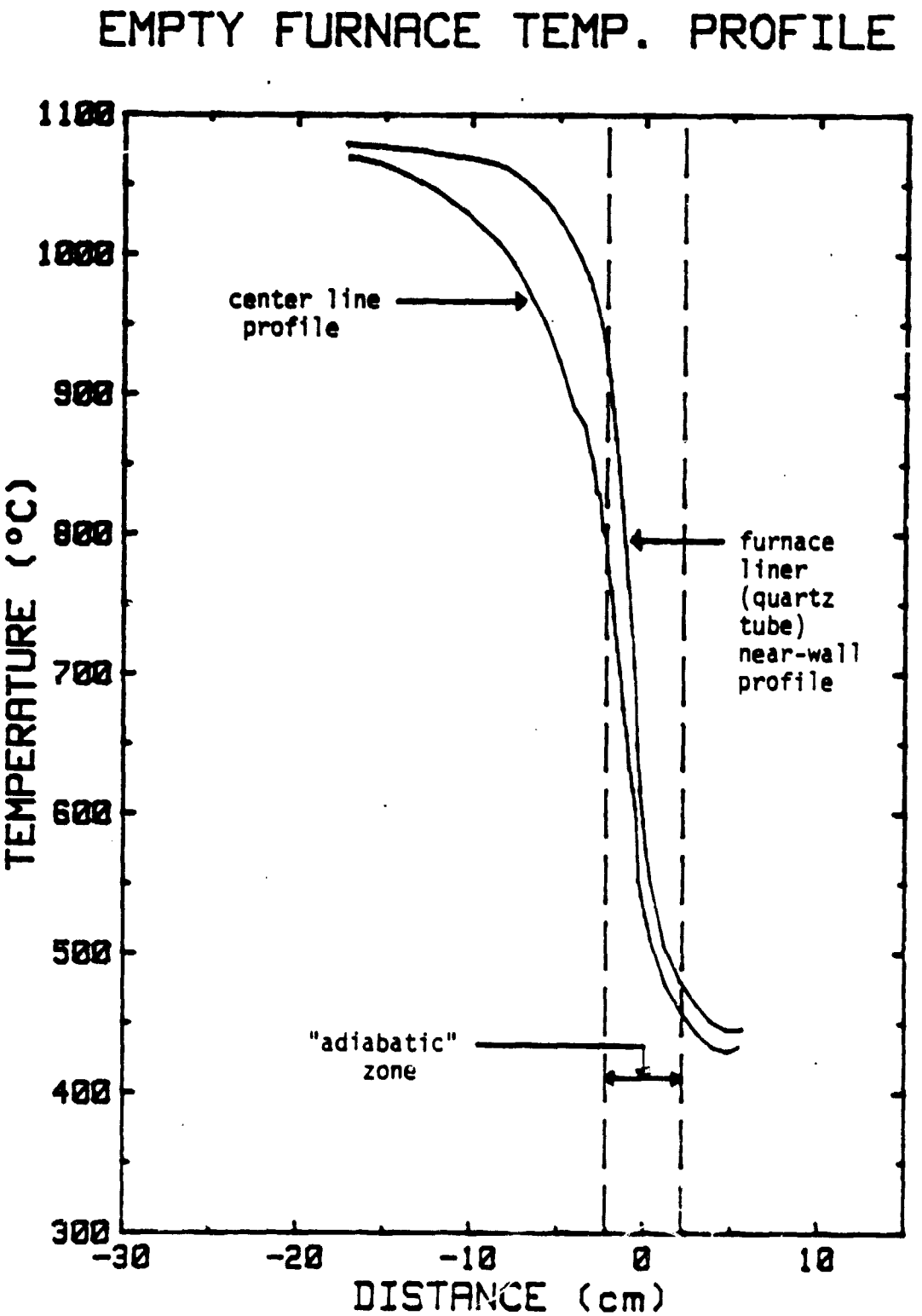

Figure 13: Plugged empty furnace profile with a 1.43 cm tickler heater set at 1045°C.

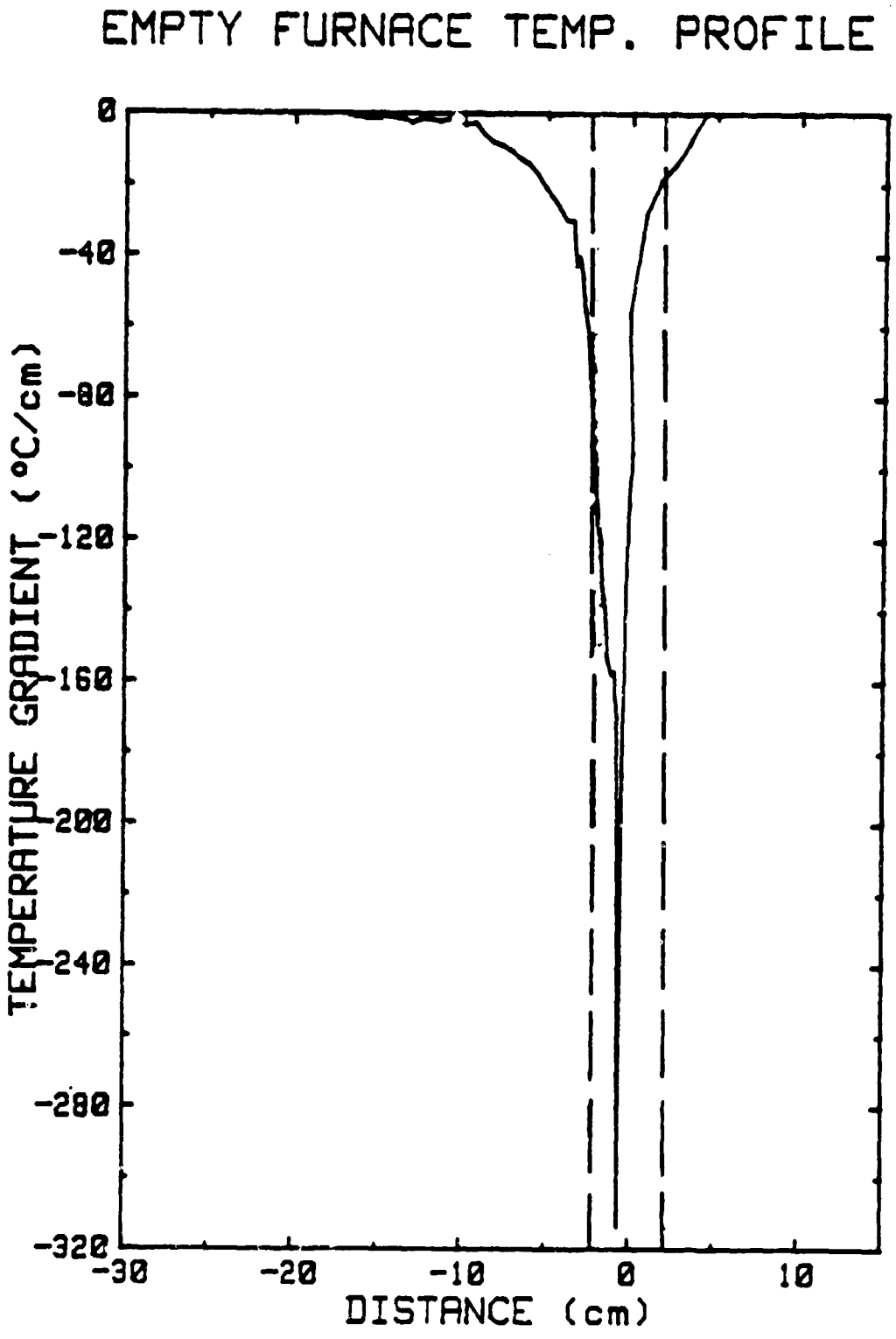

Figure 14: Plugged empty furnace profile. The furnace liner near-wall temperature profile with 1.43 cm tickler heater set at 1045°C.

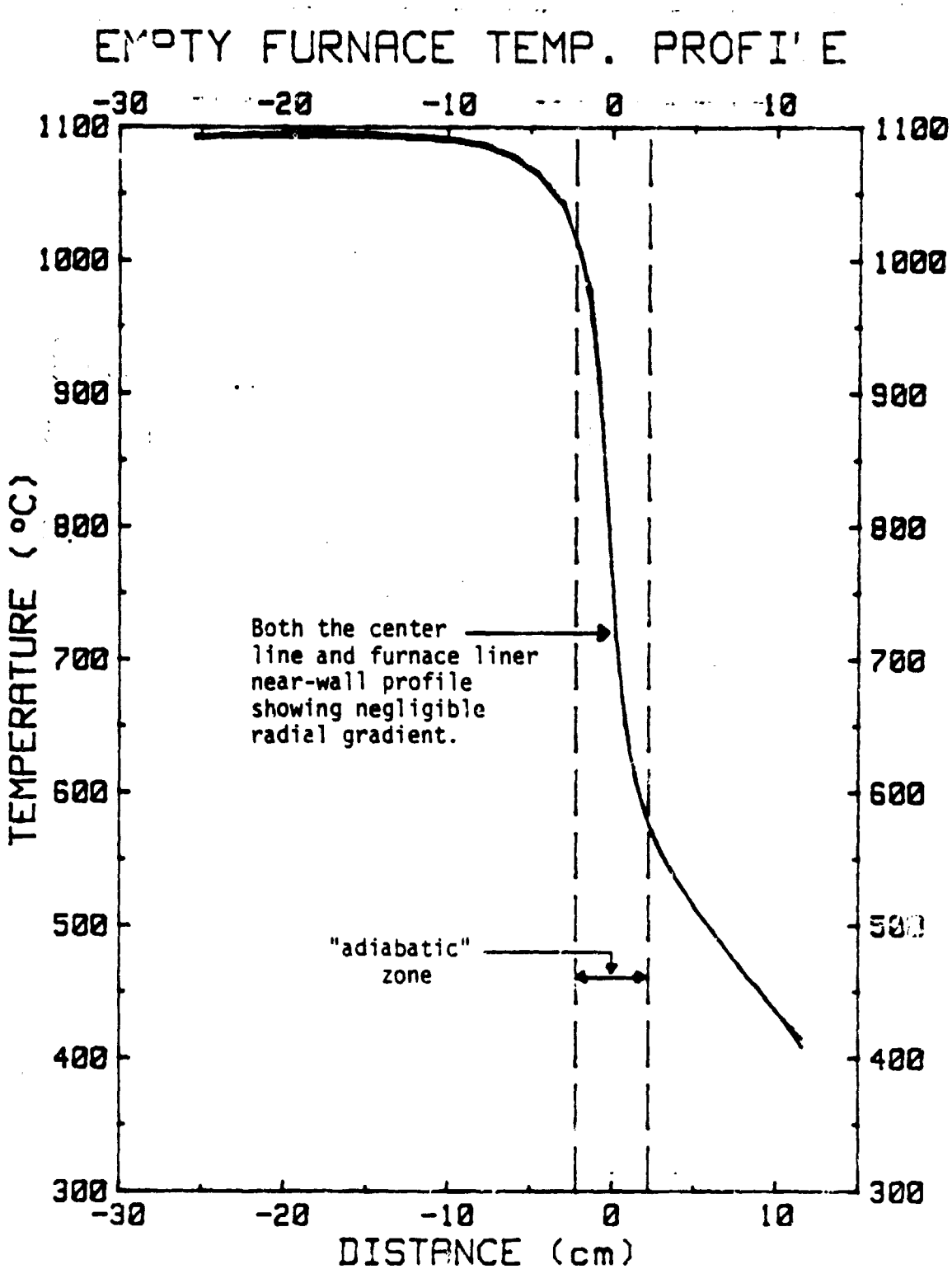

Figure 15: Plugged empty furnace temperature profile with a 2.3 cm tickler heater set at 1045°C.

shows an almost complete elimination of temperature differences between the near-wall and the center-line profiles. This means that any radial temperature gradient is almost removed by effective plugging. Figure 15 also shows that the axial temperature gradient was increased to 130° C/cm due to a combined effect of a longer tickler heater (2.3 cm) and a relatively good plugging.

It is known that the presence of a load in a furnace shifts the isotherms[2] which means a shift also in the temperature profile. The conduction of heat by the load tends to flatten the furnace profile. The motion of the load pushes heat toward the cold zone and therefore shifts the isotherms. The temperature difference between the near-wall and the center-line of a loaded furnace as shown in figures 16 and 17a is very small when compared with that of the unplugged furnace profiles of figure 10. It is noticed that in figures 16 and 17a, for a given position the center-line temperature is lower than the near-wall temperature up to a point. After this point the center-line temperature becomes higher and remains higher than the near-wall temperature for the rest of the furnace. Of course, this is in contrast with the empty furnace profiles in which the center-line temperature remained lower than the near-wall temperature all through the furnace. Employing the same assumptions made for figure 12, the loaded furnace profile can be converted into isotherms as shown in figure 17b. However, in contrast with figure 12, the isotherms change from convex (looking from the hot zone) to concave, going toward the cold zone.

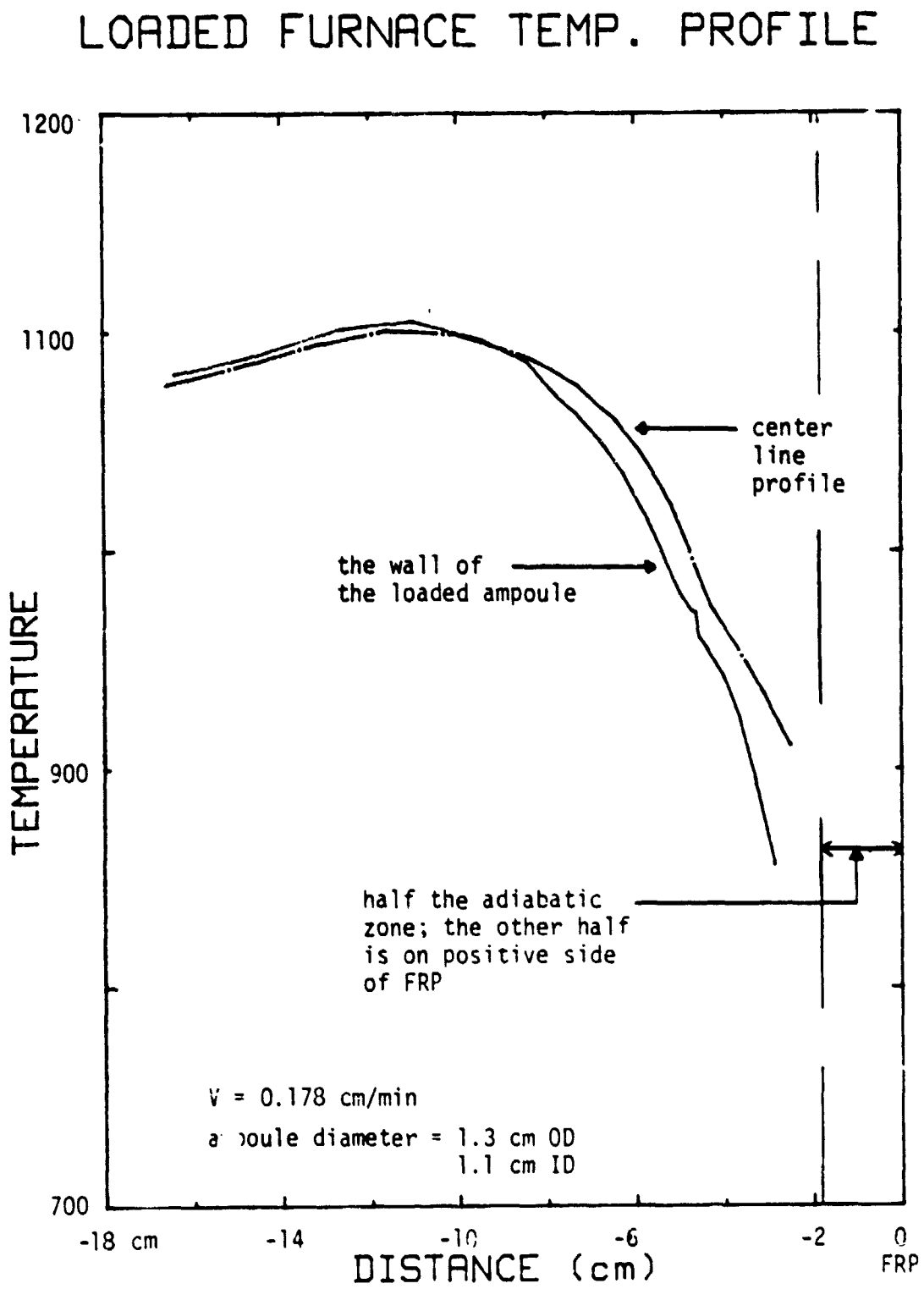

Figure 16: Temperature profile of both the center and the wall of an ampoule loaded with silver.

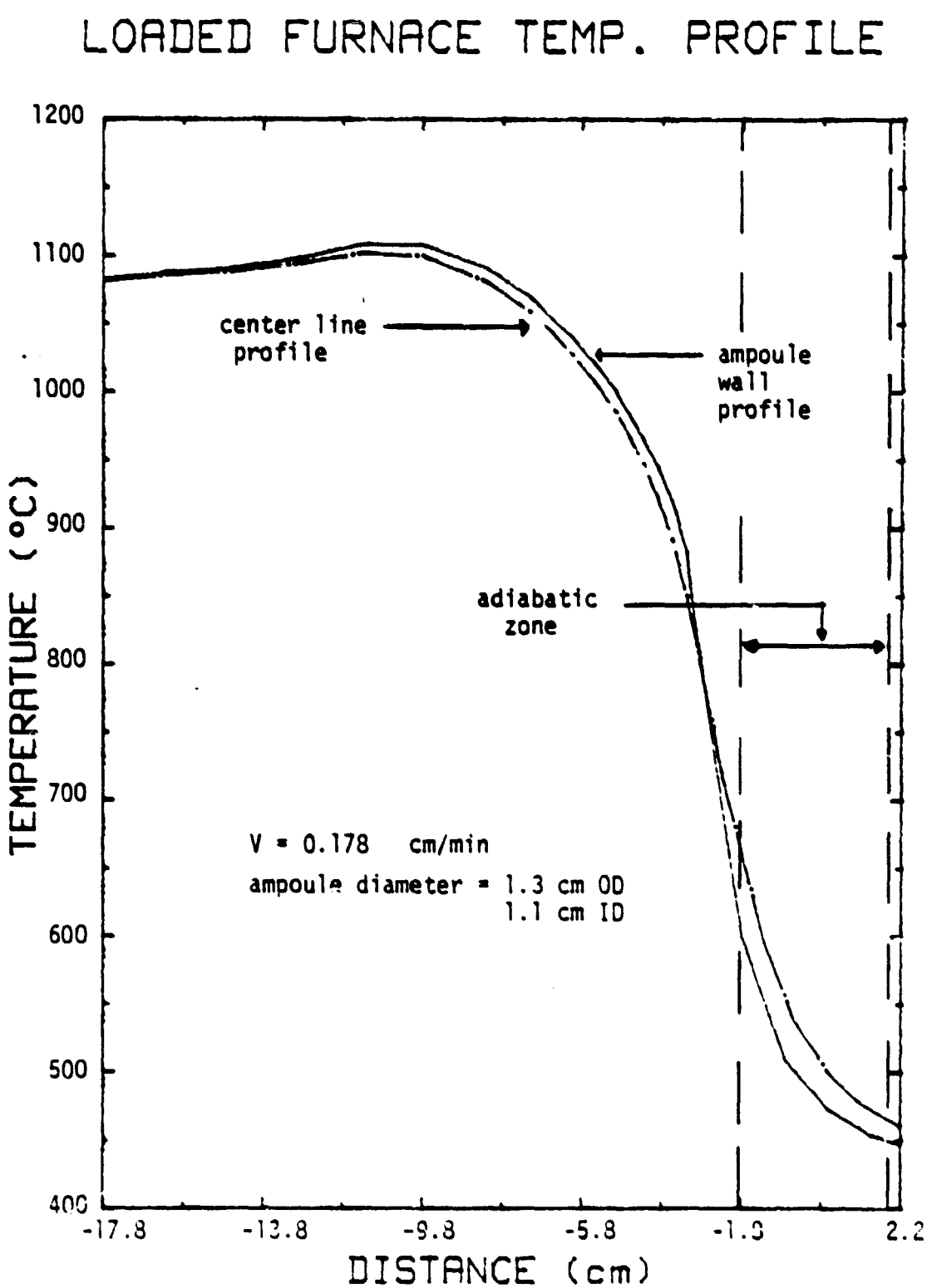

Figure 17a: Temperature profile of both the center and wall of a sealed but unloaded ampoule run through the furnace.

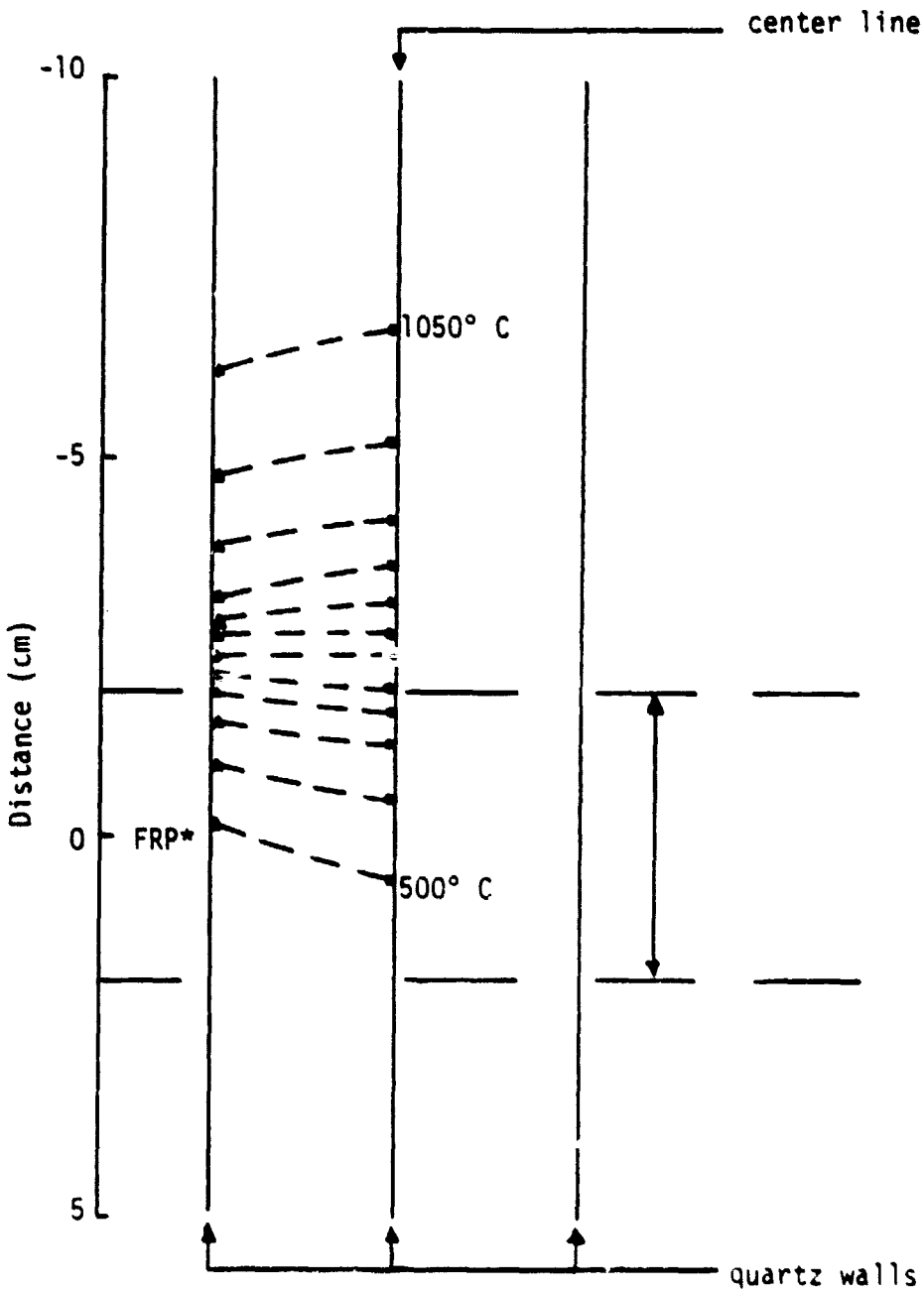

Figure 17b: Isotherms, taken at 50°C intervals. Furnace was loaded with an empty quartz ampoule. See Figure 17a.

*Furnace reference point.

C. Melt-Solid Temperature Measurements

1. Interface position determination

The raw data from the melt-solid experiments described in Chapter III is in the form of temperature versus time. These data are reduced to temperature versus distance and temperature gradient versus distance along the furnace. Curves based on these reduced data show a discontinuity in slope at the melt-solid interface. For each of the dynamic or stationary experiments described in Chapter III, a plot of temperature and/or temperature gradient against position, z, in the furnace is made to determine the interface position. It is obvious then that many curves of this type were in this investigation, however, in order to avoid clutter, only a few examples of each type will be given here and in Appendix II in order to represent the three materials used in this investigation.

The complete set of data points obtained in one of the dynamic experiments is shown in figures 18 and 19. Both figures portray a discontinuity in the regions marked AB. However, the derivative of the temperature with respect to distance is a more sensitive condition as indicated by the more pronounced discontinuity in figure 19. On expanding figure 18 within the region marked AB, the interface position with respect to the furnace, can be determined more clearly as shown in figure 20. This gives the first interface position monitored for a boule of $Pb_{1-x}Sn_xTe$ and for the indicated conditions. The freezing point of the material is determined by noting the temperature at the point of discontinuity. The curves

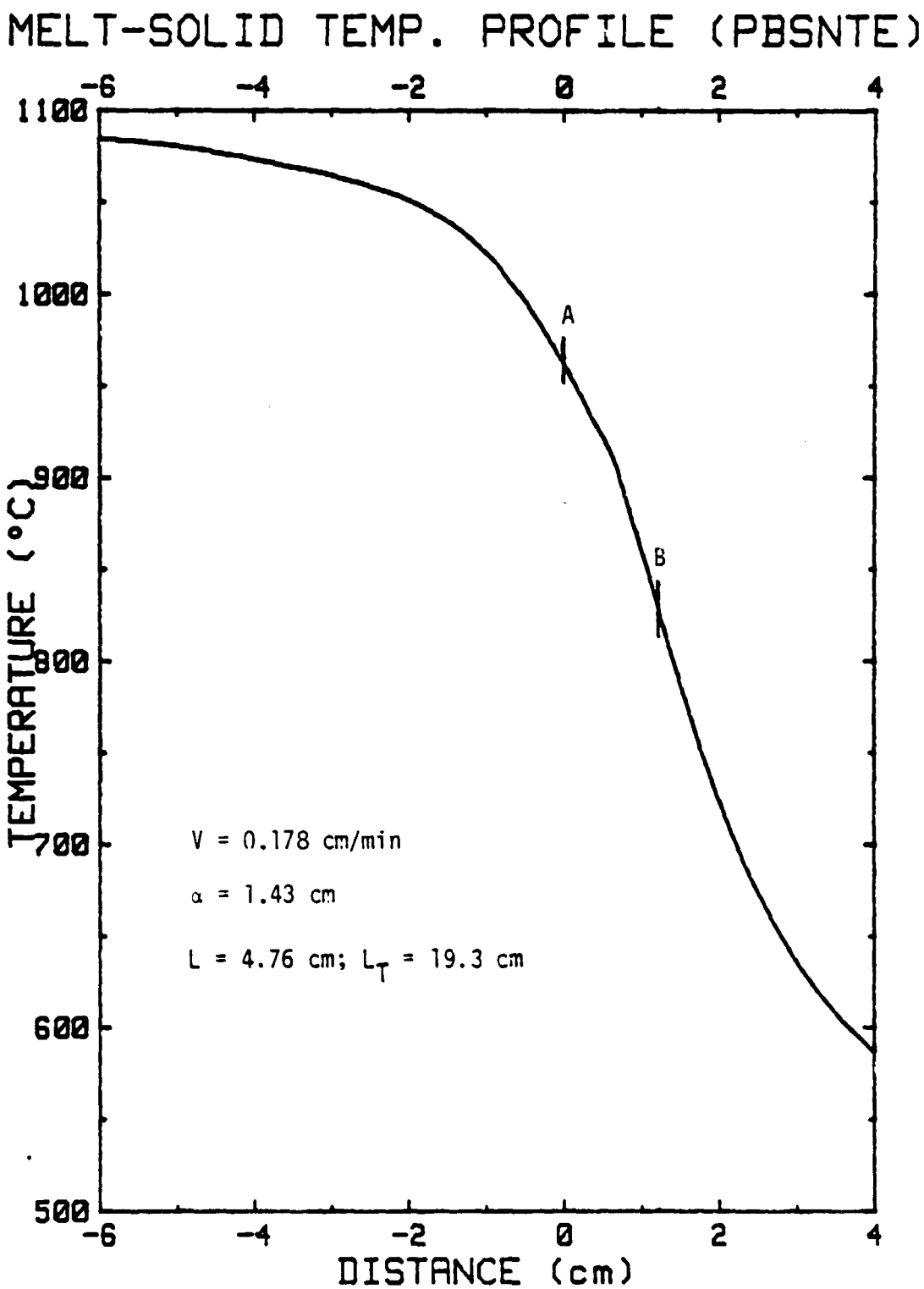

Figure 18: Dynamic temperature measurement from the melt into the solid showing all data points. Expansion within the region marked AB gives the temperature plot of Figure 20.

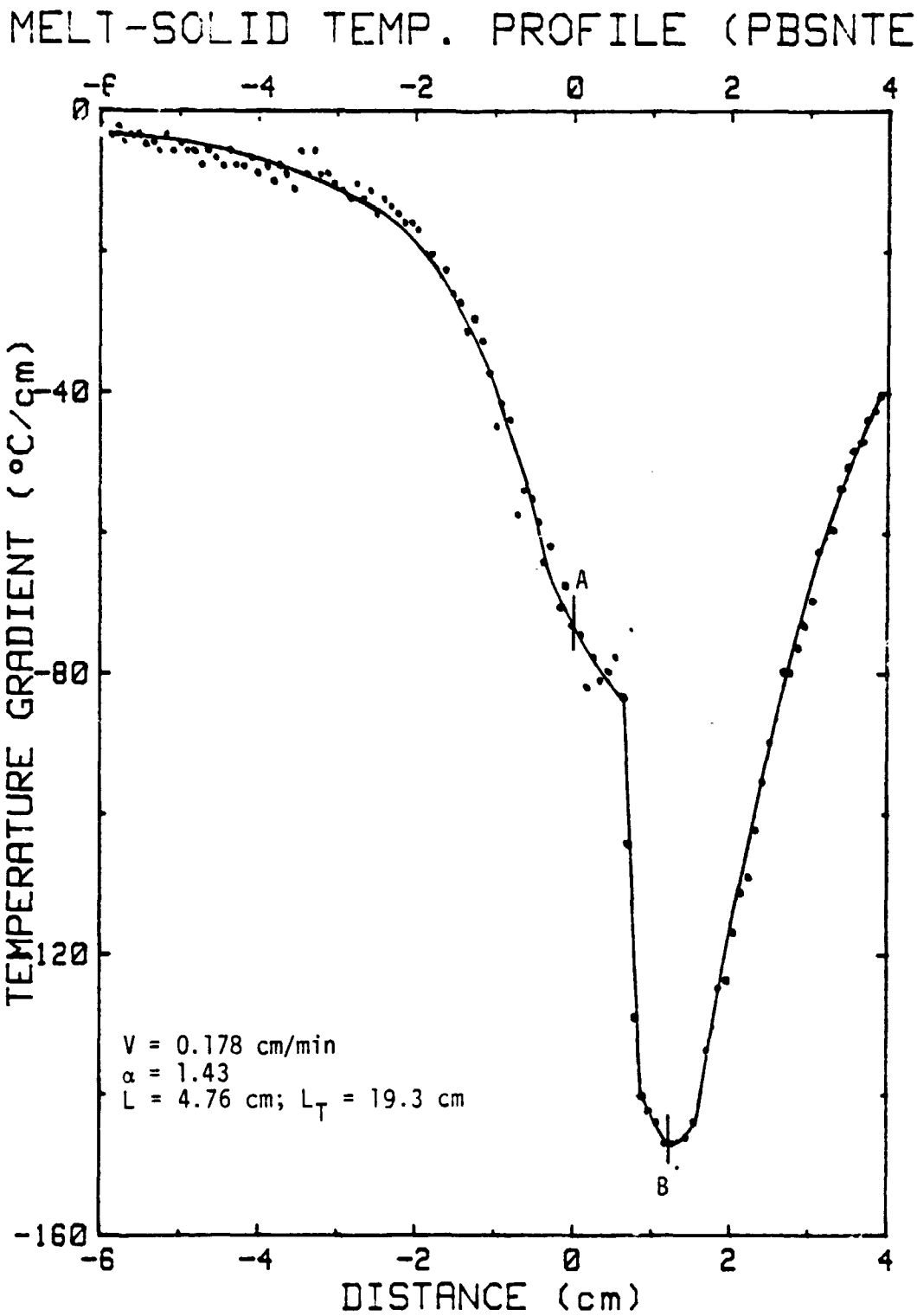

Figure 19: First dynamic interface position determination showing all data points taken at 30 second intervals.

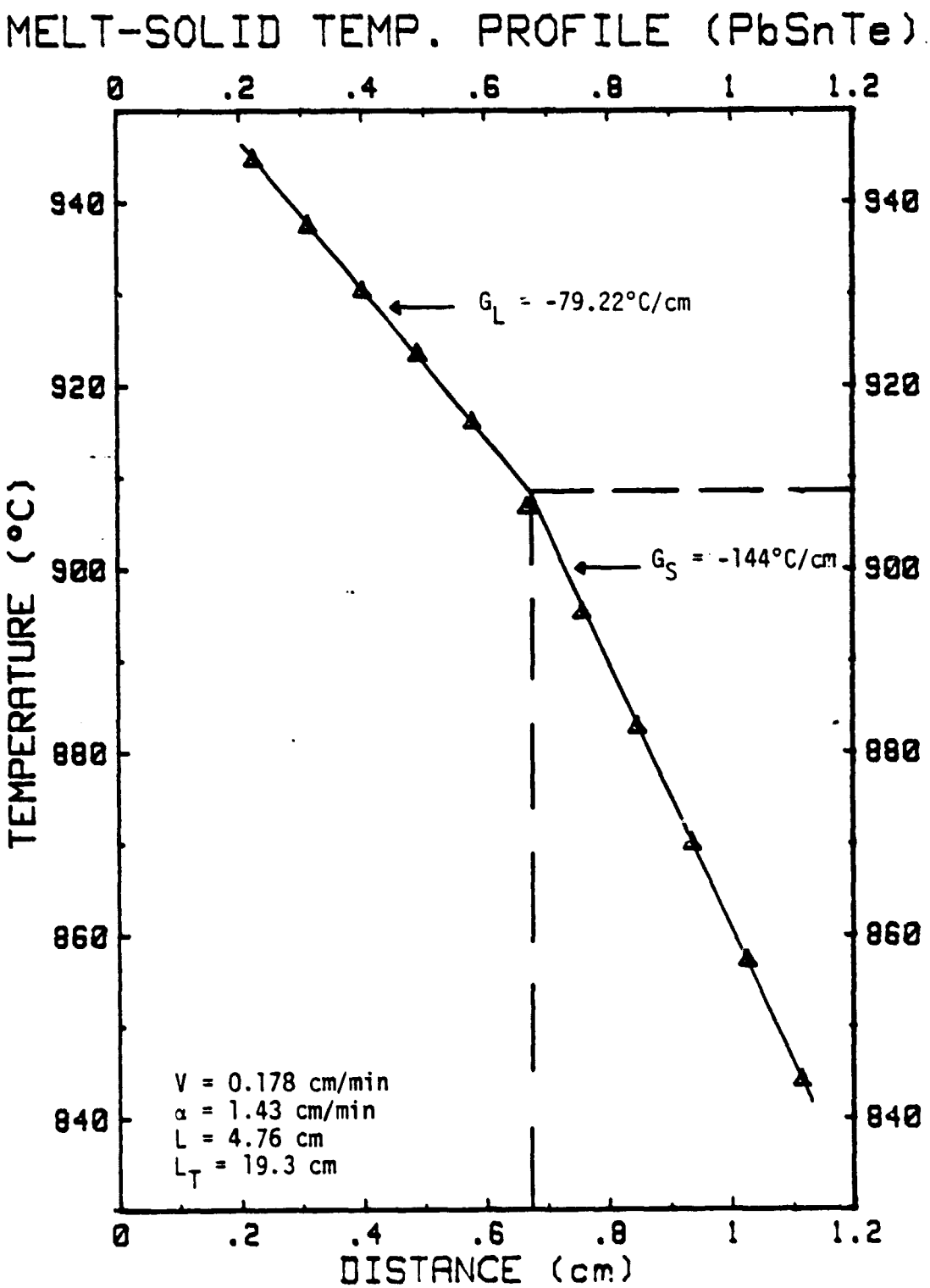

Figure 20: First dynamic interface position and freezing point determination. This is figure 18 expanded within the region marked AB.

for the second through the fifth interface positions monitored in this particular run are in Appendix II. Also shown in this Appendix are examples of the same type of curves generated for the interface position and freezing point determination for silver and germanium.

2. Materials constants

From the experimental technique employed in this investigation, two material constants can be determined. These are the freezing point and the ratio of the melt to solid thermal conductivities at the freezing point. It has been mentioned that a plot of temperature versus distance from the melt into the solid, exhibits a discontinuity in slope at the melt-solid interface and that the temperature corresponding to this point of discontinuity is the freezing temperature of the material. From figures like figure 20, the freezing points of silver and germanium were determined from an average of about 15 runs each to be $960.1 \pm 0.9^{\circ}$ C and $937.3 \pm 1.5^{\circ}$ C respectively. The uncertainty values are one standard deviation from the mean. These values are in good agreement with the literature values[34] of 961.9° C and 937.4° C for the respective freezing points. As would be expected for an alloy material which changes composition during freezing, the freezing point of $Pb_{1-x}Sn_xTe$ varied as freezing progressed. The measured freezing points and the corresponding compositions will be indicated later in this section.

Theoretically,[2,3] it is known that the thermal conductivities in the solid and melt phases influence the temperature profile during a

directional solidification (DS) experiment. Table 1 shows the measured temperature gradients at 900°C for the three materials, lead-tin-telluride, germanium and silver. Note that for the same furnace temperature settings, the temperature gradient is reduced as the thermal conductivity of the load material increases. The thermal conductivities of the solid phase, K_S, Of many materials are easy to find in the literature whereas those of the melt phases, K_L, especially of high melt-point materials, are very diffucult to find. However, proper heat balance analysis across the interface in a DS experiment can in theory yield the thermal conductivity ratio of the melt and solid phases as the freezing point. Assuming a planar interface and ignoring both radiative and convective heat transfer, the equation for the heat balance is

$$K_L G_L + \rho RH = K_S G_S \tag{24a}$$

where ρ = density

R = melt-solid interface velocity

H = latent heat of freezing

$G_{L,S}$ = temperature gradient in the liquid and solid, respectively

Furthermore, if a stationary experiment is considered, that is $R = 0$, then the equation reduces to

$$K_L G_L = K_S G_S \text{ or } \frac{G_S}{G_L} = \frac{K_L}{K_S} \tag{24b}$$

Since G_S/G_L can be determined from figure 20, K_L/K_S can also be determined. Thermal conductivities of both the solid and liquid phases of silver[32] and germanium[33] are recorded in the literature. So part of

Furnace Condition		Temperature Gradient at 900°C	Tickler Heater Setting
Empty		127°C	1045°C
Loaded With	PbSnTe	118°C/cm	1045°C
	Ge	99°C/cm	1045°C
	Ag	35°C/cm	1045°C

Table 1: Effect of a load material on the furnace temperature gradient at 900°C. A 2.3 cm tickler heater was used in all the cases.

the reason for performing the DS experiments with silver and germanium was to check the accuracy of the experimental technique in determining the K_L/K_s or K_s/K_L ratios. Table 2 shows the measured K_L/K_s or K_s/K_L ratios as compared with selected literature values. The comparison indicates that the measured value is too low for both the germanium and the silver. The error in the thermal conductivity ratios will be discussed semiquantitatively in the next chapter. In any case, the K_L/K_s ratio measured for $Pb_{1-x}Sn_xTe$ is $1.75 \pm .04$.

3. Tickler heater effects

A tickler heater (booster heater) was introduced into the furnace in order to increase the melt temperature gradient which is known to affect interface stability.[4,11] The extra heat generated near the melt-solid interface by the tickler heat can also influence the position of the interface with respect to the furnace. These possible effects were studied by carrying out the melt-solid temperature measurement experiments with each of three tickler heaters of different lengths.

The interface positions determined from any of these experiments were used to plot a graph of interface positions versus the translated length as shown in figure 21.

The figure shows that for the two materials Ge and $Pb_{1-x}Sn_xTe$, the melt-solid interface position did not significantly move with respect to the fixed furnace reference point within the solidification period that was monitored. For the same material and the same tickler

Material	Measured K_L/K_S Ratios (PbSnTe,Gr) K_S/K_L Ratio (Ag)	Thermal Conductivity Ratios Taken From Literature	Percentage by Which Measured Values Differ From Literature Values
Ag	1.54 ± .04	(2.03)[32]	32 ± 2.6%
Ge	2.09 ± .10	(2.80)[33]	34 ± 0.8%
PbSnTe	1.75 ± .04	unknown	

Table 2: Comparison of measured thermal conductivity ratios with selected literature values.

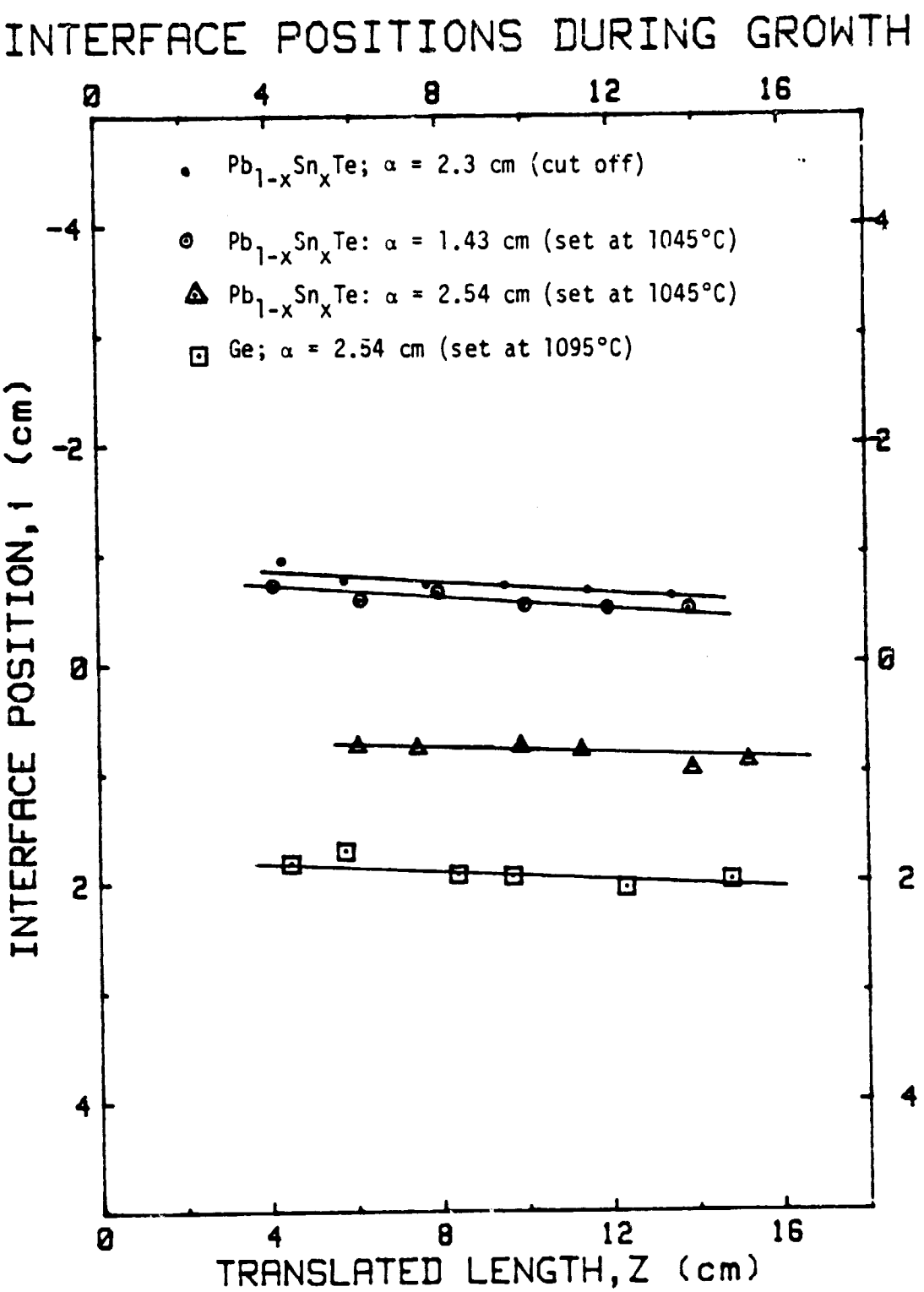

Figure 21: Crystals grown with the same ampoule translation rate but with different tickler heater lengths and settings.

heater power supply setting the interface position was depressed toward the cold zone as the tickler heater length increased from 1.43 cm to 2.54 cm. The interface position is least depressed when the tickler heater is cut off. The germanium melt-solid interface is more depressed than that of $Pb_{1-x}Sn_xTe$. Both were solidified using a 2.54 cm tickler heater but different power supply settings. It was set at 1095° C for germanium and 1045° C for $Pb_{1-x}Sn_xTe$. All the interface positions shown in the figure were determined from dynamic runs, and the tickler heater setting was constant all through each run. In any case, it can be seen from the above results that the shift in interface position can be due to the tickler heater length. The tickler heater setting can also shift the interface position. A direct demonstration of interface position shifts due to tickler heater temperature setting is shown in figure 22. These interface positions are determined from stationary runs. The only cause of solidification in this case is the change in the tickler heater power supply setting. This shows that for a given material the interface position shifts towards the hot zone as the tickler heater setting temperature is lowered. Within the experimental error, the interface position varied almost linearly with the tickler heater temperature setting.

Temperature gradient in the melt immediately ahead of the interface is an important factor in crystal growth from the melt in general and especially in the Bridgman-Stockbarger technique. This is particularly

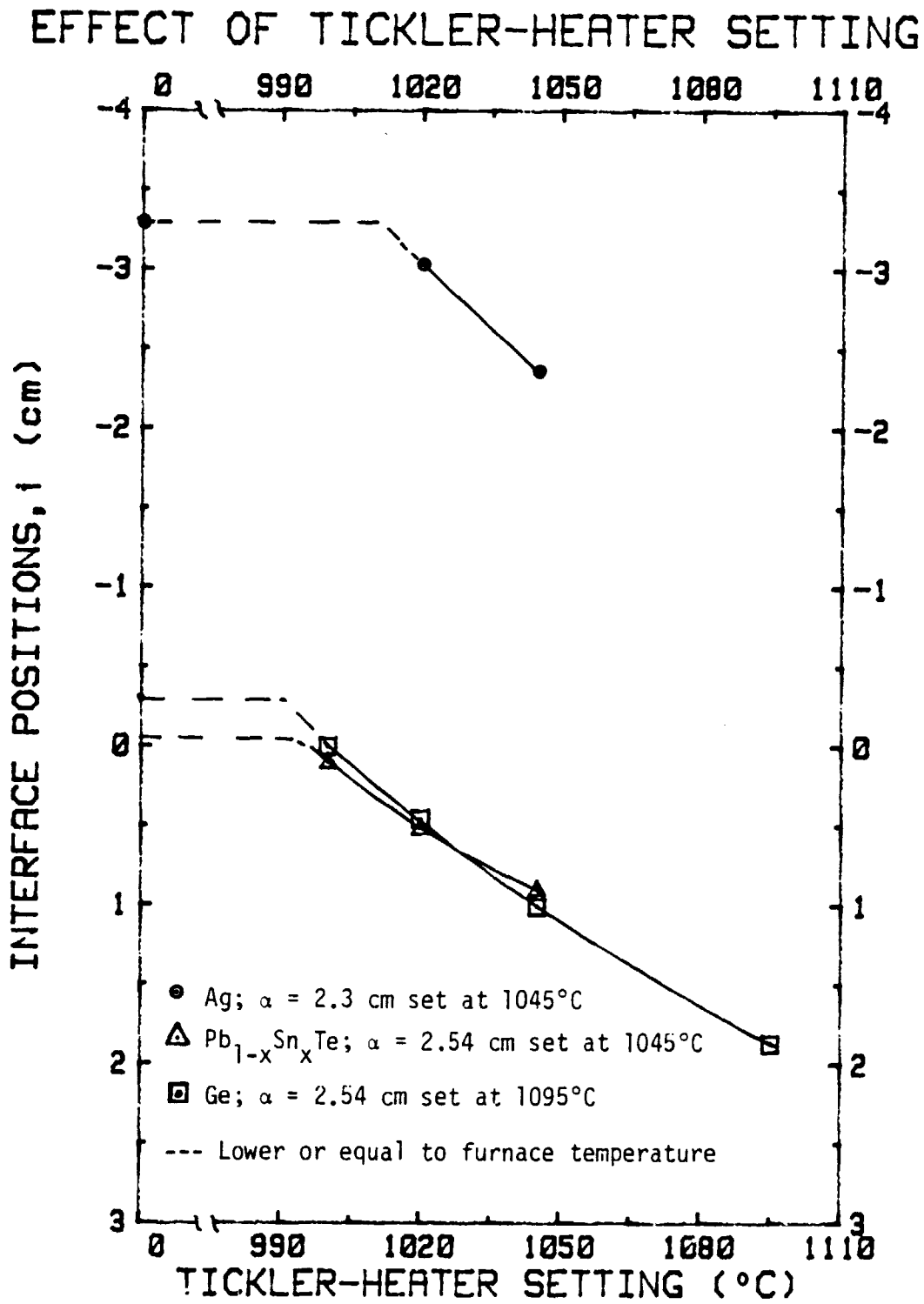

Figure 22: Effect of tickler setting on interface position. This is a stationary run so all interface movement was due to a reduced tickler heater setting.

true in the growth of alloys which require the avoidance of both thermal and constitutional supercooling. Table 3 shows an increase in melt temperature gradient with an increase in tickler heater length for the furnace configuration employed in this investigation. For the same tickler heater length and temperature setting the temperature gradient in the melt is lowest for silver which has a relatively high K_L value.

In conclusion, for the furnace constructed and used in this investigation, the temperature gradient in the melt immediately ahead of the interface can be adjusted by a change in the length and/or temperature setting of the tickler heater. These changes also result in shifts in the interface position.

4. Ampoule translation rate effect

Two translation rates, .046 cm/min and .178 cm/min were used in the DS experiments. The effect of the ampoule translation rate V on the melt-solid interface position of a material, viz $Pb_{1-x}Sn_xTe$, is shown in figure 23. The interface shifted toward the cold zone with an increase in translation rate. This effect is expected to be true also for both silver and germanium. However, the degree of the shift may be different for different materials. This will be explained in the next chapter.

A very important result shown also by figure 23 is the fact that as more material is solidified (higher L value), the melt-solid interface position, i, is constant for the semiconductor, $Pb_{1-x}Sn_xTe$. This is also

Material	Tickler Heater Length* and Power Supply Settings	Temperature Gradient in the Melt Ahead of the Interface
PbSnTe	2.3 cm cut off	72° C/cm
	1.43 cm 1045°C	80° C/cm
	2.54 cm 1045°C	87° C/cm
Ge	2.3 cm 1045°C	50° C/cm
	2.54 cm 1095°C	63° C/cm
Ag	2.3 cm 1045°C	35° C/cm
	2.54 cm 1045°C	40° C/cm

*6 heater wire windings per cm.

Table 3: Temperature gradient in the melt immediately ahead of the interface showing an increase with tickler heater length.

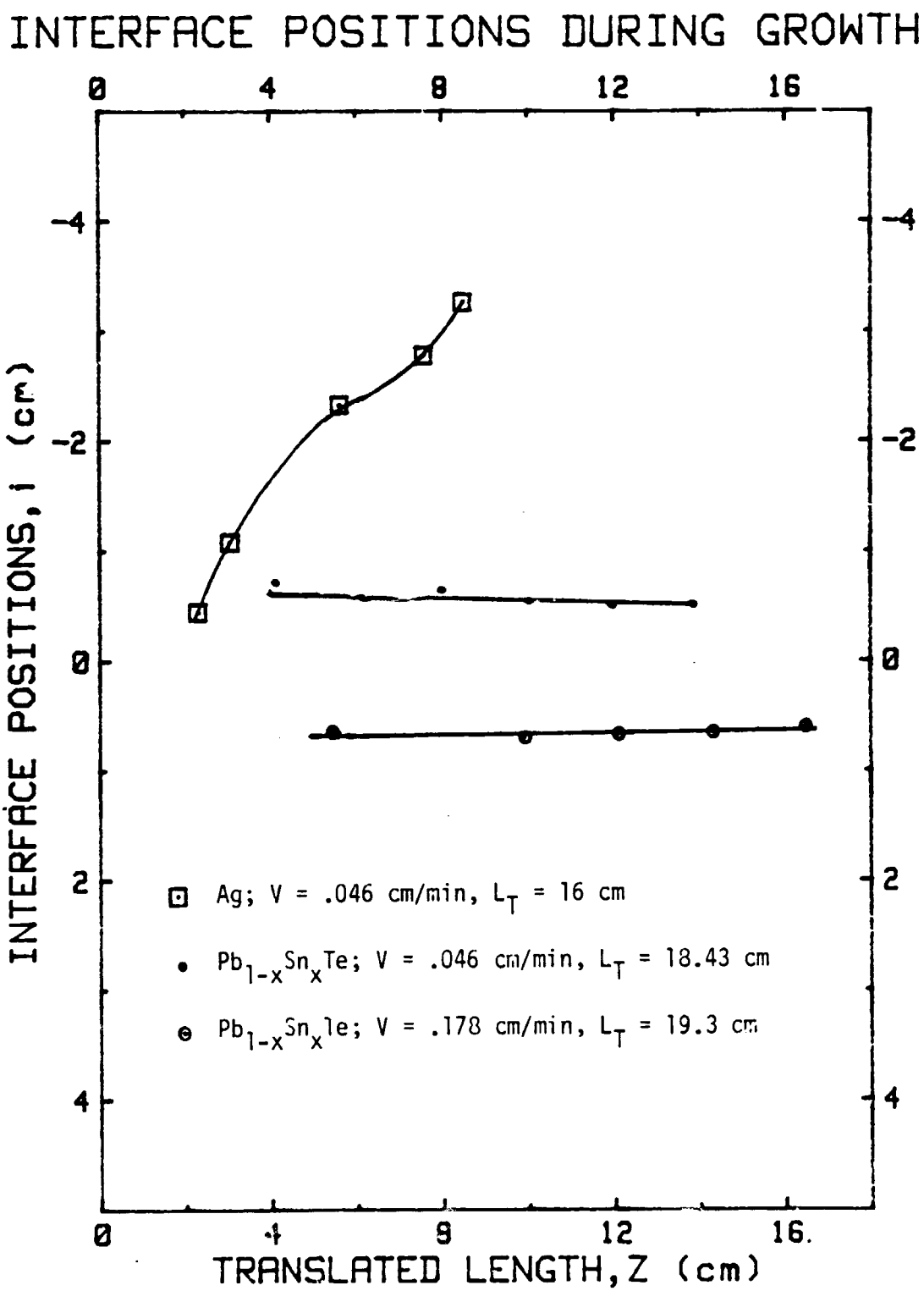

Figure 23: Rods solidified at two different ampoule translation rates but with a 1.43 cm tickler heater set at 1045°C.

true for Ge as was already mentioned in connection with figure 21. However, for a metal, Ag, there is an appreciable variation in the interface position as freezing progresses. In fact, it moves toward the hot zone (higher negative i values) and apparently in a nonlinear manner. This is interpreted to mean a shift in the isotherm that corresponds to the freezing temperature which in turn means a continuous change in the temperature profile that the material sees. The different temperature profiles seen by four interfaces monitored in one DS experiment with Ag are shown in figure 24. The profile shifts toward the hot zone as freezing progresses and hence a decrease in the temperature gradient in the melt at the freezing temperature also occurs.

5. Growth rate variations

The metal, silver, showed a continuous variation in the instantaneous growth rate as freezing progressed. The semiconductors, $Pb_{1-x}Sn_xTe$ and Ge showed a constant growth rate within the growth period monitored. These results are deduced from figure 25, since the frozen length, L, is directly dependent on the translated length Z. The crystal growth rate $R = dL/dt$ where dL/dt is given by differentiating equation (23) with respect to time, t

$$R = \frac{dZ_a}{dt} - \frac{di}{dZ_a}\frac{dZ_a}{dt} = V\left(1 - \frac{di}{dZ}\right) \qquad (25)$$

where the ampoule translation rate $V = dZ_a/dt$ and $dZ_a = dZ$.

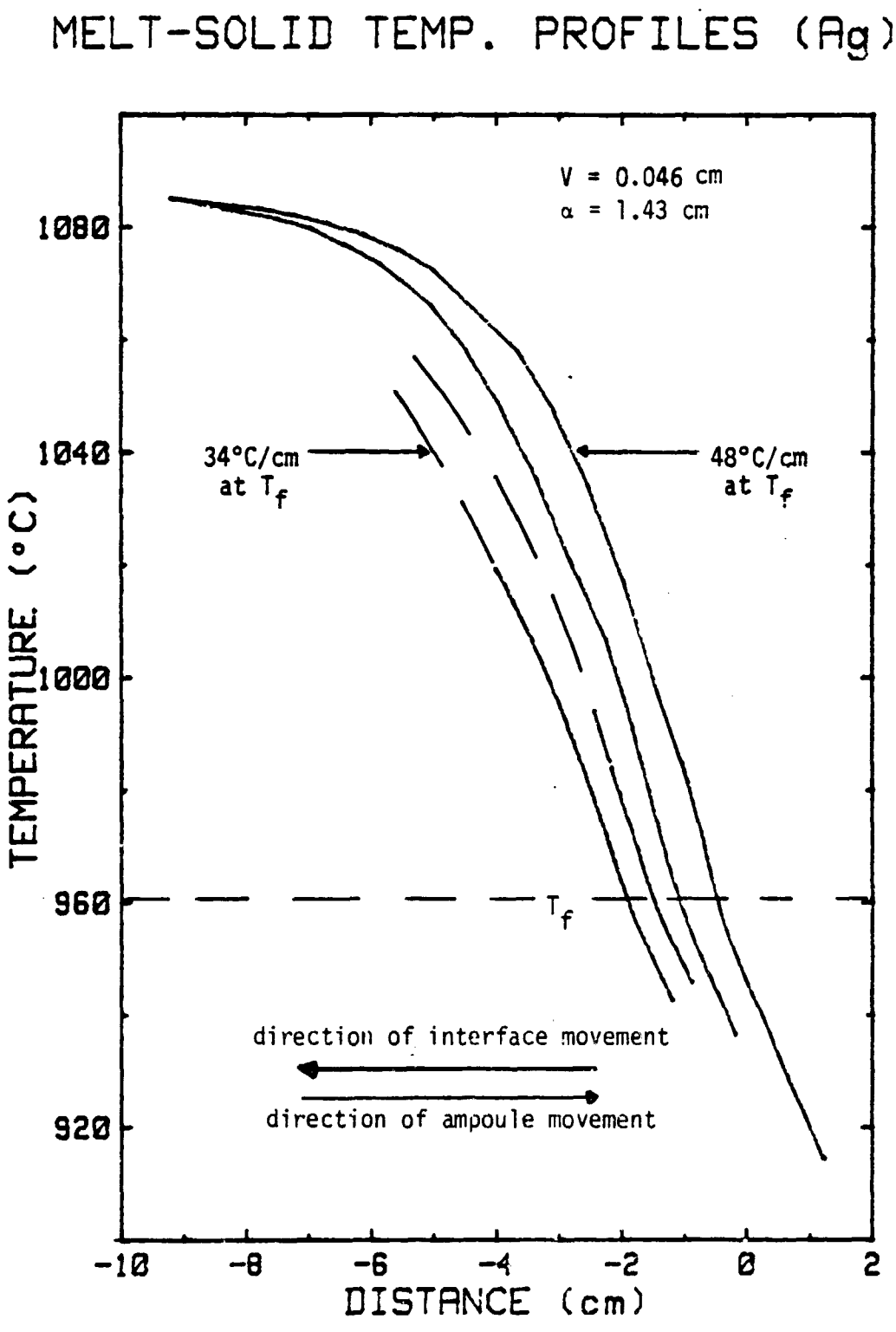

Figure 24: Change in temperature profile seen by the material as freezing progresses.

This equation simply means that the growth rate is the sum of the ampoule translation rate, V, and t' e amount, di/dt by which the growth rate differs form the translation rate. Note that the difference between the instantaneous growth rate R and the ampoule translation rate, V which is proportionate to the derivative of the interface position with respect to the translated length, was close to zero for both Ge and $Pb_{1-x}Sn_xTe$. However, for silver this difference was initially high; then it became progressively smaller and at a critical point, it turned up and became progressively higher. Using equation (25) it can be seen from figure 25 that the growth rate of silver remained higher than the ampoule translation rate all through the growth period shown. At one point the silver growth rate was higher than the translation rate by as much as 110%. The growth rate of Ge and $Pb_{1-x}Sn_xTe$ was equal to the translation rate all through the growth period monitored.

It is expected from equation (25) that if the crystal growth rate, R, and ampoule velocity are constant, the fraction of material solidified, L/L_T will have a linear dependence on the translated length. The fraction solidified is the length solidified normalized with the total boule length. The translated length, Z, is made dimensionless by dividing with the diameter, d, of the boule. Figure 26 shows a plot of L/L_T against Z/d or each material tested. For the semiconductors, Ge and $Pb_{1-x}Sn_xTe$, the relationship is essentially linear within the growth period shown. For the metal, silver, the relationship is nonlinear as could be expected from the curve for silver in figure 25.

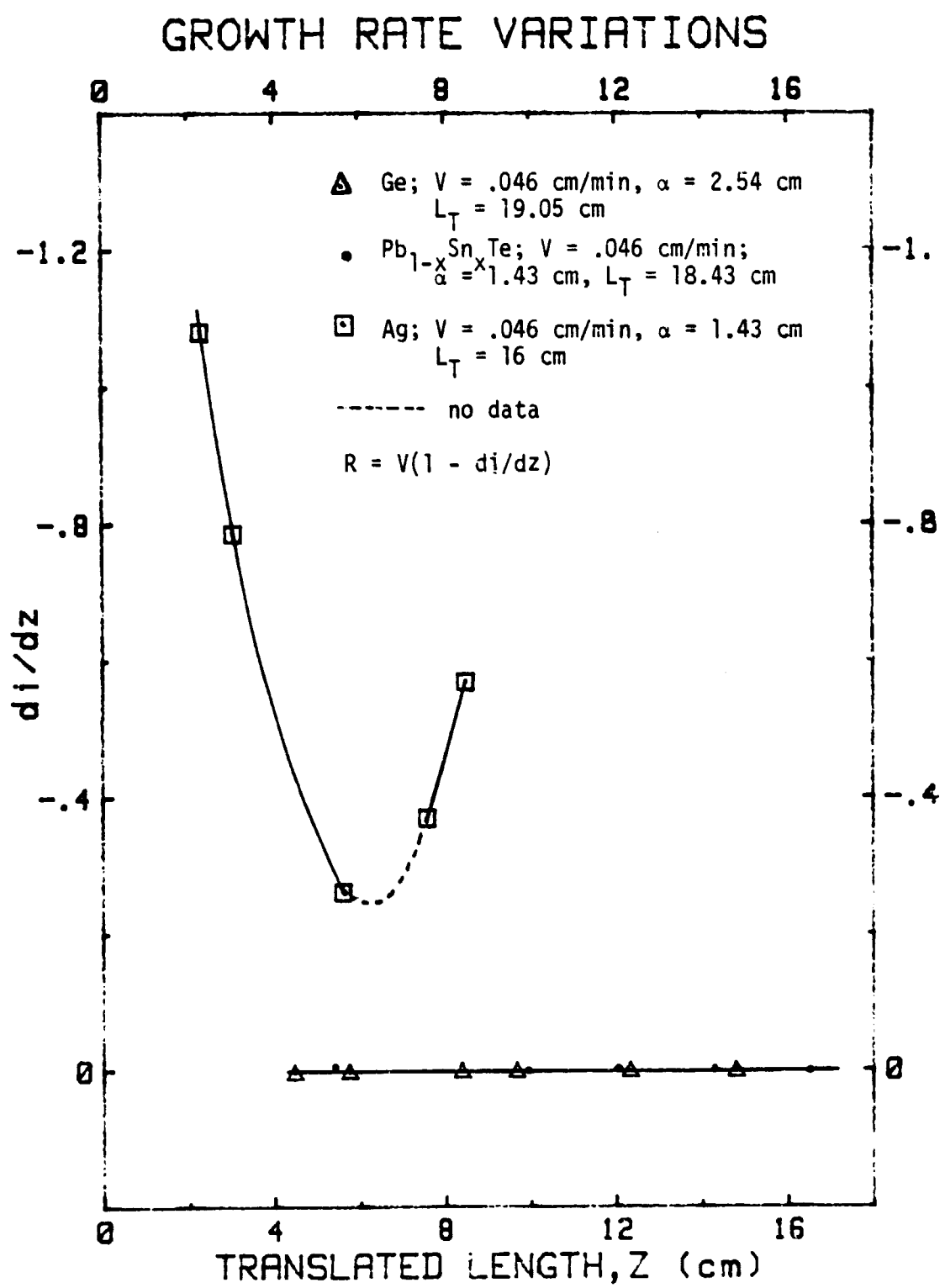

Figure 25: Growth rate variations due to the length of material solidified.

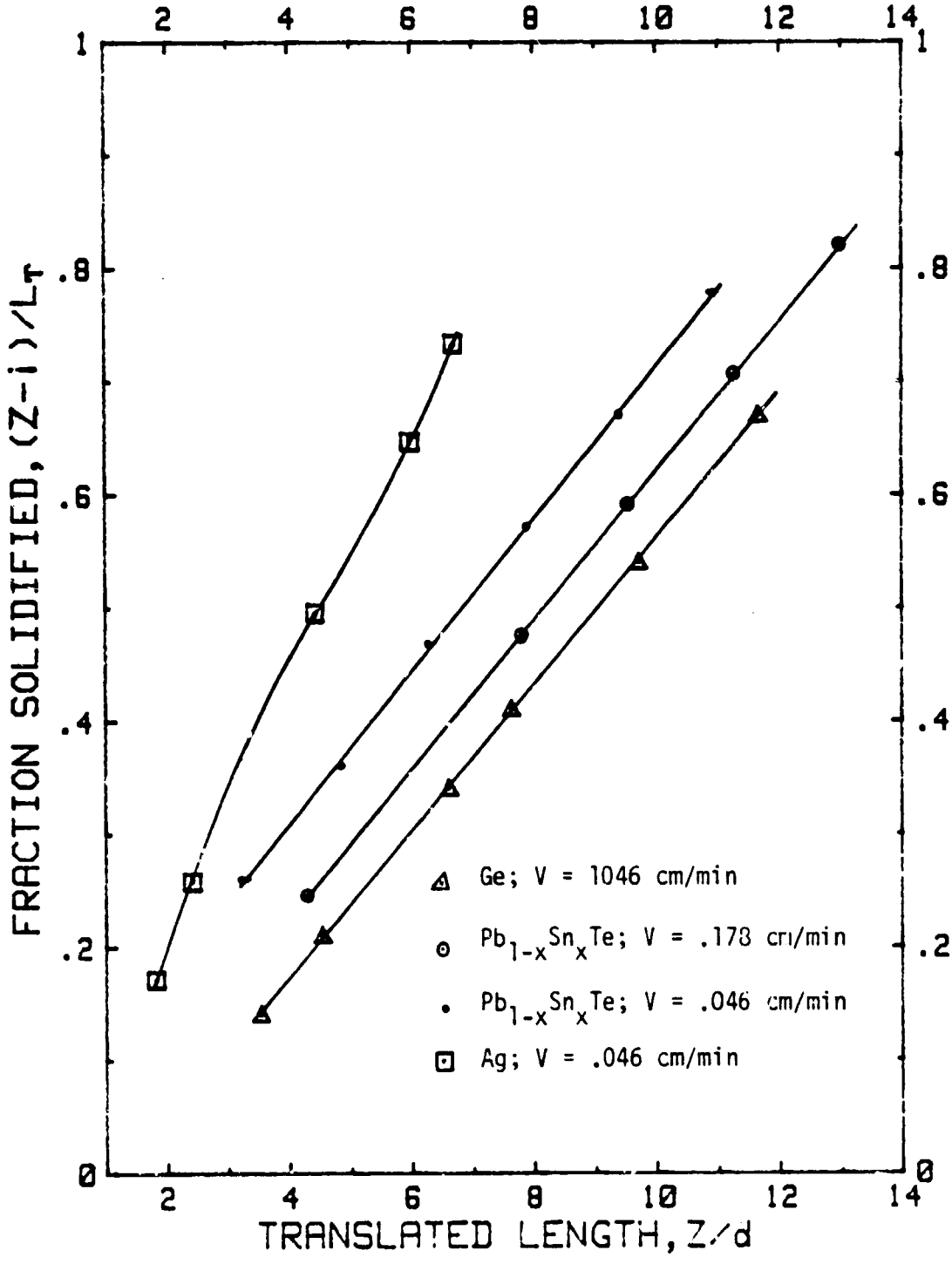

Figure 26: Normalized solidified-length versus translated length-dimensionless.

D. Composition Analysis

As already mentioned in this chapter, the freezing temperature for the alloy semiconductor, $Pb_{1-x}Sn_xTe$, varied as more of the material was frozen. This is in agreement with what would be expected for a pseudo-binary isomorphous system. A qualitative x-ray analysis was performed on the grown rod crystal to determine the solute profile and consequently to determine the compositions that yielded the various freezing temperatures measured in this investigation.

Figure 27 shows the concentration profile of the crystal rods grown at the indicated translation rates. The curve is fitted to equation (12) in Chapter II, but with the effective segregation coefficient, k_{eff} substituted for the equilibrium segregation coefficient, k, which gives

$$C = k_{eff}\, C_o\, (1 - g_s)^{k_{eff}^{-1}} \qquad (26)$$

This is done because equation (12) only applies to the particular case where there is complete mixing in the liquid and no diffusion boundary layer. However, if the k, in equation (12) is changed to k_{eff} then the equation becomes a more general one for a system with mixing in the melt. Note that from the definition of k_{eff}, equation (10) the general equation reduces to the particular equation (12) when δ is zero where δ is the thickness of the diffusion boundary layer. From the general equation (26), the k_{eff} is calculated for both composition-distance

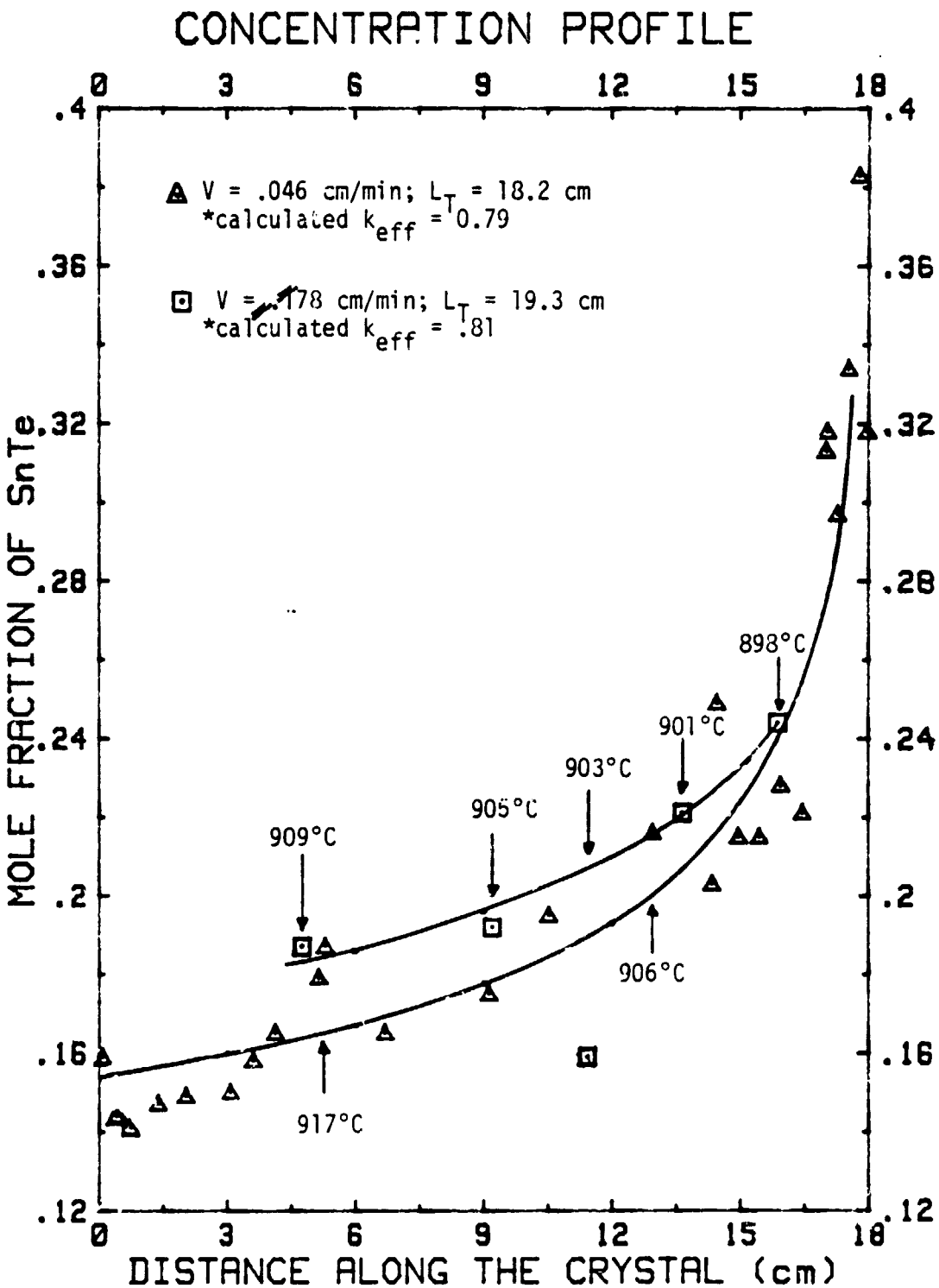

Figure 27: Concentration profiles of $Pb_{1-x}Sn_xTe$ crystal rod grown at different translation rates. It also shows the measured solidus temperatures.

*Calculated from the equation $C = k_{eff}C_o(1 - g_s)^{k_{eff}-1}$

curves, giving a value of .790 for a translation rate of .046 cm/min and .810 for a translation rate of .173 cm/min. These values are obtained by using the above equation (26) in the logarithmic form namely,

$$\ln C = \ln k_{eff} Co + (k_{eff} - 1) \ln (1 - g_s) \qquad (27)$$

The least squares fit to the above equation (27) for the entire data gives a straight line whose intercept is $\ln k_{eff} Co$ and slope is $(k_{eff} - 1)$. From this, both Co and k_{eff} can be calculated. The Co calculated by this method is .195 mole fraction SnTe for the material grown at .046 cm/min and .215 mole fraction of SnTe for that at .178 cm/min. These values compare favorably with the value 0.2 mole fraction determined by weighing during sample preparation.

Also shown in figure 27 are some of the interfacial temperatures measured at the same Z values for which the composition measurements were made. This temperature composition data in effect represents an effective nonequilibrium phase diagram which will be discussed in Chapter VI. Notice here that the temperature composition data closely correspond to those numbers obtained from the liquids line of the pseudo-binary equilibrium diagram of figure 7.

A typical x-ray spectrum collected and used for the quantitative analysis is shown in figure 28. It gives the M and L x-ray lines of lead and L lines of both tin and tellerium. On carrying out a grain boundary etch on this sample using the method described in Chapter III, a micrography of the surface reveals some grain boundaries as shown in

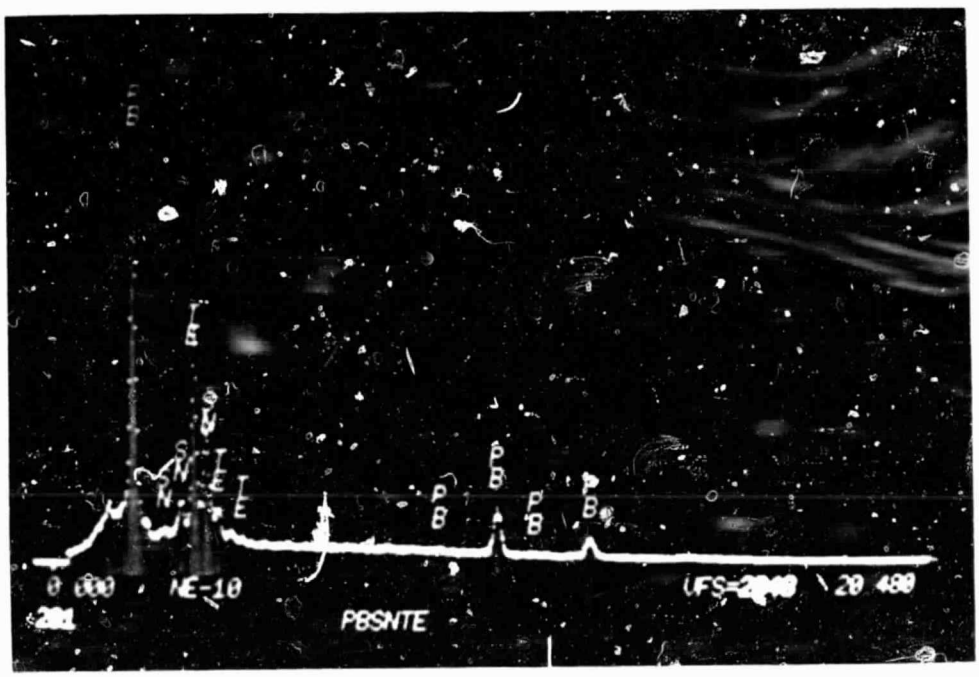

Figure 28: Energy dispersive x-ray spectrum of a cross-section of a $Pb_{1-x}Sn_xTe$ rod. This is an example of the spectra used in the quantitative x-ray analyses.

figure 29. Also shown in figure 29 is an x-ray spectrum typical of the grain boundaries. The Pb and Sn lines are almost completely absent from the grain boundary x-ray spectrum. This may mean that the grain boundary etch preferentially etches out the lead and tin leaving tellerium etch boundaries. No similar spectrum of mostly tellerium was observed in the unetched specimens.

A sample of the EDS results plotted in figure 27 for V = .046 cm/min is shown in Table 4 in terms of the atomic percentages of the elements. It is noted that at every point analysed, the sum of the atomic percentages of the metals, Pb and Sn, is always approximately equal to the atomic percentage of the nonmetal, tellerium. This may indicate that the crystal grows by the incorporation of stoichiometric molecules of PbTe and SnTe as opposed to the atoms of the elements.

In line with the above result, it was important to ensure that grains of pure lead, tin or tellerium were not included in the grown sample due to poor mixing and/or non-reaction of the elements. As already described in Chapter III, the elements are weighed out in a proportion that should give stoichiometric $Pb_{1-x}Sn_xTe$ when properly mixed and reacted for about twelve hours in the furnace. Several samples were taken from the grown material and powdered for x-ray diffraction experiments. Table 5 shows one result of such an experiment. The data shows no d spacing that matches any of the three elements, as seen by comparison with the data for the pure elements taken from the standard ASTM x-ray index cards shown in Table 6.

Position Along the Crystal Rod (cm)	Atomic Fraction of the Elements		
	Pb	Sn	Te
5.3	.398	.093	.508
6.7	.409	.084	.507
19.13	.405	.088	.507
10.52	.397	.097	.506
12.94	.385	.106	.508
14.33	.394	.101	.505

Table 4: Result of quantitative x-ray analysis of the interface positions monitored during the $Pb_{1-x}Sn_xTe$ growth at V = 0.46 cm/min.

Note that the composition is always approximately .5 metal (Pb and An) and .5 nonmetal (Te).

Diffraction Angle 2θ	d spacing	I/I_1
27.67	3.22	100
39.65	2.27	80
49.11	1.85	40
57.29	1.61	30
64.83	1.44	45
71.84	1.31	35

Table 5 : X-ray diffraction data measured for the grown $Pb_{1-x}Sn_xTe$

Material	d spacing (Å) and Relative Intensity					
Pb	d spacing	2.88	2.48	1.49	2.85	
	I/I_1	100	50	32	100	
Te	d spacing	3.23	2.35	2.23	3.86	
	I/I_1	100	37	31	20	
β-Sn	d spacing	2.92	2.79	2.02	2.91	
	I/I_1	100	90	74	100	

Table 6 : X-ray diffraction data taken from the standard ASTM cards.

From Table 5, the lattice constant of the sample can be calcualted using the formula for a cubic system and was found to be .64 nm.

It is assumed, at least for the first to freeze portion of the crystal rod (low sclute concentration), that Vegard's law is obeyed. Based on the assumption, the composition of the sample can be calculated as shown in Appendix I. The results of this calculation is .143 mole fraction of SnTe which compares favorably to the composition measured by the x-ray analysis result shown in figure 27 for the first to freeze region.

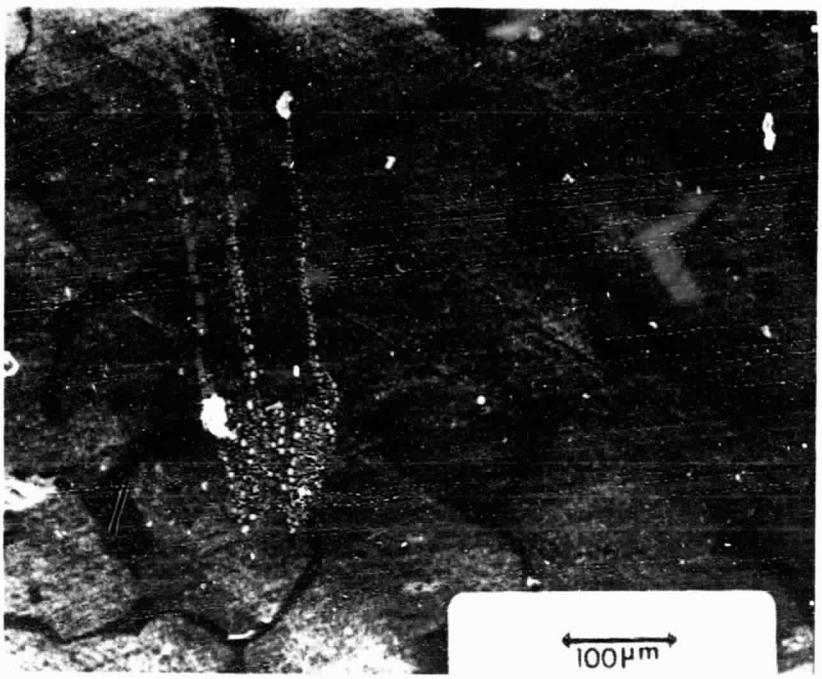

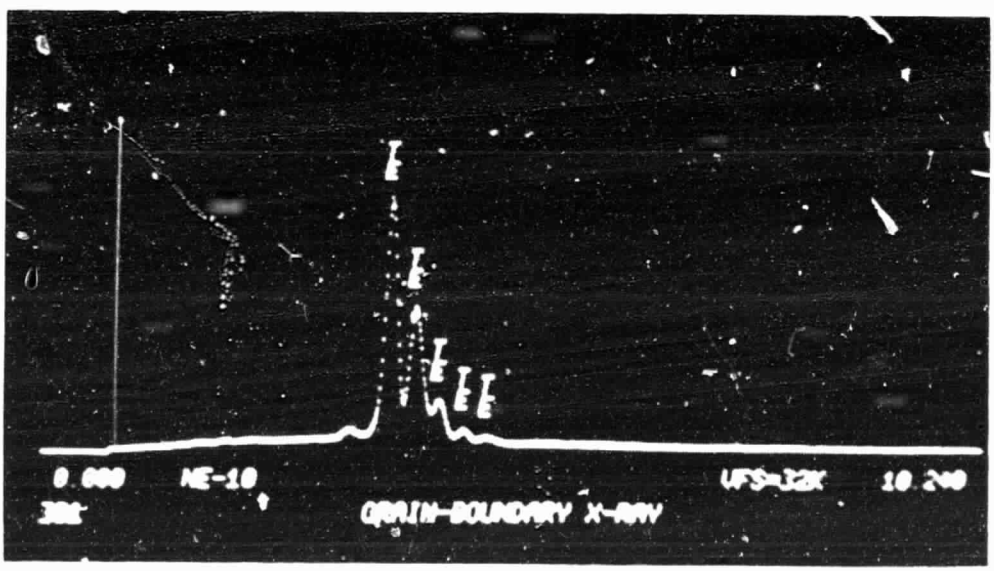

Figure 29: The x-ray spectrum shown is typical of as etched grain boundaries of $Pb_{1-x}Sn_xTe$ shown in the upper part of the figure. The grain boundaries are depleted of Pb and Sn.

CHAPTER V

ERROR ANALYSIS

A. Melt-Solid Thermal Conductivity Ratio

The thermal conductivity ratios are determined from a measurement of the temperature gradients present in the material in the growth furnace. The errors in conductivity, therefore depend on the errors in the thermal gradients which can be assessed from the scatter in the data. The temperature gradients of the melt and solid respectively, G_L and G_S used in the calculation of the thermal conductivity do show a scatter in the data. This scatter reflects the time dependent error in the position reading and the error in the temperature reading. There is no easy way to assign an error to the temperature reading. However, given the fact that the freezing point measured for the pure samples, Ge and Ag, were in good agreement with the literature values, it can be assumed that the error in the temperature reading is small. The scatter in G_L and G_S measured at points near the interface is taken as the error in the temperature gradient measurement. This ranged from 2 to 5% and therefore cannot explain the 33% average error reported in Table 2 for the determined thermal conductivity ratios. This discrepancy is interpreted to mean that systematic error is present and several possible sources of systematic error will be discussed below.

It was mentioned in the chapter on experimental details that the thermocouples had to be protected from chemical attack during the melt-solid temperature measurement. This was achieved by running the

thermocouples through a quartz capillary tube. The fact that this capillary tube runs through both the melt and solid phases will introduce a systematic error in the thermal conductivity ratio measured for the materials. The capillary tube acts as a conductor in parallel with the material to be solidified. Therefore, the calculations of thermal conductivity from equation (24b) which utilizes temperature gradient measurements in actuality yields the thermal conductivity ratios of the glass and sample rather than that for the sample alone. The magnitude of error in the thermal conductivity determined in this manner due to the presence of the capillary tube is considered using figure 30.

For the tube plus molten material, one has a net conductivity K_{mL}

$$K_{mL} = K_L F_L + K_g F_g \tag{28}$$

where $K_{L,g}$ = thermal conductivity of melt, glass

$F_{L,g}$ = volume fraction of melt, glass,

with $F_L + F_g = 1$.

Similarly for the solid side of the interface, the net conductivity K_{mS} is

$$K_{mS} = K_S F_S + K_g F_g \tag{29}$$

where K_S and F_S are the thermal conductivity and volume fraction respectively of the solid. From the dimensions of the ampoule (Figure 5) it can be seen that

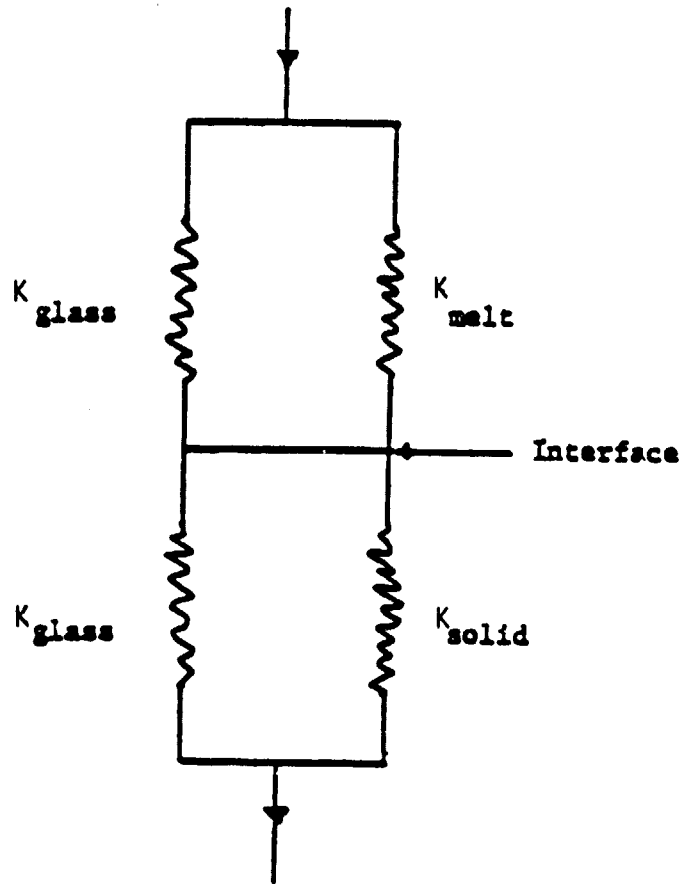

Figure 30: Parallel conductor analogy

$$F_L = F_S = .6214 \tag{30a}$$

$$F_g = .3786 \tag{30b}$$

where the quartz capillary and the thermocouple assembly was assigned the thermal conductivity of glass. The calculated thermal conductivity ratios from the measured temperature gradients are from equation (24b)

$$\frac{K_{mL}}{K_{mS}} = \frac{G_s}{G_L} \tag{31}$$

Substitution of equations (28) (29) and (30a) into equation (31) yields

$$\frac{K_L F_L}{K_S F_S} + \frac{K_g F_g}{K_g F_g} = \frac{G_S}{G_L} \tag{32a}$$

which can be rearranged to yield

$$\frac{K_L}{K_S} = \frac{G_S}{G_L} + \frac{K_g F_g}{K_S F_S} \frac{G_S - G_L}{G_L} \tag{32b}$$

The second term on the right hand side of equation (32b) is the error introduced by the presence of the capillary tube and can be expressed as a fraction error by

$$\frac{K_{mL}}{K_{mS}} - \frac{K_L}{K_S} \quad \frac{K_{mL}}{K_{mS}} = \frac{K_g F_g}{K_S F_S} \frac{G_L - G_S}{G_S} \tag{33}$$

For a given measurement of temperature gradient one can see from equation (30) that the larger the product $K_g F_g$, the larger the fractional error. For silver[32], germanium[33], and glass[34] one has $K_{S_{Ag}}$ = 3.55 watt/cm-°K, $K_{S_{Ge}}$ = 0.465 watt/cm-°K, K_g = 0.86 watt/cm-°K, $F_g/F_s(G_{L_{Ag}}/G_{S_{Ag}} - 1) = .355$, and $F_g/F_S(G_{L_{Ge}}/G_{S_{Ge}} - 1) = -.274$ to yield from equation (33) respective errors of about 1% and -5%.

The above calculated errors are very small compared to the 33% average error in the actual data shown in Table 2. It was, therefore, attempted to explain the error by considering possible geometrical effects due to the capillary tube and furnace geometry.

The effect of the possible curvature of isotherms or the presence of a radial gradient was considered; figure 31 shows a possible arrangement of curved isotherms that may exist in the loaded furnace. Note that the temperature measurements are made along the longitudinal axis which is likely not normal to the isotherms. However, equations (24a) and (24b) hold when the temperature gradient is measured normal to the isotherms. The normal temperature gradient G_N is obtained by the vectorial addition of the measured axial gradient G_M and the measured radial gradient G_r. That is

$$G_N = \sqrt{G_m^2 + G_r^2} \tag{34}$$

From the temperature measurements along the ampoule wall and along the capillary average axial as well as average radial gradients can be

determined. The normal gradients for melt and solid G_{NL} and G_{NS} were calculated from equation (34) and substituted into equation (24b) to calculate K_L/K_S ratios. This approach yielded thermal conductivity ratios which differed from the literature values by a larger amount than that for the uncorrected data in Table 2.

All the above analyses failed to provide a suitable correction factor that could be applied to the data. However, it is noted that the percent error between the values obtained here and those available in the literature was approximately the same for both germanium and silver as shown by Table 2. In view of the lack of a physically based correction procedure, this percent error (33%) was used as an empirical correction factor and applied to the PbSnTe results to obtain what is likely a better assessment of the actual thermal conductivity ratio. This empirical approach gave a K_L/K_S value of 2.35 ± .08 for the $Pb_{1-x}Sn_xTe$, boule where x is 0.2 for the case studied here.

There is one additional comment to be made about the use of equation (24b) to calculate the thermal conductivity ratio. When the boule and interface position are stationary, this equation is applicable; however, when the boule is being translated at a velocity V and the solid is growing at a linear rate R, then the latent heat H may make a significant contribution to the heat balance equation.

The heat energy balance equation at the interface is given by equation (24a) as follows

$$K_L G_L + \rho RH = K_S G_S \tag{24a}$$

where ρ is the density of the solid. Since the G_L and G_S are determined experimental and the material constant are known, it is possible to substitute these values into the above equation in order to quantitatively determine the relative magnitude of the latent heat term in comparison with the heat conduction terms. According to the results, the growth rate of silver, R, is twice the ampoule translation rate. For a sample calculation, a translation rate of .178 cm min^{-1} is used. This gives a growth rate of 5.9×10^{-3} cm sec^{-1}.

For silver, H = 26.5 cal/gm, ρ = 10 gm/cm^3, K_L = .4183 cal/cm-sec-^oC, K_S = .8485 cal/cm-sec-^oC. For one of the above dynamic experiments run at the above mentioned translation rate, the measured G_L and G_S values are 40.44^oC/cm and 25.56^oC/cm respectively. Therefore,

$$K_L G_L = 40.44^oC/cm \times .4183 \text{ cal/cm-sec-}^oC = 16.92 \text{ cal/cm}^2\text{-sec}$$

$$K_S G_S = 25.56^oC/cm \times .8485 \text{ cal/cm-sec-}^oC = 21.86 \text{ cal/cm}^2\text{-sec}$$

$$\rho RH = 10 \text{ cm/cm}^3 \times 10^{-3} \text{ cm/sec} \times 26.5 \text{ cal/gm} = 1.57 \text{ cal/cm}^2\text{-sec}$$

The total rate at which thermal energy flows into the interface is

$$K_L G_L + \rho RH = 18.49 \text{ cal/cm}^2\text{-sec}$$

The latent heat of fusion term comprises only about 8.5% of this heat.

For germanium, a similar calculation can be made using the measured G_L and G_S values of 58.74°C/cm and 107.38°C/cm respectively. The other relevant parameters for the germanium are ρ = 5.323 gm/cm , R = .046 cm/min, H = 114.3 cal/gm, K_L = .311 cal/cm-sec-°C, K_S = .111 cal/cm-sec-°C. This gives

$$K_L G_L = 18.25 \text{ cal/cm}^2\text{-sec.}$$

$$G_S K_S = 11.93 \text{ cal/cm}^2\text{-sec}$$

$$\rho RH = .466 \text{ cal/cm}^2\text{-sec}$$

Therefore, the latent heat term in this case is about 2.5% of the total rate of heat flow into the melt-solid interface. Here also the latent heat term is considered negligible for the translation rates used in this work.

However, notice from the above calculations that for silver

$$K_L G_L + \rho RH < K_S G_S \tag{35a}$$

and for germanium

$$K_L G_L + \rho RH > K_S G_S \tag{35b}$$

These inequalities suggest that there is another heat transfer mechanism operating at the interface. Convection in the melt is probably the other heat transfer mechanism. In order to account for this effect, one can consider an effective heat transfer coefficient for the melt, h_L,

which would include all the heat transfer coefficients regardless of the transfer mechanism, excluding the heat conduction mechanism through the liquid, $K_L G_L$. One can now write the heat balance equation as[35]

$$K_L G_L + h_L \Delta T + \rho RH = K_S G_S \tag{36}$$

where ΔT is the effective temperature difference between the melt and its surrounding environment. A comparison of equations (35 a,b) and (36) shows that the term $h_L \Delta T$ must equal about 4 cal/cm^2-sec and -6.79 cal/cm^2-sec for the above cases of silver and germanium respectively. This is consistent with the idea that convection carries heat through the melt to the interface for the silver case and away from the interface for the germanium case. Figure 32 indicates the conditions that may lead to convection in the two systems.

By measuring the temperature at the ampoule wall and at the center of the sample it was determined that the isotherms for silver were convex (viewed from the hot zone) in the melt immediately ahead of the interface and concave for germanium. For silver this means that the walls were hotter than the center leading to a lower density near the wall and a higher density at the center. Under the influence of gravity, this radial density gradient will set up a convective cell in which the mass at the center falls while the mass near the wall rises. In the case of germanium, however, the opposite condition is found; namely, near the melt-solid interface, the center is hotter than the wall and hence the

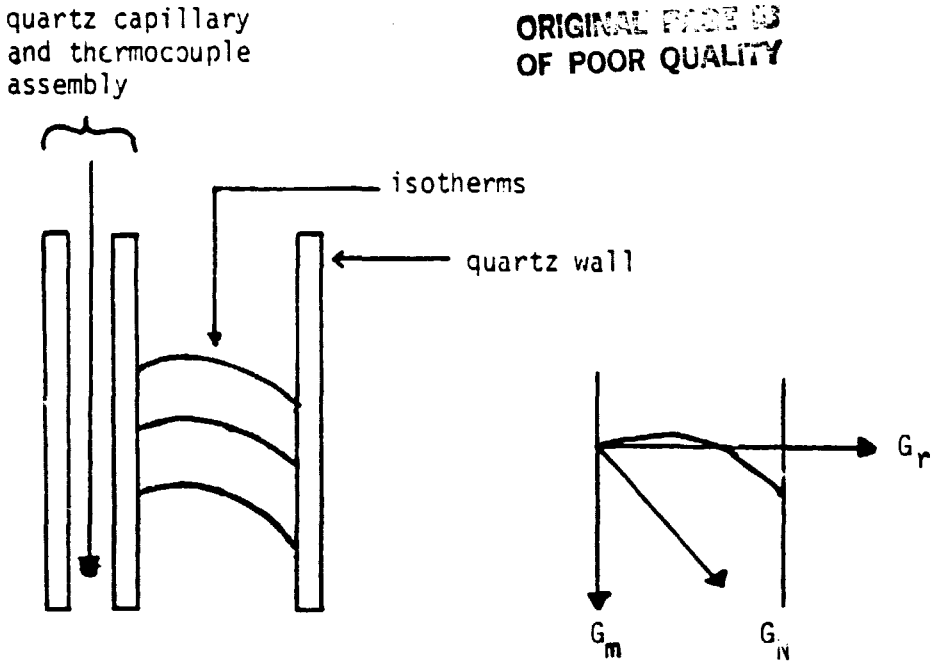

Figure 31: A sketch showing where temperature measurements are made relative to the isotherms.

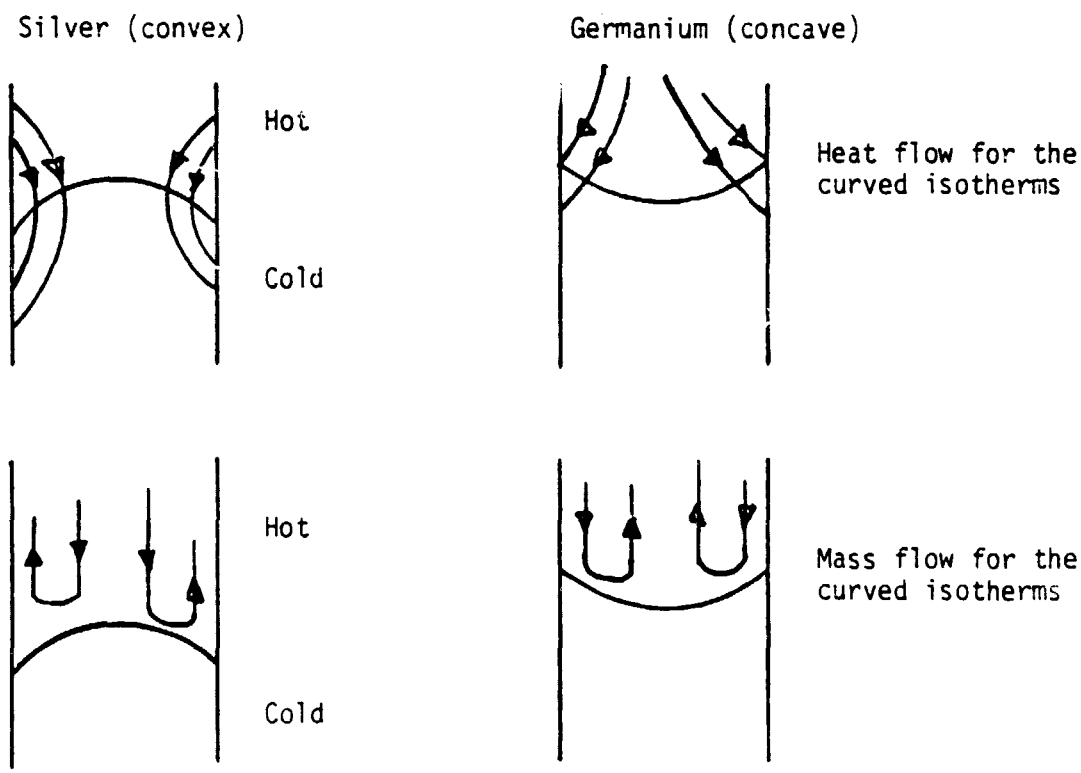

Figure 32: Possible heat and mass flow pattern for the indicated interface shapes.

mass at the wall falls while that at the center rises. The convective flow direction for germanium will therefore be opposite to that of silver. Note that equations (31) and (36) can be solved simultaneously to determine the necessary expression for the correction factor to be applied to the thermal conductivity ratio determined in this work. According to the measured and literature values of the thermal conductivity ratios, of Table 2, similar percent errors were found when the conductivity ratio was expressed as a number greater than unity; that is, the conductivity value in the numerator is that of the phase with the higher conductivity. Accordingly, for silver and germanium respectively, this procedure will give

$$\frac{K_{mS}}{K_{mL}} = \frac{K_S}{K_L} - \frac{Q}{G_S K_L} \quad (Ag) \tag{37a}$$

and

$$\frac{K_{mL}}{K_{mS}} = \frac{K_L}{K_S} + \frac{Q}{G_L K_S} \quad (Ge) \tag{37b}$$

where $Q = \rho RH + h_L \Delta T$.

The terms $Q/G_S K_L$ and $Q/G_L K_S$ are the respective correction factors which empirically account for the percent errors listed in Table 2 for the thermal conductivity ratios. The result that the errors listed in Table 2 for silver and for germanium are about the same,

i.e., 33%, is not understood and may be fortuitous, but suggests that there may be self-cancelling effects which lead to roughly the same percent error. As mentioned earlier, for lack of a better correction procedure, the one of assuming a fixed percent error will be adopted.

B. Position Error

The raw data obtained in the melt-solid temperature measurements consisted of temperature versus time. Since the translated length, Z, is the product of the translation rate, V, and time, t, an expression can be written as follows

$$Z = Vt$$

so that

$$dZ = Vdt + tdV \tag{38}$$

An error of 2 seconds is known to exist in the time, recorded by the programmable thermometer used in this investigation. This follows from the fact that the meter spends 2 seconds on any channel before it reads another one. There is also an error of ± .036 cm/hr in the measured translate rate. This is actually the standard deviation of the translation rate values measured for the motor speed of 2.78 cm/hr. Finally, it is known that each of the dynamic experiments took about one hour from the start time to the time of the interface temperature measurement. Using these values, equation (38) becomes

$$dZ = [2.8 \text{ cm/hr} \times \frac{\pm 2}{3600} \text{ hr}] + [1 \text{ hr} \times \pm .036/\text{hr}] = 0.37\text{cm}$$

The initial position of the bottom of the ampoule is set by eye judgement of a pointer on the furnace graduated scale, before each of the dynamic runs. This may be the largest source of absolute position error and is conservatively assigned an error of 0.10 cm. These two errors add up to a total of ± .137 cm for the interface position determined in this work. This means that for a translation rate, 2.78 cm/hr, a positional change in the ampoule of (2.78 ± .137) cm is read instead of 2.78 cm after a period of one hour. This gives an error of about 5% in the position readings. Note that the measured temperature is affected by only that part of the position error that is time dependent. In the above case then, only the .037 cm error affects the temperature readings from the "Temperature vs. distance" curves.

It has been observed in connection with figure 23 that the melt-solid interface position of $Pb_{1-x}Sn_xTe$ was essentially constant. However, note that from figure 27 the freezing temperature is lowered as freezing progresses. This means a slight shift in the freezing isotherm toward the cold zone. The freezing temperature changed by about 11°C between the first and last interface position monitored. From table 3 the gradient in the melt of the $Pb_{1-x}Sn_xTe$ is about 80°C. For this type of temperature gradient, an 11°C change in freezing temperature should correspond to a positional shift in interface of about 0.13 cm. While this is consistent with figure 23 which shows a slight shift of about 0.1 cm

in interface positions monitored at the slow translation rate of .046 cm/hr, this amount of shift is nevertheless within the .137 cm calculated for the error in the experimental determination technique of the interface position and hence will be neglected.

C. Concentration Profile Error

In order to check the precision of the energy dispersive x-ray analysis, a number of concentration determinations were made at one point on a sample using the same amount of count time, the same voltage and the same beam current. The standard deviation of the measurements is ± .006 mole fraction which is taken to be the precision of the measurements.

During the alloy preparation, by weighing of the components, it is known that the initial concentration, C_o, of the melt column of the $Pb_{1-x}Sn_xTe$ is .2 mole fraction of SnTe. However, from the composition analysis discussed in Chapter IV, the best fit to the concentration profiles of figure 27 gave an initial concentration value which differed from .2 mole fraction of SnTe by about 5%. This is interpreted to mean that the accuracy of the composition analysis is about 5%.

CHAPTER VI

DISCUSSION

A. Furnace Characterization

1. Introduction

It is generally known that a furnace environment affects the quality of simgle crystals grown in the furnace. Some of the furnace environment properties which have been shown to affect crystal quality are the axial[4] and radial[3] temperature gradient and the insulation thickness or length of the adiabatic zone (region without a direct control heat source). A tickler heater (booster heater) was used in this investigation to affect the axial temperature gradient. The tickler heater is a direct heat source and when placed at the end of the adiabatic zone, in effect reduces the length of the adiabatic zone of the furnace. The extra heat generated by the tickler heater should shift the isotherms in the furnace. Again, it is known that the furnace temperature profile is dependent on the properties[2,3] of the load in the furnace. Chang et al.[2] have shown that the isotherms of their modelled Bridgman type furnace do shift as the Biot number of the load is changed. The Biot number, hS/K, is defined as the ratio of heat loss from the sample surface to heat conduction, where h is the load's heat transfer coefficient, S is the load radius and K is the thermal conductivity of the load material.

A considerable amount of effort was put into characterizing the empty furnace used in this investigation in order to understand the environment in which the solidification experiments were performed.

While temperature profile determinations are easier to make in an empty furnace than in a loaded one, both do obey the same fundamental heat flow principles. So a knowledge of the empty furnace profile of a crystal growth furnace can point to the trend in profile that may be expected during growth. For instance, an elimination or reduction of radial temperature gradients in an empty furnace usually corresponds to a similar situation in a loaded furnace and represents a good crystal growth condition for obtaining a planar interface. In effect, the result of an empty furnace characterization may be seen as a first approximation of the heat flow pattern to be expected in the loaded furnace, and hence the following discussion is concerned with characterizing the temperature profile under various furnace conditions.

2. Effect of Plugging the Furnace Ends

The result of leaving both the hot and cold zone ends unplugged in a vertical Bridgman type furnace is shown in figure 10. Notice the enormous difference between the temperatures of the near-wall of the quartz liner and the center-line of the furnace for any given axial position. This indicates the presence of large radial gradients. On plugging the furnace ends, an equilibration is reached after about 3 minutes and depending on how effective the plugging is, the temperature differential between the quartz near-wall and the center line is either reduced or essentially eliminated, as shown in figures 11 and 15 respectively. Again, this indicates a reduction or elimination of radial temperature

gradients. The temperature difference between the quartz near-wall and the furnace center-line may be caused by a "chimney" effect. This simply means that air is blowing into the furnace from the cold zone as hot air rises. However, due to frictional forces, the air near the wall is not rising as fast as the air in the center. So the wall retains its heat better than the center which is subjected to a flux of cooler air than that of the wall Also, the heat lost through the air flux will lower the temperature f both the hot and cold zones leading to a low axial gradient. If a tight plugging of the furnace ends is achieved such that essentially no air enters or leaves the furnace, then the radial gradient can be reduced remarkably and the axial temperature gradient increases.

It has been mentioned that both the axial nd radial temperature gradients affect the quality of crystals grown in the furnace. Since plugging of the furnace ends affects these furnace properties, as discussed above, it must invariably affect the quality of crystals grown in the furnace. Therefore, proper plugging is essential to crystal growth in a vertical Bridgman type furnace in order to avoid the material problems due to high radial and low axial temperature gradients. Improper plugging leads to air flow in the furnace which creates a condition for the furnace wall to be substanially hotter than the center.

3. Effect of Loading

The experimental results show that a load introduced into the furnace will have a temperature profile different from that of the empty

furnace. From Table 1, it can be seen that for the same furnace and tickler heater settings, the empty furnace profile was changed from a gradient of 127°C/cm at 900°C to 118°C/cm, 99°C/cm and 35°C/cm by $Pb_{1-x}Sn_xTe$, germanium and silver respectively. This shows that as the load in the furnace changed from a low thermal conductivity material, $Pb_{1-x}Sn_xTe$, to a higher thermal conductivity material, silver, the amount of change in the temperature gradient of 900°C increased.

The ability of a load to conduct heat means that if placed in a temperature gradient, the load will tend to go toward a thermal equilibrium by trying to eliminate the temperature gradient. So the load placed in the Bridgman type furnace will spread heat from the hot to cold zone in an attempt to remove the imposed temperature gradient. However, since there is a constant heat source set to maintain the gradient, the effect of the load is to reduce the temperature gradient. The higher the thermal conductivity, the more effective the load in spreading heat and reducing the temperature gradient.

Figure 24 shows that the loaded furnace profile continuously shifted as the freezing of the silver progressed. This continuous shift in profile may be related to a change in the value of the overall Biot number seen by the various zones of the furnace. As mentioned in the introduction of this section, it has been shown theoretically[2] that the Biot number, hS/K, is a parameter which affects the furnace temperature profile. An increase in this parameter is shown to correspond to a

shift in the isotherms toward the cold end of the furnace plus a decrease in the spacing between the isotherms. The decrease in the spacing of the isotherms corresponds to a higher axial temperature gradient. Clyne[5] has shown for aluminum that the shift in the thermal profile of the load is dependent on the proportion of the lengths of the specimen that is located in the hot and cold zones.

For the same material, say silver, the heat transfer coefficient, h, is not expected to change substantially going from the melt into the solid phase, as compared to a factor of about two change in thermal conductivity values recorded for most semiconductors and metals. So changes in the value of h is neglected. For silver with $K_S \approx 2K_L$, this means that as the solid is formed, the Biot number, hS/K, is reduced in the cold zone. Also, the proportion of the entire starting column of material that is in the cold zone is increasing leading to a better coupling with the cold zone. These two conditions of a high solid thermal conductivity and a longer length of solid in the cold zone reinforces each other and leads to a shift in isotherms toward the hot zone as shown by figure 24.

The above discussions seem to indicate that the thermal conductivity of the load in a furnace is a factor that affects how the load temperature profile compares with the empty furnace profile. The higher the thermal conductivity, the more the deviation from the empty furnace profile. As the load is traversed through the furnace, the change in the proportion of the length of the load that is in the cold zone causes a shift of isotherms toward the hot zone.

4. Effect of Tickler Heater

In the furnace configuration used in this investigation, the tickler heater is placed within the adiabatic zone starting at the boundary of the hot and the adiabatic zones. As can be seen from figure 11, this is within the region in which the furnace temperature profile rolls off from the hot zone to the cold zone. As already mentioned, the tickler heater in this furnace configuration basically reduces the length of the adiabatic zone. The heat generated in this region not only results in a positional delay in the roll-off "knee" but also increases its temperature. This can be seen by comparing figures 11 and 15. The tickler heater generates heat only on the hot zone side of the insulation or adiabatic zone; whereas the temperature on the cold zone side is fixed by the control thermocouple in the cold zone. Since as discussed above, the roll-off from the hot to the cold zone is delayed, it means that the gap within which the profile has to roll-off and fall to the fixed cold side temperature is smaller leading to a higher axial temperature gradient. As will be discussed in the next section, the above mentioned condition corresponds to a shift in isotherms toward the cold zone.

B. Melt-Solid Interface Positions

1. Introduction

As discussed in the preceding section, a load put into a furnace can alter the temperature profile of the furnace. However, the discussion did not include the effect of the movement of the load, which

will be discussed here. Fu and Wilcox have shown theoretically[2] that the furnace isotherms shift toward the cold zone as the Peclet number, Pe, increases. The Peclet number, $V\rho C_p S/K$, is defined as the ratio of heat carried by motion of the load to heat conduction, where V is the load translation rate, ρ is the density, C_p is the heat capacity, S is the load radius and K is the thermal conductivity.

The tickler heater has been shown to generate heat within the roll-off region, thereby increasing the axial temperature gradient of the empty furnace. In this section, this result will be correlated with shifts in the melt-solid interface and increases in the temperature gradient in the melt immediately ahead of the interface. These are important parameters in crystal growth by the Bridgman technique. Finally, the materials constants which were the offshots of the technique used in the interface position determination will be discussed.

2. Tickler Heater Effect on Interface Positions

The melt-solid interface has been previously referred to as representing the isotherm that corresponds to the freezing temperature of the material on the assumption that there is no compositional variation across the interface. In this sense then, any condition that shifts the furnace isotherms also shifts the interface.

It has been shown in the preceding section that the extra heat generated by the tickler heater raises the temperature of the roll-off "knee" and shifts the profile toward the cold zone. This shift means that any

given axial position within the roll-off region sees a higher temperature than it did without the tickler heater. This is another way of saying that the position of a given isotherm, 900°C for example, is taken by a higher temperature isotherm such as 950° while the 900°C isotherm is displaced further toward the cold zone. The interface, as an isotherm, also gets shifted for the same reasons. Of course, the longer the tickler heater length and/or the larger the tickler heat temperature setting, the more heat is generated in the roll-off region and the more the shift in interface position. The heat generated by the tickler heater has also been shown in the preceding section to result in an increase in the empty furnace axial temperature gradient. Recall that the empty furnace profile points to the trend in the profile to be expected during the crystal growth. So it is expected that for the same reasons given in the section on furnace characterization that the temperature gradient in the melt of a given material should increase with tickler heater length and/or setting. This is consistent with the results in Table 3.

3. Effect of Translation Rate

It has been pointed out in the introduction that a theoretical work[2] by Fu and Wilcox has shown that as the Peclet number, Pe, increases, the furnace isotherms and therefore the melt-solid interface are shifted toward the cold zone. Note that from the definition of Pe, $V\rho C_p S/K$, for a given material, the only variable is the translation rate, V. The above theoretical result then corresponds to a shift in isotherms with

an increase in the load translation rate. Also, equations (15 a,b) can be used to show that ϕ, the dimensionless temperature, get bigger as Pe gets bigger. Again, for the same material, this means that a given isotherm is replaced by a higher temperature one as the ampoule translation rate is increased.

The above mentioned theoretical results are consistent with figure 23 which shows that the melt-solid interface of the same material $Pb_{1-x}Sn_xTe$ shifted toward the cold zone with an increase in the translation rate, V, from .046 cm/min to .178 cm/min. Physically, the thermal mass of the load may be responsible for the load not dissipating heat as fast as it is being moved. So some of the heat carried from the hotter region is moved to the cooler region. This will make the cooler region hotter than it should normally be in a stationary condition. Of course, the higher the rate of sample translation, the less time the load has to dissipate heat to the immediate environment, the more heat is carried down to the cooler sections and therefore the further down the position of a given isotherm.

4. Materials Constants

The freezing point measured for germanium in this work is 937.3 ± 1.5°C which is in agreement with the current literature value[34] of 937.4°C. For silver, the measured freezing point, 960.1 ± .9°C, is about 2°C lower than the current literature value of 961.93°C. These results may be related to the purity of the samples. The germanium used in the

investigation was 99.9999 percent pure whereas the silver was only 99.99 percent pure. From the phase diagrams of silver and oxygen or silver and sulphur, it can be seen that a small amount of these elements can suppress the freezing point of silver significantly. In fact, an oxygen content of about 0.0001 mole fraction, according to the phase diagram, will suppress the freezing point of silver by about 1°C. So the slightly low freezing point measured for silver is attributed to impurities like oxygen in the sample.

Another material constant determined in this investigation is the melt-solid thermal conductivity ratios for the samples. The results for germanium and silver show an error of about 33% when compared with selected literature values, as shown in Table 3. This error has been discussed extensively in Chapter V. The total error is likely a combination of errors due to the presence of the quartz capillary tube, the curvature of the interface and convection in the melt caused by radial temperature gradients. By taking temperature readings at both the wall and center of samples simultaneously, it was determined that the average radial gradient could be as high as 20°C/cm which suggests that locally the radial gradient may be significantly higher. The radial temperature gradient creates a radial density gradient which coupled with gravity can initiate and maintain convection in the melt. The calculations of Chapter V showed that the largest error is likely that resulting from convection.

A generally accepted assumption in single crystal growth by the Bridgman-Stockbarger technique is that solid-state diffusion is negligible compared to diffusion in the melt. As a result, mass redistribution during crystal growth from the melt is explained by mass transport mechanisms in the liquid only. In the growth of $Pb_{1-x}Sn_xTe$, the pseudobinary phase diagram of figure 8b suggests that a tin-rich layer should build up in the melt in front of the interface since the equilibrium segregation coefficient,[37] k, is less than unity. A number of things can happen to this tin-rich layer. It can be completely or partially swept away and homogenized with the bulk melt by convection, it may remain undisturbed in the absence of convection. Of course, each of these conditions should yield a different final solute redistribution curve.

One possibility is the steady-state case in which there is no convection in the melt, and liquid mass transport is by diffusion only. In this case, according to equation (7a), one expects a concentration profile that should have a constant composition over most of the length of the grown rod. Obviously, the data points in figure 27 do not exhibit any appreciable constant composition portion and so do not fit the steady state theory. Two other solute redistribtuion theories are: (a) complete mixing in melt by Pann[17] and (b) partial mixing in the melt with a diffusion boundary layer of thickness, δ, by Burton, Prim and Slichter[10]. Both theories describe the solute redistribution according to equation (12)

$$C_S = kC_o(1 - g_s)^{k-1} \tag{12}$$

except that in the latter theory, the equilibrium distribution coefficient, k, is replaced by an effective distribution coefficient, k_{eff}, as equation (26). Note that this partial mixing case is growth rate dependent, through the definition of k_{eff} given by equation (10)

$$k_{eff} = \frac{k}{k+(1 - k)e^{-R\delta/D_L}} \tag{10}$$

where R = crystal growth rate

δ = effective diffusion layer thickness

D_L = diffusion coefficient in the melt

It is known from literature[37] that the equilibrium segregation coefficient, k, ranges from .60 to .74 for liquid composition of about .2 to .5 mole fraction of SnTe. However, when the data of figure 27 were fitted to equation (12), k values of 0.79 and 0.81 were obtained for the respective growth rates of .046 cm/min and .178 cm/min, both of which differed from the expected range values for the equilibrium segregation coefficient. This suggests that of the three theories discussed above, the BPS boundary layer approach gives the best description of the data measured in this investigation.

From the above discussion, one is lead to believe that figure 27 is indicative of the presence of free convection in the melt, with a boundary layer of thickness, δ. While the difference between the

measured k_{eff} and the literature value of k can be attributed to other causes such as a breakdown in the assumptions leading to equation (26), it is nevertheless reasonable to expect free convections to result from the radial temperature gradient which is known to exist in the melt and hence give rise to the k_{eff} value of the BPS theory.

From equation (10), a characteristic value, δ/D_L, for systems with free convection present in the melt can be calculated from a knowledge of k , R and k_{eff}. For the case of lead-tin telluride, the selected[37] k value is .69. For the growth rate of .046 cm/min and .178 cm/min, the respective δ/D_L values are calculated to be 685 sec/cm and 212 sec/cm. A greater confidence is placed on the value of 685 sec/cm which is for the slower growth rate because it is based on many data points as opposed to that for the fast growth rate. This fact is evident in figure 27. Clark[38] has determined the diffusion coefficient, D_L, of SnTe in PbTe as 7×10^{-5} cm^2/sec. Using this D_L value, the thickness of the diffusion boundary layer is calculated to be about .05 cm which is the same order or magnitude as the δ values listed in the literature[35] for alloy systems undergoing progressive freezing with free convection present.

C. Growth Rate

The results shown in figure 25 indicate that the growth rate of silver varied as freezing progressed and also that at all times it remained higher than the ampoule translation rate. In contrast, the growth rate of germanium and that of lead-tin-telluride remained approximately constant

and equal to the translation rate. As already mentioned in Section A of this chapter, the profile seen by the load in a furnace seems to be dependent on the proportion of the load lengths that are in the hot or cold zone. As more of the load enters the cold zone, there is a better coupling between the specimen and the cold zone while at the same time there is a weak coupling with the hot zone. The net effect is that a given isotherm, e.g., the freezing isotherm, migrates toward the hot zone. However, for a poor conductor like the semiconductors, germanium and lead-tin-telluride, once the first portion is frozen, heat transfer to the cold zone via conduction through the specimen is poor or essentially eliminated. Because of its poor conductivity, the solid essentially acts as an "insulator", separating the melt-solid interface from the cold zone. In this case, coupling with the cold zone is poor. Therefore, the loss of heat necessary for continued growth is sustained only by the mechanical drop of the sample toward the cold zone. This may explain the result that the growth rate of the semiconductors was equal to the ampoule translation or drop rate. For the metal silver, on the other hand, the better coupling through the high thermal conductivity solid phase sustains a continued migration of the interface toward the hot zone, i.e., a continued displacement of the freezing isotherm toward the hot zone. This added heat loss through the growth crystal is seen (from figure 25) to force the freezing isotherm to migrate faster than the ampoule drop rate and hence the continued change in interface position.

Figures 25 and 26 also show that the rate of migration of the interface slowed down during the solidification process until about 66% of the melt column was frozen and then the migration of the interface slowed a speed-up in the rate of advancement with translation of the boule. This may be related to the nonsymmetric nature of the furnace temperature profile, which goes from a low through a high and back to a low magnitude of the temperature gradient. Because the gradients were only measured near the interface, there is no gradient data from which one could calculate the expected isotherm shift with translation rate and boule length. However, qualitatively it is possible for the boule to cause isotherm shifts as varying rates as a function of the translated boule distance, z.

The results suggest that for materials with very low thermal conductivity, the only means of effective heat loss that can contribute to solidification rate is provided by the sample drop rate into the cold zone. However, for materials with high thermal conductivity, there is the shift in freezing isotherms due to better coupling with the cold zone. This plus the ampoule drop rate may make the rate of interface movement or the growth rate higher than the sample translation rate. Obviously, the magnitude of this effect is affected by the translation rate.

D. Solute Redistribution

The changing interfacial temperatures of the $Pb_{1-x}Sn_xTe$ due to changing compositions were determined from the melt-solid temperature

measurements. Examples of the measured freezing temperatures are shown in figure 27. From this figure, then both the concentration and the freezing temperature corresponding to that concentration can be determined at the chosen points. In effect, the solidus curve of the material can be determined from the combination of x-ray analysis, composition data, and the melt-solid temperature measurements technique used in this investigation. However, the pairs of concentration and temperature data taken from figure 27 tend to fall on the liquidus line of the pseudobinary phase diagram of figure 8b. The samples used for the x-ray analysis were obtained by cutting across the rod crystal at the chosen points along the axis. This was then prepared as discussed in Chapter III. The x-ray analysis was then done at points on the cross sectional surface on the assumption that the crystal was grown with a planar interface. However, as already mentioned in this chapter, temperature measurements made simultaneously at the wall of the ampoule and the center of the sample indicate the presence of radial temperature gradients which consequently correspond to a curved isotherm and hence a curved melt-solid interface. For the case of lead-tin-telluride, the isotherms and hence the melt-solid interface are concave (viewed from the hot zone). The amount of curvature is represented by the magnitude of the radial temperature gradient. Unfortunately, the radial gradients were not measured for this case. In order to estimate the radial gradient, a proportionality between the axial temperature

gradient of lead-tin-telluride and its radial gradient will be assumed to be the same as that measured for germanium. The measured axial temperature gradient for germanium is 99°C/cm from Table 1. A maximum radial gradient of 20°C/cm was also measured for germanium at the temperature, 900°C. The axial temperature gradient for lead-tin-telluride is from Table 1, 118°C/cm. From this data, the radial temperature gradient of lead-tin-telluride is assumed to be 24°C/cm.

Figure 30 has already been used to describe the radial positions at which the temperature measurements were made with reference to the curved-interface. Now if the sample is cut in a planar cross section and x-ray analysis performed at the center, it becomes obvious that the measured concentration will correspond to a different isotherm than that at the point where the temperature reading was taken. The center of the x-ray samples is about 3.5 mm from the radial position where the temperature readings were taken. For a radial gradient of 24°C/cm, this center position therefore corresponds to an isotherm 8.4°C lower than the measured one. In order to obtain an estimate of the correct solidus temperatures at the radial points, the compositions were measured by x-ray analysis, one has to correct the measured temperature by subtraction of 8.4°C. Table 7 shows the corrected solidus temperature which are to be compared with those values taken from the bulk phase diagram of figure 8b for the selected measured concentrations. The corrected solidus temperatures compare very well with those from the phase diagram. While one can

Measured Concentration Mole Fraction SnTe	Measured Solidus Temperature Corrected for Interface Curvature	Solidus Temperature Taken from Reference 30 or Figure 8b
.186	901°C	898°C
.191	897°C	896°C
.206	895°C	894°C
.220	893°C	892.3°C
.242	890°C	889.2°C

Table 7: Measured solidus temperature corrected for the melt-solid interface curvature.

use the melt-solid temperature measurement technique and the x-ray analyses to generate the solidus line of a given alloy system, care must be taken to properly correlate the temperature measurements and the composition measurement so that they correspond to the same isotherm and interface.

CHAPTER VII

SUMMARY AND CONCLUSION

A. Growth Rates

The instantaneous growth rate of directionally solidified silver was shown to remain higher than the amopule translation rate all through the growth period monitored. The growth rate was continuously changing all through the growth period and at the early stages of growth was as much as 110% higher than the ampoule translation rate. On the other hand, the growth rates of both Ge and $Pb_{1-x}Sn_xTe$ were essentially constant and equal to the ampoule trnaslation rate within the monitored growth period.

The continued migration toward the hot zone of the freezing isotherm of silver can be related to better heat coupling with the cold zone as more material is solidified. The apparent rate increase after about 66% of the melt column has been frozen is possibly a result of the non-symmetric nature of the furnace temperature profile.

From the discussion of the results, it is concluded that the growth rate of poor conductors like Ge and $Pb_{1-x}Sn_xTe$ is determined by the sample drop rate over the range of growth rates studied (.046 cm/min - .178 cm/min). However, the growth rate of high conductivity materials like metals may differ from the sample drop rate because of the added shift in the freezing isotherm due to better heat coupling with the cold zone.

B. Materials Constants

The measurement of temperature profiles on either side of a solid-liquid interface is an experimental technique employed in this research

to provide freezing temperatures of a 99.9999% pure germanium sample and a 99.99% pure silver sample. The respective measured freezing points were 937.3 ± 1.5°C and 960.1 ± 0.9°C, which are in good agreement with literature values[34] of 937.4°C and 961.8°C. The discrepancy observed for silver is consistent with a small inpurity level (e.g., .01% oxygen). This experimental technique was also used to determine the freezing temperatures of an alloy system at recorded points along the rod, as freezing progressed. Using a quantitative x-ray analysis, the composition of the points for which freezing temperatures were recorded can be obtained, thereby completing a temperature versus composition curve which should correspond to the solidus line of the alloy system. A comparison of the composition-distance profile for lead-tin-telluride showed that of the three theoretical curves available in the literature, the one of Burton et al.[10] (BPS theory) most closely fit the data. The BPS theory assumes a boundary zone of width δ into the melt through which mass transfer is by diffusion. Partial mixing of the melt and negligible diffusion in the solid is assumed. This theory leads to a continuously varying composition along the grown rod as shown in figure 27. Based on this theory, an effective segregation coefficient, k_{eff}, of .790 and .810 for the $Pb_{1-x}Sn_xTe$ was measured for the translation rates of .046 cm/min nad .178 cm/min respectively.

Using a diffusion coefficient calculated by Clark[38], the thickness, δ, of the diffusion layer was calculated in this investigation for

$Pb_{1-x}Sn_xTe$ to be 0.047 cm and 0.015 cm for the translation rates of 0.046 cm/min and 0.178 cm/min respectively. The value of 0.047 cm is taken to be the more reliable value because it is based on a larger set of data points.

Another direct measurement from the temperature profiles is the melt-solid thermal conductivity ratio of $Pb_{1-x}Sn_xTe$. This is determined to be 2.33 ± .05. The solid thermal conductivity, K_S, of $Pb_{1-x}Sn_xTe$ at the freezing point (x = .2) is given in the literature[36] as 0.023 Watts cm^{-1} K^{-1}. With this K_S value and the K_L/K_S ratio given above the melt thermal conductivity, K_L can be calculated to be about 0.054 Watts cm^{-1} K^{-1}. Of course, this value is expected to vary with composition.

C. Tickler Heater and Plugging Effects

A tickler heater (booster heater) has been used effectively to increase the temperature gradient, G_L, in the melt ahead of the interface. With the furnace configuration used in this investigation, the tickler heater essentially reduces the length of the adiabatic zone and generates heat within the temperature profile roll-off region of the furnace. In so doing, the temperature of the roll-off "knee" is elevated and the location of the entire roll-off region is displaced toward the cold zone of the furnace. This leads to an increase in axial temperature gradient, which has important implications for the growth of a single crystal.

The change in furnace temperature profile due to the tickler heater also corresponds to a condition in which any given isotherm within the roll-off region is pushed down toward the cold zone. This also includes the freezing isotherm or the melt-solid interface which was shown to move toward the cold zone with an increase in the extra heat generated in the roll-off region. The increase in heat generation has been achieved by increasing the length or temperature setting or the tickler heater.

Finally, it has been shown that improper plugging of the furnace ends may lead to a convective cold air flux in the furnace which makes the furnace liner walls hotter than the center line. This situation is shown to lead to high radial and low axial temperature gradients. Therefore, proper plugging of the furnace ends is essential to avoid to the materials problems caused by high radial and low axial temperature gradients.

D. Load Material and Translation Rate Effects

The temperature profile seen by the load during bulk crystal growth using the Bridgman-Stockbarger technique is shown to change as more of the melt column is frozen. The data suggest that the temperature profile depends on the proportion of sample length in the hot and cold zones of the furnace and on the relative and absolute values of the thermal conductivities of the melt and solid. Figure 24 shows that for a high thermal conductivity material, silver, the profile sifts toward the hot zone. This shift in profile was not detectable for either Ge or $Pb_{1-x}Sn_xTe$.

This result was interpreted to mean that if the thermal conductivity of the load is negligibly small, then the length of material in the hot or cold zone has a negligible effect on the furnace temperature profile.

Table 1 shows how the furnace profile can be flattened to low axial gradient as the load material is changed from a poor conductor, $Pb_{1-x}Sn_xTe$ to a good conductor, Ag. The lowering of the axial temperature gradient corresponds to a shift in the isotherms toward the hot zone, and also an increase in the spacing between isotherms. However, the translation of the load through the furnace shows the opposite effect of pushing isotherms toward the cold zone. This is demonstrated by the shift in freezing isotherms or the interface toward the cold zone with an increase in translation rate.

APPENDIX I

Data Reduction Program

A

Listed below is the program used in the reduction of the data from temperature versus time to temperature or temperature gradient versus distance.

```
16    CREATE "TEMP4",6
20    CREATE "GRAD4",6
30    OPTION BASE 0
40    ASSIGN #7 TO "TEMP4",T
50    ASSIGN #8 TO "GRAD4",G
60    INPUT "INITIAL DISTANCE=",S1
70    INPUT "INITIAL TEMP=",Y1
80    INPUT "MOTOR SPEED =",C
90    PRINT "MOTOR SPEED = ";C
100   N=1
110   PRINT "NO","TIME","DISTANCE","TEMP","TEMP GRAD"
120   INPUT "TIME,TEMP=",X,Y
130   S=S1+X*C
140   IF S<>S1 THEN 180
150   PRINT 1,X,S,Y,0
160   Z=S
170   GOTO 220
180   N=N+1
190   D=(Y1-Y)/(S1-S)
200   Z=S1+X*C/2
210   PRINT N,X,S,Y,Z,D
220   S1=S
230   Y1=Y
240   PRINT #7;Y,S
250   PRINT #8;D,Z
260   GOTO 120
270   END
```

B

The lattice constant calculation using values determined by x-ray diffraction (see Table 6A) is calculated by

$$d = \frac{u\lambda}{2 \sin\theta}$$

$CuK_\alpha = 1.5418$

Using $\theta = 27.67^\circ$, $d = 3.224\text{Å}$

For a cubic system (lead-tin-telluride has a Rocksalt structure)

$$a^2 = d^2(h^2 + k^2 + l^2)$$

$$a = d\sqrt{(h^2 + k^2 + l^2)}$$

From Table 6a, hkl = 200

Therefore

$$a = 6.42\text{Å}\ (Pb_{1-x}Sn_xTe)$$

From the ASTM cards

$$a_{(PbTe)} = 6.443\text{Å}$$

$$a_{(SnTe)} = 6.302\text{Å}$$

Therefore

$$a_{(PbSnTe)} = a_{(PbTe)} - .14X$$

where x is the mole fraction of SnTe.

$$x = \frac{a_{(PbTe)} - a_{(PbSnTe)}}{.14} = .143$$

APPENDIX II

Example of Melt-Solid Interface Position and Freezing Point Determination Curves

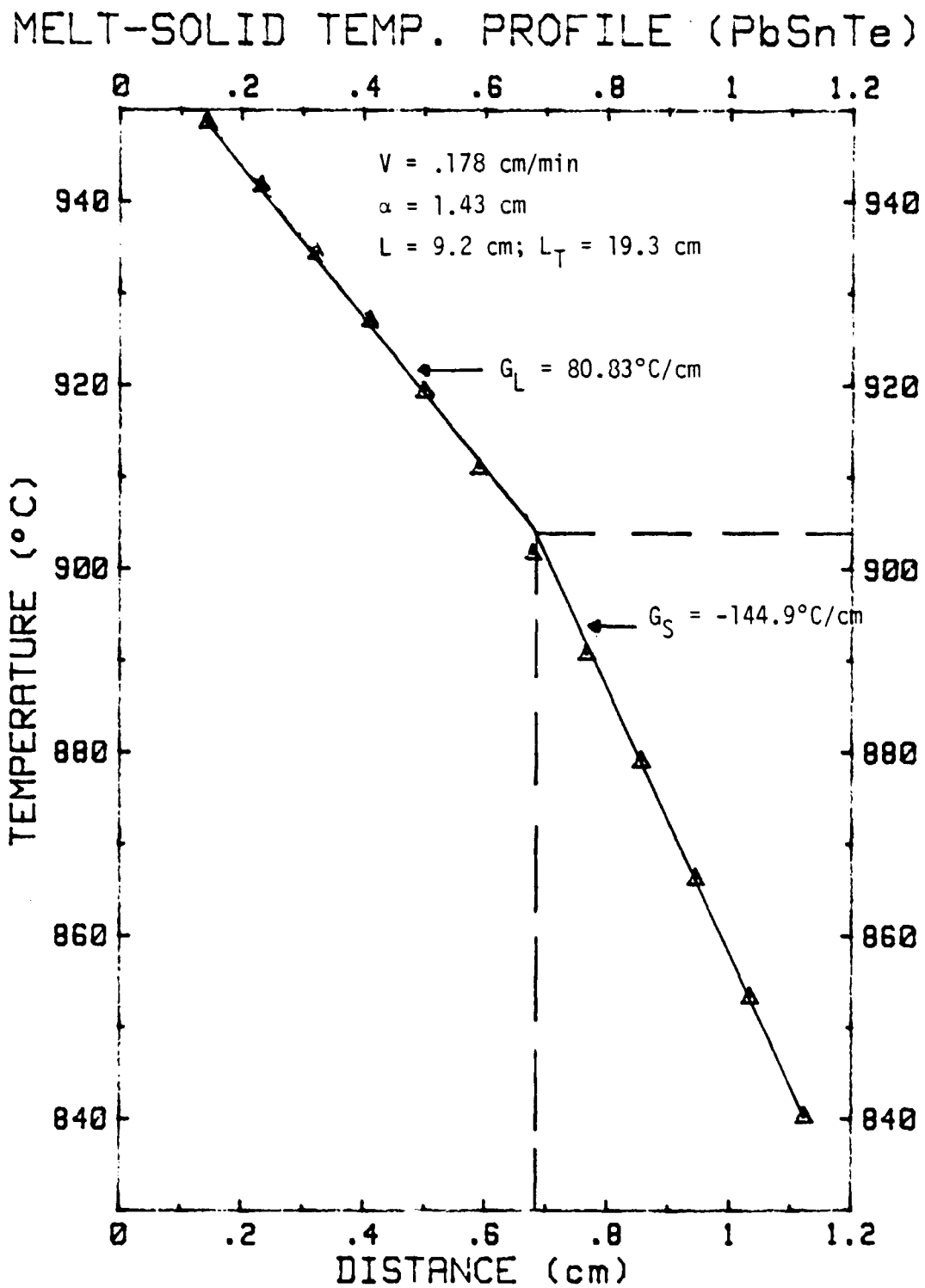

Figure 81. Second dynamic interface position and freezing point determination. Readings were tkaen every 30 seconds.

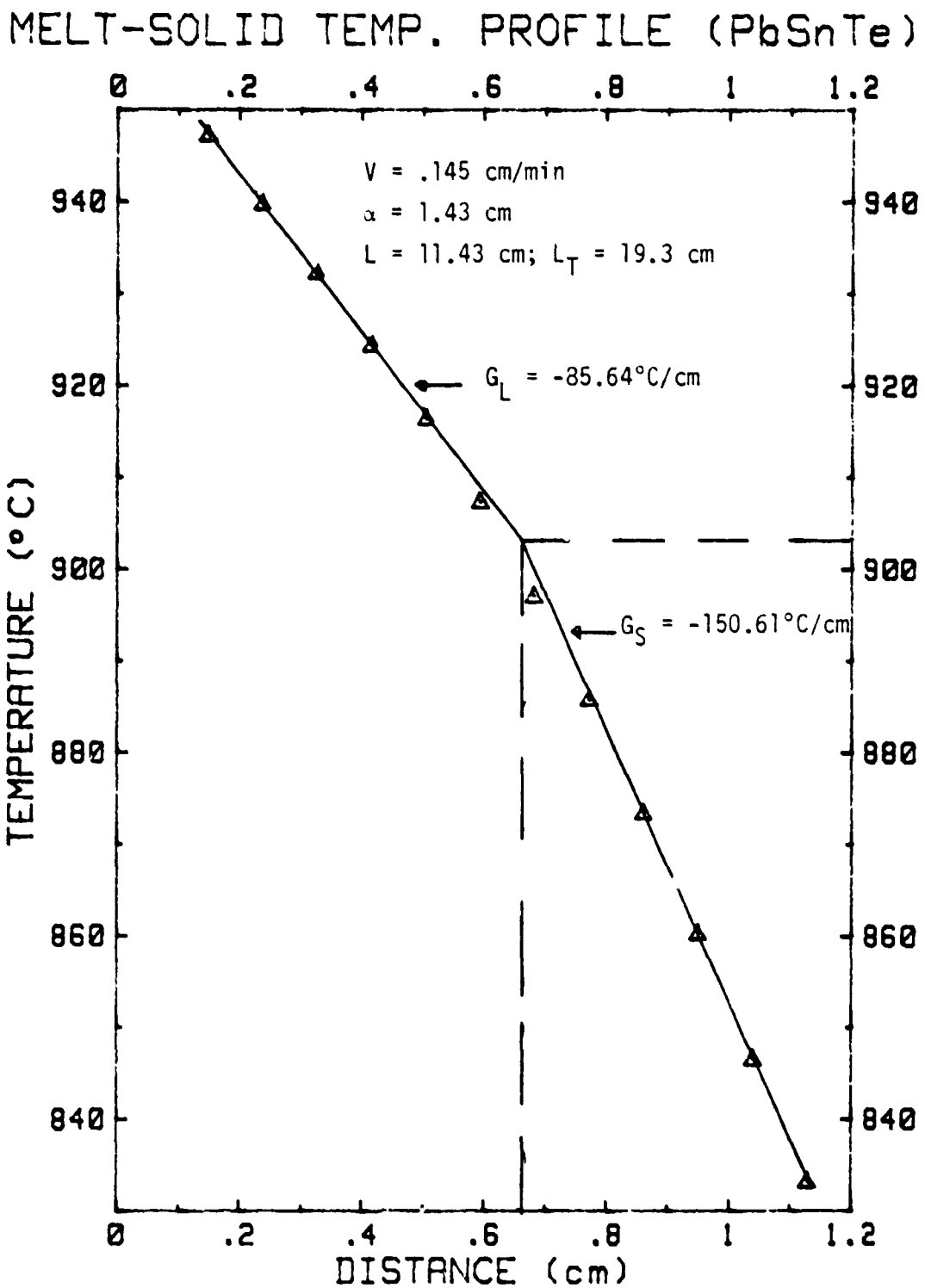

Figure 82. Third dynamic interface position and freezing point determination. Readings were taken every 30 seconds.

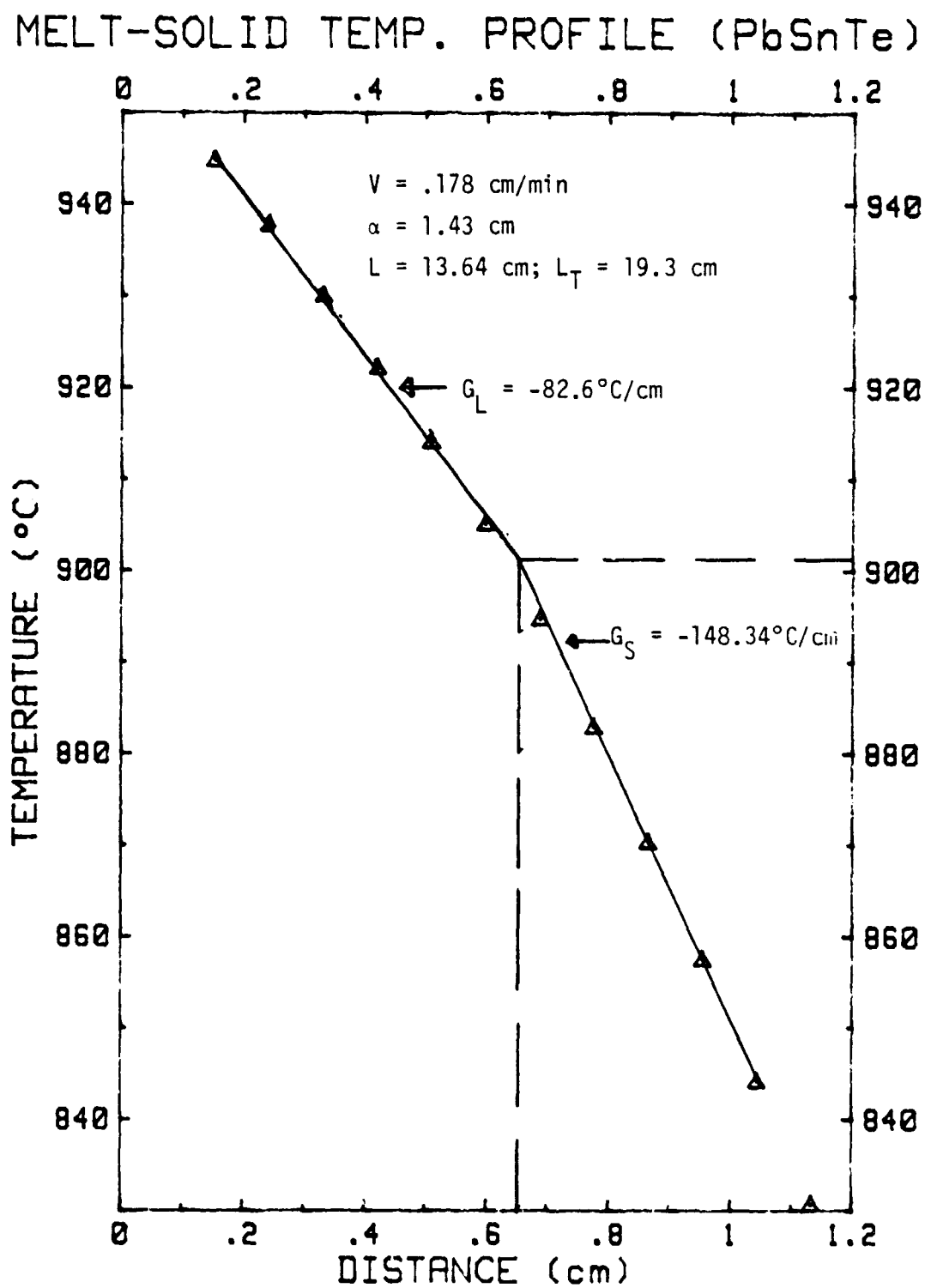

Figure B3. Fourth dynamic interface position and freezing point determination. Readings were taken every 30 seconds.

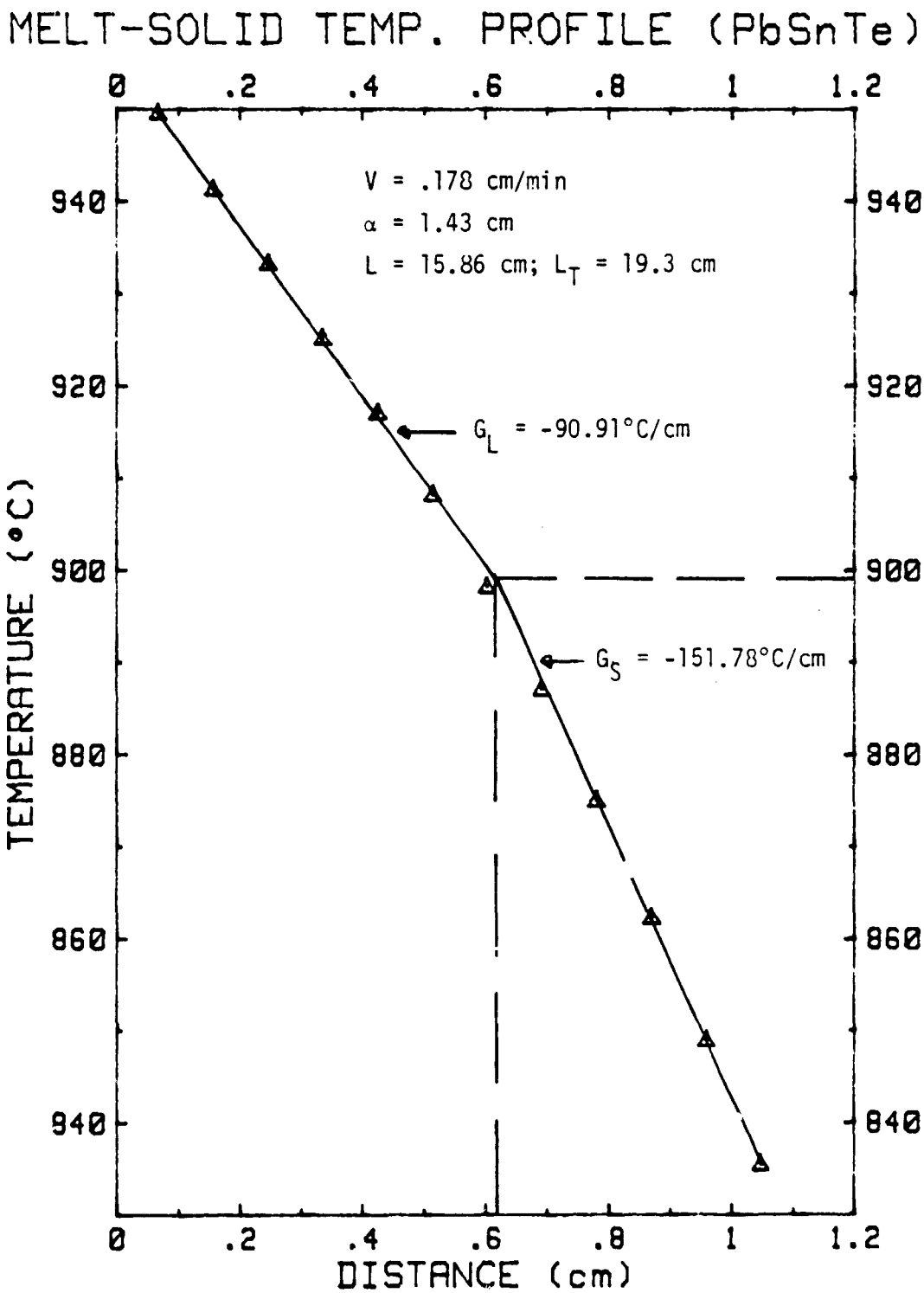

Figure 84. Fifth dynamic interface position and freezing poing determination. Readings were taken every 30 seconds.

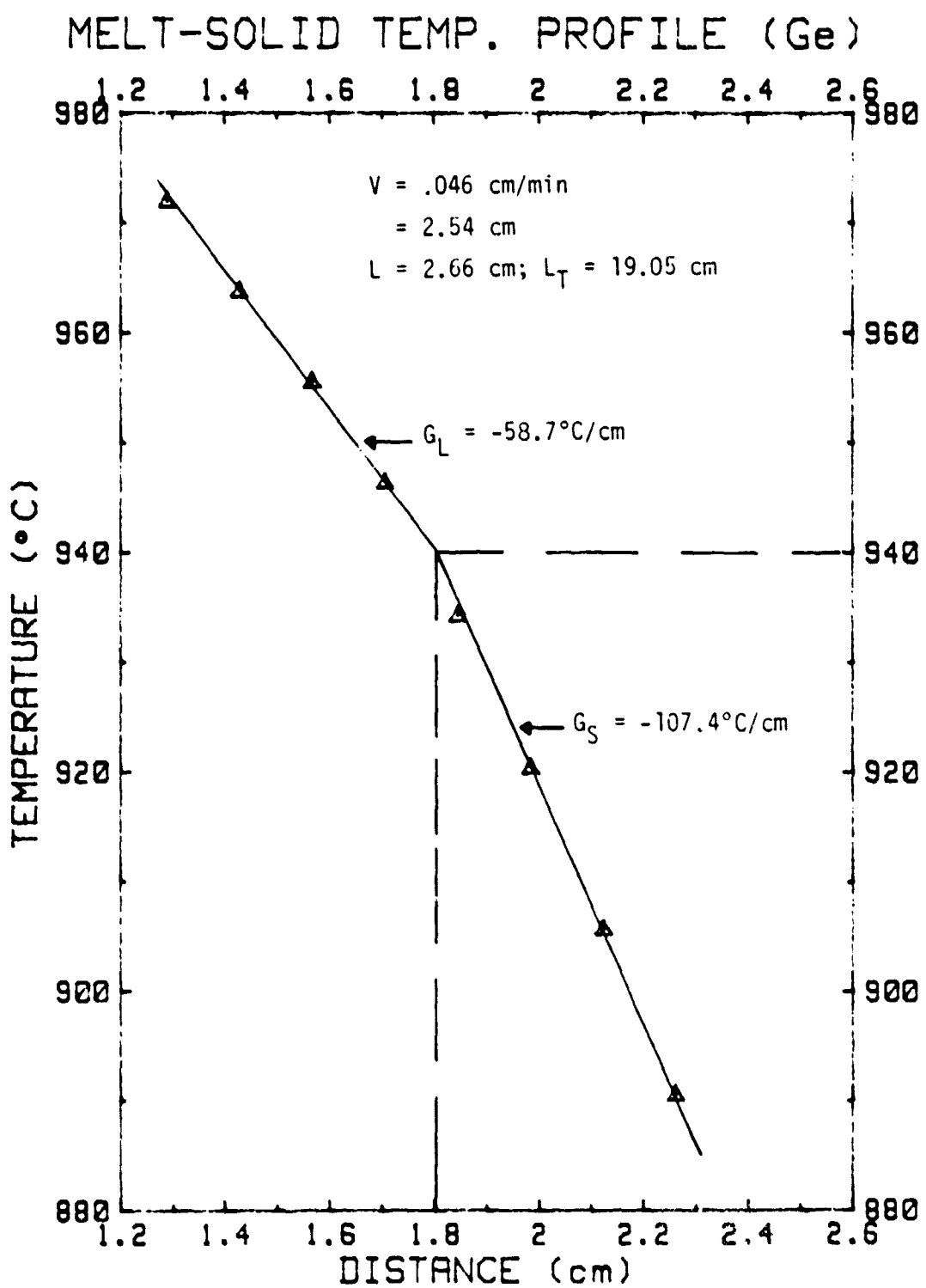

Figure B5. First dynamic interface position and freezing point determination.

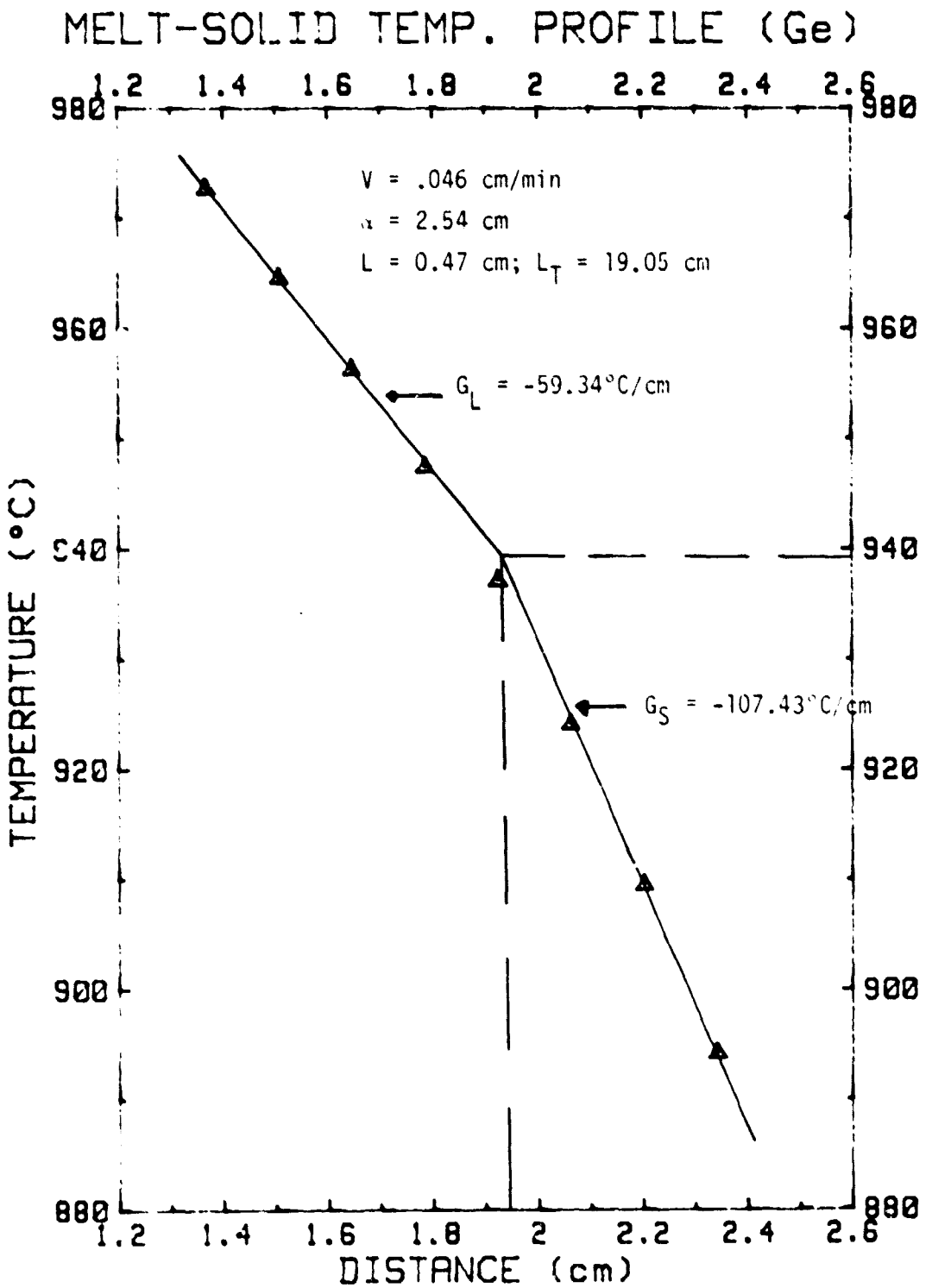

Figure B6. Second dynamic interface position and freezing point determination.

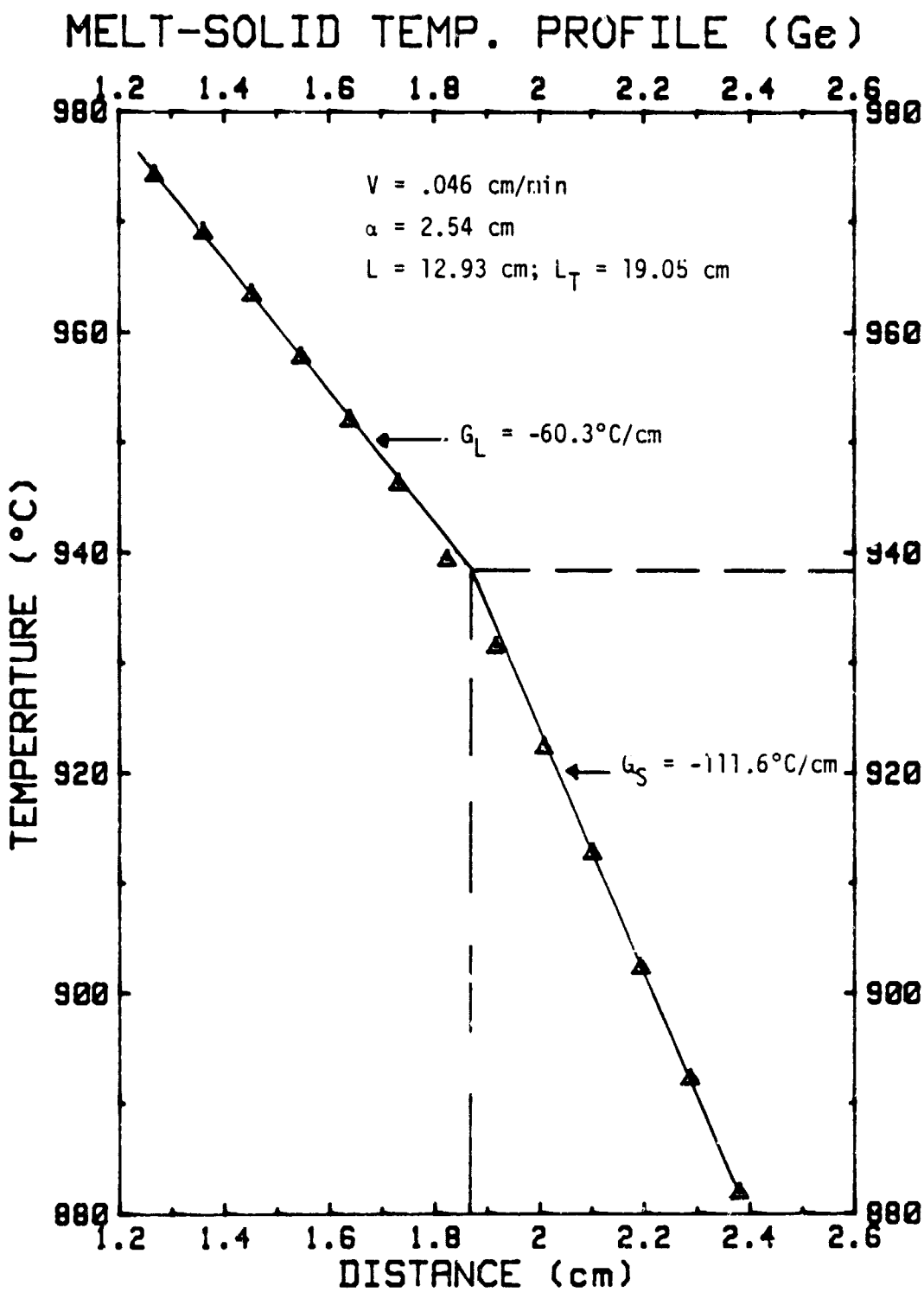

Figure B7. Stationary interface position and freezing point determination. Tickler heater was set at 1094°C.

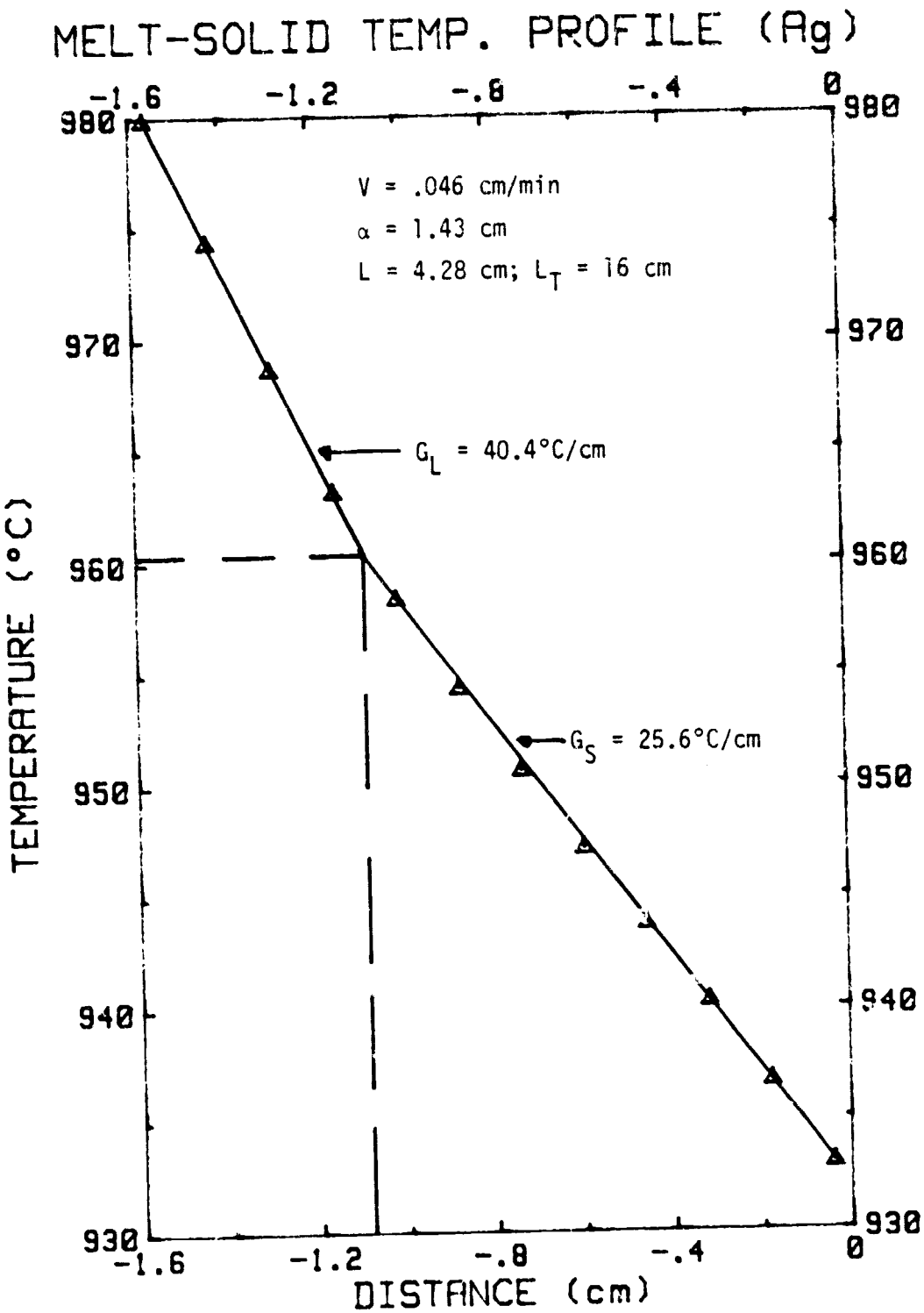

Figure B8. First dynamic interface and freezing point determination.

BIBLIOGRAPHY

1. P. W. Bridman, Proc. Am Acad. Arts Science, Vol. 60 (1925), p. 303.

2. Ta-Wei Fu, W. R. Wilcox J. Crystal Growth, Vol. 48 (1980), p. 416.

3. C. E. Chang, W. R. Wilc , J. Crystal Growth, Vol. 21 (1974), p. 135.

4. J. W. Rutter, B. Chalme , Canadian J. Physics, Vol. 21 (1952), p. 15.

5. T. W. Clyne, J. Crystal rowth, Vol. 50 (1980), p. 684.

6. J. O. Dimmock, I. Melng lis, A. J. Strauss, Physical Review Letters, Vol. 16, No. 26 (1966), . 1193.

7. H. Levinstein, Physics day, Nov. 1977, pp. 23-27.

8. W. A. Tiller, K. A. Jac on, J. W. Rutter, and B. Chalmers, Acta Meta, Vol. 1 (1953), p. 28.

9. D. T. J. Hurle, Solid S te Electro, Vol. 3 (1961), p. 37.

10. J. A. Burton, R. C. Pri and W. P. Slichter, J. Chem. Phys., Vol. 21 (1953), p. 1987.

11. W. W. Mullins, R. F. Sek ka, J. App. Physics, Vol. 35, No. 2 (1964), p. 444.

12. V. G. Smith, W. A. Till , and J. W. Rutter, Canadian J. Phys., Vol. 33 (1955), p. 723.

13. C. J. Wagner, J. Metals, Vol. 6 (1954), p. 154.

14. M. C. Flemings, Solidifi ation Processing, McGraw Hill Series (1974), p. 35

15. G. H. Gulliver, "Metalli Alloys," (Appendix), Charles Griffin & Co., Ltd., London, 1922 taken from Ref. 14).

16. E. Scheil, Z. Metalk. Ve . 34 (1942), p. 70 (taken from Ref. 14).

17. W. G. Hann, Trans AI , ol. 194 (1952), p. 747 (taken from Ref. 14).

18. C. E. Chang. Ph.D. D cation, University of Southern California, Los Angeles (1973) (Take from Ref. 3).

19. K. M. Kim, A Lichtensceiger, and H. C. Gatos, J. Electrochem , V 25, No. 3 (1978), p. 475.

20. A. F. Will, Gatos, J. Electrochemical Soc., Vol. 119 (1972), p. 1218.

21. A. F. Witt, H. C. Gatos, M. Lichtensteiger, C. J. Herman, J. Electrochem. Soc., Vol. 125, No. 11 (1978), p. 1832.

22. A. S. Yue, J. B. Clark, AIME Trans., Vol. 218 (1960), p. 55.

23. D. P. Woodruff, Phil. Mag. (1967), Vol. 17, p. 283.

24. R. J. Naumann,"Working Paper," Nov. 18, 1980.

25. S. W. Chi, Heat Pipe Theory and Practice, p. 1.

26. W. C. Dash, in Growth and Perfection of Crystals (R. H. Doremus, B. W. Roberts and D. Turnbull, eds), Wiley, New York, 1958, p. 361.

27. R. D. Rosi, RCA Rev., Vol. 19, 1958, p. 349.

28. L. S. Birks, Electron Probe Microanalysis (1963), p. 6.

29. R. Castaing, Thesis, University of Paris (1951), ONERA Publication No. 55 (taken from Ref. 28).

30. T. C. Harman, J. Nonmetals, Vol. 1 (1973), p. 183.

31. M. K. Nerr, J. Electrochem. Soc., Vol. 109 (1962), p. 433 (taken from Ref. 26).

32. Thermophysicsl Properties of Matter, Vol. 1, p. 348.

33. L. Flippou, Int. J. of Heat Mass Transfer, Vol. 16 (1973), p. 865.

34. CRC Handbook of Chemistry and Physics.

35. M. Zief, W. R. Wilcox, Fractional Solidification, Vol. 1 (1967), p. 161.

36. R. E. Taylor, H. Groot, Thermophysicsl Properties of PbSnTe; Report to NASA (Langley), January 1980.

37. A. R. Calawa, T. C. Harman, M. Finn and P. Youtz, Trans. AIME, Vol. 242 (1968), p. 374.

38. I. O. Clark, Masters Thesis, George Washington, University, Washington, DC, 1980.